

# Millennial-scale variability of marine productivity and terrigenous matter supply in the western Bering Sea over the past 180 kyr

J.-R. Riethdorf<sup>1,\*</sup>,<sup>5</sup> D. Nürnberg<sup>1</sup>, L. Max<sup>2</sup>, R. Tiedemann<sup>2</sup>, S. A. Gorbarenko<sup>3</sup>, and M. I. Malakhov<sup>4</sup>

[1] {Helmholtz Centre for Ocean Research Kiel (GEOMAR), Wischhofstr. 1-3, D-24148 Kiel, Germany}

[2] {Alfred Wegener Institute for Polar and Marine Research, Am Handelshafen 12, D-27570 Bremerhaven, Germany}

[3] {Pacific Oceanological Institute, Far Eastern Branch, Russian Academy of Sciences, Baltiskaya St. 43, 690041 Vladivostok, Russia}

[4] {North Eastern Interdisciplinary Science Research Institute (NEISRI), Far Eastern Branch, Russian Academy of Sciences, Portovaya St. 16, 685000 Magadan, Russia}

~~[\*]~~-~~[5]~~ {~~now at:~~ Department of Ocean Floor Geoscience, Atmosphere and Ocean Research Institute, University of Tokyo, 5-1-5 Kashiwanoha, Kashiwa, Chiba 277-8564, Japan}

Correspondence to: ~~J.-R. Riethdorf~~[D. Nürnberg](mailto:riethdorfdnuernberg@geomar.de) ([riethdorfdnuernberg@geomar.de](mailto:riethdorfdnuernberg@geomar.de))

## Abstract

We used piston cores recovered in the western Bering Sea to reconstruct millennial-scale changes in marine productivity and terrigenous matter supply over the past ~180 kyr. Based on a geochemical multi-proxy approach our results indicate closely interacting processes controlling marine productivity and terrigenous matter supply comparable to the situation in the Okhotsk Sea. Overall, terrigenous inputs were high, whereas ~~primary-export~~ production was low. Minor increases in marine productivity occurred during ~~warm~~ intervals of Marine Isotope Sstage 5 and interstadials, but pronounced maxima were recorded during interglacials and Termination I. ~~Seasonal sea-ice is suggested to act as the dominant transport agent f~~Theor

29 terrigenous material is suggested to be derived from continental sources on the eastern Bering  
30 Sea shelf and to be subsequently transported via sea-ice, which is likely- to drive changes in  
31 surface productivity, terrigenous inputs, and upper-ocean stratification. From our results we  
32 propose glacial, deglacial, and interglacial scenarios for environmental change in the Bering  
33 Sea. These changes seem to be primarily controlled by insolation and sea-level forcing which  
34 affect the strength of atmospheric pressure systems and sea-ice growth. The opening history  
35 of the Bering Strait ~~and the Aleutian passes~~ is considered to have had an additional impact.  
36 ~~Sea-ice dynamics are thought to drive changes in surface productivity, terrigenous inputs, and~~  
37 ~~upper-ocean stratification.~~ High-resolution core logging data (color b\*, XRF scans) strongly  
38 correspond to the Dansgaard-Oeschger climate variability registered in the NGRIP ice core  
39 and support an atmospheric coupling mechanism of Northern Hemisphere climates.

40

## 41 **1. Introduction**

42 The subarctic North Pacific (N Pacific) is a high-nitrate, low-chlorophyll (HNLC) region  
43 (e.g., Kienast et al., 2004; Tyrrell et al., 2005), characterized by salinity-driven stratification  
44 (permanent halocline), which is suggested ~~as a potential~~ control ~~mechanism of late~~  
45 ~~Quaternary~~ glacial/interglacial variations in atmospheric carbon dioxide (CO<sub>2</sub>) concentrations  
46 (Haug et al., 1999, 2005; Sigman and Boyle, 2000; Sigman et al., 2004, 2010; Jaccard et al.,  
47 2005). The halocline prevents the formation of deep water (Warren, 1983; Emile-Geay et al.,  
48 2003) and modulates the supply of nutrient-rich deep water into the euphotic zone, thereby  
49 influencing the extent of marine productivity and ~~nitrate~~ nutrient utilization. Since the halocline  
50 also acts as a barrier for atmospheric-oceanic gas exchange, the modern N Pacific with its  
51 high carbon export efficiency (Honda et al., 2002) is considered a net sink of atmospheric  
52 CO<sub>2</sub> (Takahashi et al., 2002a).

53 Several studies have reported low ~~marine export production~~ productivity in the N Pacific  
54 during glacial times (Narita et al., 2002; Kienast et al., 2004; Jaccard et al., 2005, 2009, 2010;  
55 Brunelle et al., 2007; Shigemitsu et al., 2007; Galbraith et al., 2008; Gebhardt et al., 2008).  
56 However, it remains unclear, whether ~~reduced marine productivity and low atmospheric CO<sub>2</sub>~~  
57 ~~were~~ this was caused by ~~increased polar~~ stronger stratification or by enhanced sea-ice cover.  
58 Both processes would result in a less efficient ~~biologically driven drawdown~~ export of organic  
59 ~~matter~~ carbon to the deep ocean and its subsequent degradation to CO<sub>2</sub> ("biological pump"),

60 and hamper the release of deep-sequestered CO<sub>2</sub> to the atmosphere. Interglacial maxima in  
61 export productivity at ODP Site 882 were related to reduced stratification rather than to  
62 sea-ice influence (Jaccard et al., 2005). Since the modern Bering Sea is marked by high  
63 marine productivity and seasonal sea-ice formation (e.g., Springer et al., 1996; Niebauer et al.,  
64 1999) it might have had a different influence on past ocean-atmosphere CO<sub>2</sub> exchange.  
65 Paleooceanographic reconstructions in the Bering Sea also revealed reduced surface  
66 productivityexport production during the last glacial period, which increased during  
67 Termination I and remained high in the Holocene (Gorbarenko, 1996; Cook et al., 2005;  
68 Gorbarenko et al., 2005; Okada et al., 2005; Okazaki et al., 2005; Brunelle et al., 2007, 2010;  
69 Itaki et al., 2009; Khim et al., 2010; Kim et al., 2011). This variability was explained by a  
70 complex interplay of changes in sea surface temperatures (SST), sea-ice extentcoverage,  
71 inflow of Pacific surface waters, and upper-ocean stratification (e.g., Katsuki and Takahashi,  
72 2005; Brunelle et al., 2007, 2010; Kim et al., 2011).

73 Knowledge of past sea-ice variability in the Bering Sea comes from diatom and radiolarian  
74 assemblages, and IP<sub>25</sub> biomarker studies (Cook et al., 2005; Katsuki and Takahashi, 2005;  
75 Tanaka and Takahashi, 2005; Max et al., 2012). Although sea-ice is considered an important  
76 transport agent for terrigenous material, geochemical or sedimentological studies assessing  
77 past terrigenous matter supply in the N Pacific are rare. Existing studies focused on the  
78 Okhotsk Sea (Sato et al., 2002; Nürnberg and Tiedemann, 2004; Nürnberg et al., 2011), the  
79 NW Pacific (Shigemitsu et al., 2007; VanLaningham et al., 2009), and the Southern Ocean  
80 (Latimer and Filippelli, 2001). For the Okhotsk Sea Nürnberg and Tiedemann (2004)  
81 suggested that nearly synchronous glacial/interglacial changes in biological and terrigenous  
82 fluxes were modulated by sea-ice processes driven by variations in the strength of the  
83 Siberian High. For the Bering Sea some provenance studies involving sedimentological and  
84 geochemical characteristics of surface sediments are available, but were mainly conducted on  
85 the eastern Bering Sea shelf (Gardner et al., 1980; Lisitzin, 2002; Asahara et al., 2012;  
86 Nagashima et al., 2012). These studies and results from the Meiji Drift in the NW Pacific  
87 indicate that a large fraction of the supplied terrigenous material was delivered from Yukon-  
88 Bering Sea sources (VanLaningham et al., 2009). However, downcore records reflecting the  
89 compositional variability of terrigenous matter in the Bering Sea are missing.

90 Recent progress has been made in detecting millennial-scale climate variability in Bering Sea  
91 sediments (Cook et al., 2005; Gorbarenko et al., 2005, 2010; Okazaki et al., 2005; Brunelle et

92 al., 2010; Khim et al., 2010; Kim et al., 2011; Max et al., 2012; Rella et al., 2012). Most of  
93 these studies are restricted to the last ~70 kyr or focus on deglacial changes in the northern,  
94 southern, and southeastern Bering Sea. Together with studies from the NE Pacific (e.g.,  
95 Hendy and Kennett, 2000) they imply that short episodes of increased marine productivity are  
96 connected with interstadials recorded in Greenland ice cores. However, the existing  
97 reconstructions within the N Pacific realm are constrained by the shallow lysocline, which  
98 ~~within the N Pacific realm~~ limits the use of carbonate-based proxies and causes  
99 stratigraphic uncertainties. In the Bering Sea according reconstructions are thus restricted to  
100 shallow shelf areas or morphological-topographic highs. Here, we present millennial-scale  
101 reconstructions of marine productivity/export production and terrigenous matter supply for the  
102 hitherto only poorly studied western Bering Sea. Results were derived from a suite of  
103 geochemical proxies and high-resolution core logging data covering the last ~180 kyr.

104

## 105 **2. Regional setting**

106 The Bering Sea links the Pacific Ocean with the Arctic Ocean via the only shallow (~50 m)  
107 Bering Strait. In its eastern and northern part it is characterized by a wide and shallow (0-200  
108 m) continental shelf area. Pacific surface waters, transported by the westward flowing  
109 Alaskan Stream, enter the Bering Sea through several passes within the Aleutian Island Arc  
110 (e.g., Takahashi, 2005). Inside the Bering Sea, a large-scale cyclonic surface circulation  
111 pattern develops with the Bering Slope Current (BSC) and the East Kamchatka Current acting  
112 as eastern and western boundary currents, respectively (Fig. 1). Outflow occurs through the  
113 Bering Strait into the Arctic Ocean and through the Aleutian passes, mainly Kamchatka Strait,  
114 into the N Pacific (Stabeno et al., 1999). Deep waters flow northward and eastward from  
115 Kamchatka Strait with return outflow above 3,000 m water depth (Reed et al., 1993; Stabeno  
116 et al., 1999). The oceanographic and climatic conditions are characterized by a strong  
117 seasonal variability of SST and sea-ice coverage that result from the interaction of the  
118 Siberian High and the Aleutian Low. The Arctic Oscillation, Pacific Decadal Oscillation, and  
119 the Pacific–North American pattern are reported to be related with decadal variations of both  
120 atmospheric pressure cells (Niebauer, 1988; Mantua et al., 1997; Niebauer, 1998; Overland et  
121 al., 1999, 2002). During winter, a strong Siberian High leads to results in advection of cold  
122 Arctic air masses and mainly northerly wind directions (Stabeno et al., 1999). This causes a

123 significant cooling of the sea surface, sea-ice formation, as well as enhanced vertical mixing  
124 in the mixed layer, thereby returning nutrients from the subsurface. In contrast, during  
125 summer, the reduced strength of the Aleutian Low and enhanced insolation result in a  
126 stratified mixed layer and increased marine productivity.

127 Primary productivity is dominated by diatoms mainly blooming during spring, whereas  
128 increased biological CaCO<sub>3</sub> fluxes (coccolithophores, planktonic foraminifera) occur during  
129 spring and late summer/early fall (e.g. Takahashi et al., 2002b). Highest annual production  
130 rates are associated with shelf areas and vary regionally between >200 and >800 gC m<sup>-2</sup>  
131 (Arzhanova et al., 1995; Springer et al., 1996; Stabeno et al., 1999). Available nutrients are  
132 reported to be often fully consumed during seasonal blooms (Niebauer et al., 1995).

133 Sea-ice ~~formation~~ begins to form during October/November on the northern Bering Sea  
134 continental shelf (Anadyr Bay, Bering Strait), reaching its maximum distribution in  
135 March/April, and subsequently ~~disintegrating~~ declines until July (Tomczak and Godfrey,  
136 1994; Niebauer et al., 1999; Lisitzin, 2002). ~~It~~ Sea-ice formation takes place in shallow shelf  
137 areas, bays, and coastal areas. As in the Arctic, coastal polynyas play an important role for the  
138 build-up of sea-ice, and consequently for water mass ventilation due to brine rejection  
139 (Niebauer et al., 1999; Stabeno et al., 1999). Processes entraining sediment into newly formed  
140 ice involve tidal sea-level oscillations, wind mixing, resuspension of sediments from the  
141 seafloor (suspension freezing), beach-ice formation, nearshore anchor ice formation, and  
142 seabed freezing (e.g. Nürnberg et al., 1994; Stein, 2008, and references therein; Nürnberg et  
143 al., 2011, and references therein). Especially during fall and winter, storms affect reworking  
144 and resuspension processes by sea-ice crushing, mixing of the water column, and detachment  
145 of the sediment-laden ice from the coast. The sediment freight is released by sea-ice melting,  
146 especially during spring/summer, and then contributes to (hemi-) pelagic sedimentation.

147

### 148 **3. Material and methods**

149 This study is based on piston cores SO201-2-77KL, -85KL, and -101KL from Shirshov  
150 Ridge, western Bering Sea (Fig. 1, Tab. 1). The cores were recovered along a ~280 km-long  
151 north-south transect from ~~shallow-intermediate~~ to deep ~~intermediate~~-water levels- (630-2135  
152 m) during R/V Sonne cruise SO201-KALMAR Leg 2 in 2009 (Dullo et al., 2009). The  
153 sedimentary succession is characterized by monotonous sequences of mainly clay- and silt-

154 sized siliciclastic material, which are repeatedly interrupted by layers of diatomaceous ooze.  
155 Except for the younger part of the Holocene, which mainly consists of diatom-rich sediment,  
156 our sediment cores contained low but sufficient concentrations of CaCO<sub>3</sub>~~sufficient carbonate~~  
157 to also allow for high-resolution paleoceanographic–foraminifera-based reconstructions.  
158 However, ~~for~~ cores 85KL and 101KL sediments younger than 7.5 ka BP and 12.5 ka BP,  
159 respectively, ~~are-were~~ not preserved/recovered.

### 160 **3.1 Stratigraphic approach**

#### 161 **3.1.1 Core logging**

162 Color reflectance measurements were carried out using a Minolta CM 508d hand-held  
163 spectrophotometer at 1 cm-spaced intervals (Dullo et al., 2009). Reflectance data were  
164 automatically converted by Spectramagic software into CIE L\*, a\* and b\* color space  
165 (CIELAB).

166 The Avaatech X-ray fluorescence (XRF) core scanner at Alfred Wegener Institute for Polar  
167 and Marine Research, Bremerhaven, was used to determine relative changes in the  
168 sedimentary elemental composition. Core scanning was performed on the split core surface  
169 covered with SPEX CertiPrep 3525 Ultralene foil (4 µm thick). Each core segment was triple-  
170 scanned for analysis of elements Al through to Ba at 1 mA, but at different tube voltages and  
171 count times (10 kV, 10 s; 30 kV, 15 s; 50 kV, 30 s), using a sampling resolution of 1 cm.  
172 Results are considered semiquantitative (Richter et al., 2006; Tjallingii et al., 2007) and are  
173 given as count rates (in cps) or as log-ratios (natural logarithm) of element count rates.

#### 174 **3.1.2 Stable oxygen isotopes**

175 For stable oxygen isotope ( $\delta^{18}\text{O}$ ) stratigraphy we used endobenthic foraminifer species  
176 *Uvigerina peregrina* and *Uvigerina auberiana*, since *Uvigerina*  $\delta^{18}\text{O}$  values are reported to be  
177 in equilibrium with seawater (Shackleton and Hall, 1984).  $\delta^{18}\text{O}$  was measured every 5 cm on  
178 2-3 tests of *U. peregrina*, ~~or, if not present, of *U. auberiana*~~, collected from the 315-355 µm  
179 size fraction. For core 77KL we used tests of *U. auberiana* when *U. peregrina* was not  
180 present. The mMeasurements were performed at GEOMAR, Kiel, using a ~~Thermo-Finnigan~~  
181 MAT253 mass spectrometer (Thermo Scientific, Germany) coupled with a ~~Thermo-Scientific~~  
182 Kiel IV Carbonate device (Thermo Scientific, Germany). Results were referenced to the  
183 NBS19 standard and calibrated to the VPDB scale. Long-term precision (n > 1000 samples)

184 for  $\delta^{18}\text{O}$  of the used carbonate standard (Solnhofen limestone) was  $\pm 0.06\%$ . In core 77KL  
185 benthic foraminifera were only preserved until 865 cm core depth.

### 186 **3.1.3 Paleomagnetism**

187 Sedimentary natural remanent magnetization (NRM) was determined in core 85KL based on  
188 saturation magnetization in magnetic-hysteresis parameters, and by differential  
189 thermomagnetic analyses using a Faraday magnetic balance and a coercive spectrometer  
190 (Burov ~~and Yasonov, 1979~~ et al., 1986; Yasonov et al., 1998). The NRM module and direction  
191 were measured with a AGICO JR-5A spinner magnetometer after the stepwise  
192 demagnetization of a reference sample. Magnetic cleaning was performed using an alternating  
193 magnetic field with an amplitude of 10 mT to recognize the characteristic component of NRM  
194 (ChRM). Anhysteretic remanent magnetization (ARM) was generated in the preliminarily  
195 demagnetized samples using a AGICO AMU-1A anhysteretic magnetizer under a constant  
196 field of 0.05 mT and a maximum alternating field of 100 mT. Relative paleointensity of the  
197 magnetic field (RPI) was then calculated by normalization of ChRM to ARM. Scalar  
198 petromagnetic properties (SPP) were additionally determined (Enkin et al., 2007; Malakhov et  
199 al., 2009). All measurements were conducted at NEISRI, Magadan.

200 Takahashi et al. (2011) reported on the transformation of oxide magnetic minerals into  
201 paramagnetic  $\text{FeS}_2$  in Bering Sea sediments. They associated the formation of  $\text{FeS}_2$  with  
202 sulfate reduction processes under anaerobic methane oxidation. We performed quality control  
203 of the magnetic hysteresis parameters (Day-plot, orthogonal projections of AF  
204 demagnetization of NRM, et al.) and the thermomagnetic analyses of the magnetic fraction,  
205 which also indicate an influence by sediment diagenesis in core 85KL. Specifically, the  
206 thermomagnetic analyses suggest the occurrence of paramagnetic  $\text{FeS}_2$  in the major  
207 ferrimagnetic phase from 880 cm to 1760 cm core depth. We assume that the dissolution of  
208 very fine-dispersed almost single-domain magnetic particles and the preservation of coarse  
209 pseudo-single-domain and multi-domain particles just led to decreasing RPI values within  
210 that depth interval. However, this most probably had no effect on the relative variability of the  
211 reconstructed geomagnetic field.

### 212 **3.1.4 Age models**

213 The chronostratigraphic approach included high-resolution core logging data (color  $b^*$ , XRF  
214 scanning), benthic  $\delta^{18}\text{O}$  stratigraphy, magnetostratigraphy, and accelerator mass spectrometry

215 (AMS) radiocarbon dating of planktonic foraminifera for absolute age control. A detailed  
216 presentation of the stratigraphic framework for the last 20 kyr, including the AMS-<sup>14</sup>C dating  
217 results, is provided in Max et al. (2012). The pre-deglacial (>20 ka BP) stratigraphic  
218 framework of our cores is primarily based on the graphic correlation between color b\*  
219 recorded in core 85KL and the Dansgaard-Oeschger (D-O; e.g., Dansgaard et al., 1993)  
220 climate variability registered in the NGRIP  $\delta^{18}\text{O}$  record (NGRIP members, 2004; GICC05  
221 timescale, Rasmussen et al., 2006) (Fig. 2A). For ages >122 ka BP and for identification of  
222 the Marine Isotope Stage (MIS) 5.5 climate optimum (~125 ka BP) color b\* and XRF Ca/Ti  
223 log-ratios were correlated to the Sanbao stalagmite  $\delta^{18}\text{O}$  record (Wang et al., 2008). The  
224 Laschamp (~42 ka BP), Norwegian-Greenland Sea (~65 ka BP), and Blake (~117 ka BP)  
225 paleomagnetic excursions were identified in the RPI record and correlated with the PISO-  
226 1500 geomagnetic paleointensity stack (Channell et al., 2009). Further ages were derived  
227 from comparison of benthic  $\delta^{18}\text{O}$  values and SPP (not shown) with the global reference stack  
228 LR04 (Lisiecki and Raymo, 2005), which was also used to identify boundaries of stages MIS  
229 1 to 6. The stratigraphy of core 85KL was transferred via intercore correlations (color b\*,  
230 XRF Ca/Ti log-ratios) to cores 77KL and 101KL (Fig. 2B), for which similar stratigraphic  
231 approaches were carried out. All age-depth points are provided in Appendix A.

232 Figure 3 shows the age models for our cores by direct comparison with the used reference  
233 records and a respective age versus depth diagram. Age models were tested via spectral  
234 analysis of the color b\* and benthic  $\delta^{18}\text{O}$  records in the time domain to detect orbital  
235 frequencies. Spectral analysis was performed using the AnalySeries 2.0 software (Paillard et  
236 al., 1996). Despite the shortness of our records with respect to orbital-scale changes, we found  
237 dominant cyclicities of ~23 and ~39 kyr, which within appropriate bandwidths match  
238 frequencies of orbital precession ( $0.047\pm 0.005 \text{ kyr}^{-1}$ ) and obliquity cycles ( $0.025\pm 0.0015 \text{ kyr}^{-1}$ ) (Fig. 3).

### 240 3.2 Sedimentation and accumulation rates

241 Linear sedimentation rates (LSR, in  $\text{cm kyr}^{-1}$ ) were calculated between age control points. ~~and~~  
242 ~~h~~Bulk accumulation rates ( $\text{AR}_{\text{Bulk}}$ , in  $\text{g cm}^{-2} \text{ kyr}^{-1}$ ) were calculated as the product of LSR and  
243 the dry bulk density (DBD, in  $\text{g cm}^{-3}$ , determined each 5 cm). ~~DBD was determined each 5~~  
244 ~~cm~~. Records of LSR and  $\text{AR}_{\text{Bulk}}$  are shown in Fig. 4. Cores from Shirshov Ridge have average  
245 LSR ( $\text{AR}_{\text{Bulk}}$ ) of 11-16  $\text{cm kyr}^{-1}$  (7-15  $\text{g cm}^{-2} \text{ kyr}^{-1}$ ), and hence allow for centennial- to



246 millennial-scale reconstructions. Variability and average values of LSR and  $AR_{Bulk}$  increase  
247 towards the northernmost site. In general, LSR and  $AR_{Bulk}$  are higher during cold intervals  
248 (~~stages-MIS 6, 5.4, 5.2, and 4~~) than during warm intervals (~~stages-MIS 5.5, 5.3, 5.1, 3, and 1~~),  
249 but highest during Termination I (20-10 ka BP) (Fig. 4). Holocene sediments are either ~~not~~  
250 ~~preserved~~fully recovered or subject to low LSR ( $AR_{Bulk}$ ). The piston should have prevented  
251 sediment loss during coring and at least giant piston cores are reported to rather cause  
252 oversampling (stretching) of the sediments (Széréméta et al., 2004). We therefore consider the  
253 partly ismissing Holocene sections to be the result of a change in sedimentation favoring the  
254 deposition of highly porous diatomaceous ooze and its subsequent erosion, ~~since piston cores~~  
255 ~~are reported to rather cause oversampling (stretching) of the sediments (Széréméta et al.,~~  
256 ~~2004) and because the piston should have prevented sediment loss during coring.~~  
257 ~~In this study, we report proxy concentrations rather than quantified flux rates and treat the~~  
258 ~~respective records as qualitative. Accumulation rates in contrast to proxy concentrations are~~  
259 ~~unaffected by depositional dilution or enrichment. However, if proxy concentrations in~~  
260 marine sediments cores are low or vary only little, the variability of accumulation rates  
261 mainly reflects the LSR variability (Middelburg et al., 1997). This situation applied to our  
262 sediment cores. Accordingly, we mainly report proxy concentrations rather than quantified  
263 flux rates and treat the respective records as qualitative.

### 264 **3.3 Assessment of marine productivity**

265 Past changes in marine productivity (paleo-export production) were approximated from total  
266 organic carbon (TOC),  $CaCO_3$ , biogenic opal, biogenic barium ( $Ba_{bio}$ ), and XRF logging data.  
267 This multi-proxy approach was necessary due to specific restrictions of the respective proxies.  
268 TOC preservation in sediments is highly debated (e.g., Hartnett et al., 1998; Ganeshram et al.,  
269 1999; Thunell et al., 2000; Hedges et al., 2001) as it is, e.g., influenced by oxidation processes  
270 and bottom water ventilation (De La Rocha, 2007). Also, its source can be of marine and  
271 ~~terrigenous-terrestrial~~ origin. In the N Pacific the preservation of  $CaCO_3$  is limited by the  
272 shallow lysocline. Accordingly,  $CaCO_3$  concentrations rather reflect changes in the bottom  
273 water calcite saturation state (e.g., Jaccard et al., 2005; Gebhardt et al., 2008), although  
274 changes in biological  $CaCO_3$  production can not be fully excluded to explain changes in  
275  $CaCO_3$ . Opal dissolves during settling to the seafloor, but its preservation is independent from  
276 bottom water oxygenation. Since opal-rich sediments are linked to biogenic silica production

277 (e.g., [Honjo, 1990](#); Nelson et al., 1995; Ragueneau et al., 2000; Pondaven et al., 2000; ~~Matul~~  
278 ~~et al., 2002~~) biogenic opal is most often used in N Pacific reconstructions of marine  
279 productivity. Barium, present as sedimentary barite is used in several studies to reconstruct  
280 paleoproductivity (e.g., Dymond et al., 1992; Francois et al., 1995; Dymond and Collier,  
281 1996; Gingele et al., 1999), ~~although evidence for direct biogenic barite formation does not~~  
282 ~~exist~~. Barite particles occur in areas of high new production (Dehairs et al., 1991) and  
283 laboratory experiments showed that the decay of phytoplankton in undersaturated seawater  
284 results in barite formation (Ganeshram et al., 2003).

### 285 **3.3.1 CN-analyses and biogenic opal**

286 Total carbon (TC), TOC, and total nitrogen (TN) were determined on freeze-dried bulk  
287 sediment samples of 20 mg using a Carlo Erba NA-1500 CNS analyzer. TOC was measured  
288 on previously decalcified samples and CaCO<sub>3</sub> concentrations were calculated by  
289 multiplication of the difference between TC and TOC with a factor of 8.333. Reproducibility  
290 of the TOC and TN measurements was ±0.03 wt.% and ±0.01 wt.%, respectively.

291 The ~~atomic-molar~~ ratio of TOC to TN, corrected for inorganic nitrogen compounds (referred  
292 to as [C/N]<sub>a</sub> hereafter), was used to distinguish between marine and ~~terrigenous-terrestrial~~  
293 sources of TOC. The Redfield ratio (Redfield et al., 1963) translates the C/N ratio of marine  
294 organic matter to ~7. Typical terrigenous values lie between 20-200 (Hedges et al., 1986). We  
295 applied a correction for total inorganic nitrogen (TIN), usually clay-bound inorganic  
296 ammonium (Müller, 1977), based on a linear relationship between TOC and TN (after Goñi et  
297 al., 1998). Results showed TIN concentrations of 0.01-0.02 wt.% that were assumed constant  
298 downcore.

299 Biogenic opal was measured following Müller and Schneider (1993) using molybdate-blue  
300 spectrophotometry. Silica was extracted from 20 mg of freeze-dried bulk sediment samples.  
301 Results were evaluated applying the procedure of DeMaster (1981). Replicate measurements  
302 showed a reproducibility of 1-2 wt.%.

### 303 **3.3.2 Biogenic barium (Ba<sub>bio</sub>)**

304 Concentrations of major (Al, Ti, Fe, K) and trace (Ba) elements were determined on discrete  
305 samples offrom 0.6 g of freeze-dried bulk sediment using a Philips PW1480 XRF  
306 spectrometer without determination of loss on ignition following standard procedures.  
307 Analytical precision, determined for the BHVO standard, was <2% RSD for the major

308 elements and  $\pm 30$  ppm for Ba (N = 15). Results for barium ( $Ba_{total}$ ) are the sum of biogenic  
309 ( $Ba_{bio}$ ) and nonbiogenic Ba-portions.  $Ba_{bio}$  was therefore calculated via concentrations of Al  
310 by estimating the aluminosilicate contribution of Ba considering the global average Ba/Al  
311 ratio for pelitic rocks of  $6.5 \text{ mg g}^{-1}$  (Wedepohl, 1971):

$$312 \quad Ba_{bio} = Ba_{total} - Al * 0.0065 \quad (1)$$

313  $Ba_{bio}$  was subsequently used to assess new production ( $P_{New}$ ) by applying the relationship of  
314 Nürnberg (1995) (see also Fig. 7). Annual primary production (PP) was calculated after  
315 Eppley and Peterson (1979) using the  $P_{New}$ -estimates.

### 316 3.3.3 XRF logging data (Br, Ca/Ti, Si/Al)

317 Several logging data and bulk geochemical analyses showed a similar temporal evolution. In  
318 this respect, XRF count rates of Br correlated with TOC concentrations ( $0.35 < R^2 < 0.74$ ),  
319 which supports a relationship between TOC and biophilic halogen bromine (Ziegler et al.,  
320 2008). XRF Ca/Ti log-ratios correlated with  $CaCO_3$  concentrations ( $0.07 < R^2 < 0.65$ ), which  
321 is explained by assuming a detrital origin of Ti. Normalization of XRF-derived Ca to Ti  
322 and/or Al abundances has been applied before (Jaccard et al., 2005) and is thought to reflect  
323 biogenic  $CaCO_3$  contents within the sediment. The XRF signals for Al were better than for Ti  
324 and were subsequently used for normalization. However, we favored Ca/Ti over Ca/Al log-  
325 ratios due to better correlation to  $CaCO_3$ . Although opal concentrations were close to  
326 reproducibility for most samples, they correlated with color  $b^*$  ( $0.20 < R^2 < 0.60$ ) and XRF  
327 Si/Al log-ratios ( $0.04 < R^2 < 0.73$ ). This is in accordance with other studies considering a  
328 connection between Si/Al ratios and biogenic opal (McDonald et al., 1999) and between color  
329  $b^*$  and organic matter/opal (Debret et al., 2006). All linear relationships found are considered  
330 significant strong for cores 77KL and 85KL ( $0.57 < R^2 < 0.74$ ), but insignificant weak for core  
331 101KL ( $0.04 < R^2 < 0.35$ ). Since the significance of the correlations linear correlation  
332 coefficients strongly varied between both, the respective sites and the respective proxies, the  
333 logging data were not used to apply calibration functions, but are shown together with the  
334 quantitative results.

## 335 3.4 Assessment of terrigenous matter supply

### 336 3.4.1 Coarse material, siliciclastics, and terrigenous matter

337 Changes in terrigenous fluxes were approximated from a set of sedimentological and  
338 geochemical proxies together with XRF logging data. The proportions of coarse (>63  $\mu\text{m}$ )  
339 and fine (<63  $\mu\text{m}$ ) material (in wt.%) were determined every 5 cm by weighing of the dried  
340 sediment before and after wet-sieving through a 63  $\mu\text{m}$  mesh. Magnetic susceptibility (not  
341 shown) was logged using a GEOTEK Multi-Sensor Core Logger in combination with a  
342 Bartington MS2C sensor loop each 1 cm on the unopened core segments directly after  
343 recovery (Dullo et al., 2009). Records of >63  $\mu\text{m}$  ~~did not match~~ showed only weak  
344 relationships with magnetic susceptibility records ( $R^2 < 0.13$ ), which ~~showed~~ were  
345 characterized by only low values (<15 SI units). Hence, magnetizable minerals are most  
346 probably mainly bound to the fine fractions.

347 Relative amounts of siliciclastics (%Siliciclastics) were calculated by considering the bulk  
348 sediment to be composed of siliciclastics,  $\text{CaCO}_3$ , TOC, and biogenic opal. TN concentrations  
349 were generally <0.3 wt.% and not included in the calculation:

$$350 \quad \% \text{Siliciclastics} = 100\% - (\text{CaCO}_3\% + \text{TOC}\% + \text{Opal}\%) \quad (2)$$

351 Respective accumulation rates ( $AR_{\text{Siliciclastics}}$ ) were calculated by dividing %Siliciclastic by  
352 100 and subsequent multiplication with  $AR_{\text{Bulk}}$ . The accumulation rate of the biogenic  
353 components ( $AR_{\text{Biogenic}}$ ) was calculated by subtracting  $AR_{\text{Siliciclastics}}$  from  $AR_{\text{Bulk}}$ .

354 In a second approach, relative amounts of terrigenous matter (%Terrigen) were calculated by  
355 normalizing bulk sedimentary Al and Ti concentrations to their concentration in average  
356 continental crust (Al = 3117  $\mu\text{mol g}^{-1}$ , Ti = 112.8  $\mu\text{mol g}^{-1}$ ; Taylor and McLennan, 1995).  
357 Both normalizations resulted in a similar temporal evolution of the records, but Al-normalized  
358 results, which were on average 4-6% higher than Ti-normalized results, better compared to  
359 the records of %Siliciclastics.

### 360 **3.4.2 Lithogenous elements**

361 The geochemistry of lithogenous elements can be used to approximate continental input (e.g.,  
362 Duce and Tindale, 1991; Bareille et al., 1994), dust-supply (e.g., Boyle, 1983; Calvert and  
363 Fortugne, 2001), terrestrial runoff (e.g., Schmitz, 1987; Jansen et al., 1998), and mineralogical  
364 variations (e.g., Schneider et al., 1997; Yarincik et al., 2000). As described above,  
365 concentrations of Al, Ti, Fe, and K were determined via ~~We used discrete~~ XRF bulk analyses.  
366 The elements of elements Al, Ti, Fe, and K and their respective ratios were used to identify  
367 sources of terrigenous matter and to reconstruct variations in terrigenous fluxes. In cores

368 | 85KL and 101KL XRF logging data of K/Ti log-ratios correlated well with ~~atomic-molar~~  
369 | K/Ti ratios ( $R^2 > 0.64$ ) and are shown for comparison.

370

## 371 | **4. Results and discussion**

### 372 | **4.1 Marine productivity**

#### 373 | **4.1.1 Proxy data**

374 | ~~Our Productivity proxies records for export production~~ show a similar temporal evolution in  
375 | all cores, ~~but increasing p~~Proxy concentrations ~~increase~~ towards the southernmost site,  
376 | ~~whereas the ranges of  $AR_{Biogenic}$  are comparable and low for all sites ( $< 3 \text{ g cm}^{-2} \text{ kyr}^{-1}$ ; Fig. 4).~~

377 | Results for TOC, opal,  $\text{CaCO}_3$ , as well as their approximating logging data are shown in Fig.

378 | 5. In general, ~~marine productivity concentrations and their approximating XRF data~~ remained  
379 | low during cold ~~intervals (stages-MIS 6, 5.4, 5.2, 4 to, and 2)~~, but high during warm intervals  
380 | (~~stages-MIS 5.5, 5.3, 5.1, and 1~~), with maximum values recorded during interglacials in core  
381 | 77KL. Core 101KL exhibits lowest proxy concentrations and amplitude variations (Tab. 2).

382 | Overall concentrations hardly exceed  $\sim 1$  wt.% for TOC,  $\sim 3$  wt.% for opal, and  $\sim 2$  wt.% for  
383 |  $\text{CaCO}_3$ . ~~Stages-MIS 5.3 and 5.1~~, as well as interstadials are characterized by  $\sim 1$  to 3-times  
384 | higher values at most. Notably, cores 85KL and 101KL recorded interstadial-like events  
385 | during ~~stage-MIS 6~~ (at  $\sim 173$  ka BP, 164 ka BP, 148 ka BP, 137 ka BP, and 133 ka BP),  
386 | characterized by increased proxy concentrations or their approximating XRF data. Deglacial  
387 | and interglacial maxima in TOC, opal, and  $\text{CaCO}_3$  reach values of  $\sim 2$  wt.%,  $\sim 50$  wt.%, and  
388 |  $\sim 30$  wt.%, respectively. Maxima recorded during Termination I reflect the warm phases of the  
389 | Bølling-Allerød (B/A; 14.7-12.9 ka BP, Blockley et al., 2012) and Preboreal (PB;  $\sim 11.7$ -11.0  
390 | ka BP), whereas deglacial minima are considered to correspond to the Heinrich Stadial 1  
391 | (~~HS1~~; 18.0-14.7 ka BP, Sarnthein et al., 2001) and Younger Dryas cold phases (YD; 12.9-  
392 | 11.7 ka BP, Blockley et al., 2012).

393 | During Termination I, TOC appears to lead the deglacial increase of the other productivity  
394 | proxies by  $\sim 2$  kyr ~~at our sites~~, which is in agreement with ~~previous results from the~~  
395 | ~~wholeocean~~ Bering Sea ~~realm studies~~ (Gorbarenko, 1996; Okazaki et al., 2005; Kim et al.,  
396 | 2011). Although records of TOC and XRF count rates of Br correspond well in our cores  
397 | (Fig. 5), Br does not follow this deglacial TOC-increase, suggesting a changing source of  
398 | TOC. In contrast to TOC and  $\text{CaCO}_3$ , we observed only minor increases in opal during the

399 B/A, but a subsequent gradual increase into the Holocene. These results from the western  
400 Bering Sea are comparable to opal records from the northern slope (Itaki et al., 2009; Khim et  
401 al., 2010; Kim et al., 2011). Despite showing a similar temporal evolution, opal records from  
402 Bowers Ridge (Okada et al., 2005; Okazaki et al., 2005; Brunelle et al., 2007, 2010), Umnak  
403 Plateau (Okada et al., 2005; Okazaki et al., 2005), and the southern Okhotsk Sea (Gorbarenko,  
404 1996; Gorbarenko et al., 2002a, 2002b; Narita et al., 2002; Brunelle et al., 2010) have 1.5 to  
405 3-times higher values. ~~This further indicates decreasing, diatom-dominated marine~~  
406 ~~productivity towards the northern Bering Sea.~~

407 CaCO<sub>3</sub> concentrations at our sites are generally low and related to the abundance of  
408 foraminifera and nannoplanktonic remains (coccoliths). High XRF Ca/Ti log-ratios during  
409 ~~stage-MIS 5.5 originate from~~ are the result of decreased XRF counts of Ti and not ~~offrom~~  
410 increased Ca counts. Short-lived increases of up to ~3 wt.% were recorded during MIS 6,  
411 interstadials, and Termination I ~~stage-6~~ (Fig. 5). Similar observations, especially for  
412 Termination I, were ~~previously also~~ reported for Bering Sea cores from the northern slope,  
413 Bowers Ridge, and Umnak Plateau (Cook et al., 2005; Okazaki et al., 2005; Brunelle et al.,  
414 2007, 2010; Itaki et al., 2009; Khim et al., 2010; Kim et al., 2011). At ODP Site 882 in the N  
415 Pacific interglacial maxima in CaCO<sub>3</sub> are accompanied by maxima in Ba<sub>bio</sub> (Jaccard et al.,  
416 2005). Since enhanced preservation of CaCO<sub>3</sub> is explained by a release of deep sequestered  
417 CO<sub>2</sub> from the deep ocean basin (Broecker and Peng, 1987; Marchitto et al., 2005), these  
418 CaCO<sub>3</sub> maxima were suggested to be the result of a higher bottom water calcite saturation  
419 state in response to the weakening of the N Pacific halocline (Jaccard et al., 2005). Deglacial  
420 maxima of CaCO<sub>3</sub> in Bering Sea sediments were also explained by denitrification on  
421 continental shelves, which might have resulted in an increase in alkalinity and, thus, in  
422 enhanced carbonate preservation (Chen, 2002; Okazaki et al., 2005). Today, the calcite  
423 saturation horizon in the Bering Sea is reported to lie above 500 m water depth (Feely et al.,  
424 2002) and at our sites lies above 200 m water depth (Riethdorf et al., ~~in review~~2013).  
425 Accordingly, we consider CaCO<sub>3</sub> maxima in our cores to mainly reflect a higher bottom water  
426 calcite saturation state, but enhanced biological CaCO<sub>3</sub> production can not be ruled out.

#### 427 **4.1.2 Organic carbon source**

428 Average concentrations of bulk sedimentary TN varied at ~0.1 wt.%. Hence, sediments from  
429 Shirshov Ridge contain a considerable amount of TIN, which results in [C/N]a ratios that are

430 ~~by up to 4 units higher than (uncorrected) C/N ratios (Fig. 6A).~~ [C/N]<sub>a</sub> ratios in our cores  
431 mainly vary between 10 and 15 (Fig. 6A, Tab. 2), indicating that TOC input contains ~~mainly~~  
432 ~~marine, but~~ considerable amounts of terrestrial organic material. ~~These values compare to~~  
433 ~~those found at the northern slope (Khim et al., 2010) and in the central Okhotsk Sea~~  
434 ~~(Nürnberg and Tiedemann, 2004). For the eastern and southern part of the Aleutian Basin~~  
435 ~~(Nakatsuka et al., 1995) and for the southern Okhotsk Sea (Ternois et al., 2001) lower C/N~~  
436 ~~ratios of 6-9 were reported. Strongest [C/N]<sub>a</sub> variability is observed at Site 77KL. All our~~  
437 ~~sites records~~ show a rise in [C/N]<sub>a</sub> ratios during Termination I, ~~indicating enhanced supply of~~  
438 ~~terrestrial matter. Since average concentrations of TN varied at ~0.1 wt.%, sediments from~~  
439 ~~Shirshov Ridge contain a considerable amount of TIN. Consequently, [C/N]<sub>a</sub> ratios are by up~~  
440 ~~to 4 units higher than uncorrected ratios (Fig. 6A). Lower C/N ratios of 6-9 were reported for~~  
441 ~~the eastern and southern part of the Aleutian Basin (Nakatsuka et al., 1995) and the southern~~  
442 ~~Okhotsk Sea (Ternois et al., 2001). Our ratios are closer to those found at the northern slope~~  
443 ~~(Khim et al., 2010) and the central Okhotsk Sea (Nürnberg and Tiedemann, 2004).~~ At Site  
444 77KL, the deglacial increase in [C/N]<sub>a</sub> ratios starts at ~17 ka BP, with maximum values  
445 during the YD, and a subsequent decrease into the Holocene. The same deglacial evolution ~~is~~  
446 was observed at the northern slope (Khim et al., 2010) and in the southern Okhotsk Sea  
447 (Ternois et al., 2001; Seki et al., 2003). It was related to the discharge of terrestrial material  
448 from the flooded shelf due to sea-level rise. In contrast, cores from the eastern and southern  
449 Bering Sea show a gradual decrease of C/N ratios since the last glacial maximum (LGM)  
450 (Nakatsuka et al., 1995).

#### 451 **4.1.3 Ba<sub>bio</sub> and export production**

452 ~~Our r~~Records of Ba<sub>bio</sub> are shown in Fig. 7 and overall match the TOC and opal records, which  
453 argues against a preservation effect due to sulfate reduction and associated barite dissolution.  
454 Accordingly, we consider changes in Ba<sub>bio</sub> concentrations to mainly reflect variations in Ba<sub>bio</sub>  
455 accumulation. A potential source of error in the calculation of Ba<sub>bio</sub> comes from estimating  
456 the aluminosilicate contribution of Ba via Al. Ba/Al ratios range between 5-10 mg g<sup>-1</sup> in  
457 crustal rocks (Taylor, 1964; Rösler and Lange, 1972) with a crustal average of 7.5 mg g<sup>-1</sup>  
458 (Dymond et al., 1992). We estimated the regional detrital Ba/Al ratio from surface sediment  
459 samples following Klump et al. (2000), which resulted in a value of 7 mg g<sup>-1</sup> (unpublished  
460 data). This value is close to the global average of pelitic rocks of 6.5 mg g<sup>-1</sup> (Wedepohl,  
461 1971), which was used for reconstructing Ba<sub>bio</sub> in the central Okhotsk Sea (Nürnberg and

462 Tiedemann, 2004).  $Ba_{bio}$  variability is low during most of the time covered by the cores, with  
463 average concentrations increasing from Site 101KL (~300 ppm), via Site 85KL (~400 ppm),  
464 to Site 77KL (~500 ppm) (Fig. 7, Tab. 2). Significant increases only occurred at Site 77KL  
465 during ~~stage-MIS~~ 5.5 and the Holocene with concentrations of ~1000 ppm and ~1700 ppm,  
466 respectively. Also at Site 77KL, XRF Ba/Al log-ratios covary with  $Ba_{bio}$  concentrations (not  
467 shown;  $R^2 = 0.74$ ), thereby ~~showing-revealing~~ minor increases during ~~stages-MIS~~ 5.3, 5.1, and  
468 ~~short-lived maxima~~ during interstadials. A similar range and variability as found for core  
469 77KL was observed at Bowers Ridge (Brunelle et al., 2007), ODP Site 882 (Jaccard et al.,  
470 2005), as well as ~~in~~ the sea-ice-free ~~Antarctic Zone of the~~ Southern Ocean (Nürnberg et al.,  
471 1997). Cores from the southern (Brunelle et al., 2010) and central Okhotsk Sea (Sato et al.,  
472 2002; Nürnberg and Tiedemann, 2004), as well as from the sea-ice-influenced ~~Antarctic Zone~~  
473 ~~of the~~ Southern Ocean (Nürnberg et al., 1997) exhibit generally lower glacial (~200-400 ppm)  
474 and peak interglacial (~800-1000 ppm) contents of  $Ba_{bio}$ , being more comparable to sites  
475 85KL and 101KL. Notably, Sato et al. (2002) and Brunelle et al. (2010) for the Okhotsk Sea  
476 report a deglacial lead in the rise of  $Ba_{bio}$  prior to that observed for opal contents, which we  
477 can not verify from our records.

478 We calculated  $P_{New}$ , i.e. primary production that results from allochthonous nutrient inputs to  
479 the euphotic zone, from  $Ba_{bio}$  following Nürnberg (1995) rather than from TOC, which at our  
480 sites is affected by terrestrial carbon (Fig. 7). ~~This approach was also followed by Nürnberg~~  
481 ~~and Tiedemann (2004) for a respective reconstruction in the Okhotsk Sea. Surface sediment~~  
482 ~~samples from Shirshov Ridge reveal a north-south gradient in modern  $P_{New}$  values within ~3-~~  
483 ~~54  $gC\ m^{-2}\ yr^{-1}$  translating into PP values of ~35-145  $gC\ m^{-2}\ yr^{-1}$  (estimated from  $P_{New}$ , see~~  
484 ~~Appendix B). Considering the uncertainties for  $AR_{Bulk}$  and  $Ba_{bio}$ , this result is in agreement~~  
485 ~~with Springer et al. (1996), who reported a modern PP range of 50-100  $gC\ m^{-2}\ yr^{-1}$  (average~~  
486 ~~of 61  $gC\ m^{-2}\ yr^{-1}$ ) for the 'oceanic domain' of the Bering Sea, in which our sites are located.~~  
487 ~~On the eastern Bering Sea shelf edge modern PP is reported to lie between 175-275  $gC\ m^{-2}\ yr^{-1}$~~   
488 ~~(Springer et al., 1996). Stabeno et al. (1999) reported modern PP values of >200  $gC\ m^{-2}\ yr^{-1}$~~   
489 ~~over the southeastern shelf and >800  $gC\ m^{-2}\ yr^{-1}$  north of St. Lawrence Island, whereas~~  
490 ~~Arzhanova et al. (1995) found >400  $gC\ m^{-2}\ yr^{-1}$  over the western shelf.~~  
491 ~~Our downcore results for Results- $P_{New}$  show that ~~export-primary~~ production was commonly~~  
492 ~~low (<50  $gC\ m^{-2}\ yr^{-1}$ ) at our sites during most of the last 180 kyr was commonly low (<50  $gC$~~   
493  ~~$m^{-2}\ yr^{-1}$ ) at all sites (Fig. 7, Tab. 2). Only core 77KL is characterized by two significant~~



494 maxima  $>150 \text{ gC m}^{-2} \text{ yr}^{-1}$  during Termination I. Although these maxima correspond to higher  
495 concentrations of  $\text{Ba}_{\text{bio}}$ , they ~~might be~~ likely overestimated due to the use of  $\text{AR}_{\text{Bulk}}$  in the  
496 calculation of  $\text{P}_{\text{New}}$ . Nevertheless, our downcore results are comparable to those reported for  
497 the central Okhotsk Sea (Nürnberg and Tiedemann, 2004) and the Antarctic continental  
498 margin (Gingele et al., 1999), albeit these show lower glacial values of  $<10 \text{ gC m}^{-2} \text{ yr}^{-1}$ . PP  
499 ~~was estimated from  $\text{P}_{\text{New}}$  and~~ mainly remained  $<150 \text{ gC m}^{-2} \text{ yr}^{-1}$  at our sites (not  
500 shown). Only ~~t~~ The deglacial  $\text{P}_{\text{New}}$  maxima in core 77KL would translate into significantly  
501 higher PP values ~~maxima~~ of  $\sim 250\text{-}300 \text{ gC m}^{-2} \text{ yr}^{-1}$  (Tab. 2). ~~Modern PP on the eastern Bering~~  
502 ~~Sea shelf edge is reported to lie between  $175\text{-}275 \text{ gC m}^{-2} \text{ yr}^{-1}$  (Springer et al., 1996). Stabeno~~  
503 ~~et al. (1999) reported modern PP values of  $>200 \text{ gC m}^{-2} \text{ yr}^{-1}$  over the southeastern shelf and~~  
504  ~~$>800 \text{ gC m}^{-2} \text{ yr}^{-1}$  north of St. Lawrence Island, whereas Arzhanova et al. (1995) found  $>400$~~   
505  ~~$\text{gC m}^{-2} \text{ yr}^{-1}$  over the western shelf. Consequently, at Site 77KL modern PP~~ most probably  
506 values remained permanently low at our sites and never reached values as observed today on  
507 the eastern Bering Sea shelf. have only been reached since Termination I, whereas PP  
508 remained permanently low at sites 85KL and 101KL.

## 509 4.2 Terrigenous matter supply

### 510 4.2.1 Proxy data

511 ~~Sediments from Shirshov Ridge are dominated by siliciclastic material.~~ Sediments from  
512 Shirshov Ridge contain on average  $>85\%$  siliciclastics and only  $<10\%$  coarse material (Tab.  
513 3), thereby tying terrigenous matter mainly to the fine fractions. —Light microscope  
514 observations reveal silt to fine sand-sized, angular-shaped quartz grains as major components,  
515 supplemented by minor portions of feldspar and mica. ~~Coarse ice-rafted debris (IRD) and~~  
516 ~~dropstones (1-2 cm in diameter) are~~ appear as well-rounded pebbles, but they are commonly  
517 rare although occurring over the entire length of the cores. ~~The Proxy~~ records approximating  
518 terrigenous matter supply exhibit a similar temporal evolution at ~~all our~~ sites (Fig. 8), but in  
519 contrast to the productivity proxies decreasing concentrations towards the southernmost site  
520 are observed. ~~In general~~ This and the observation that, proxy records reflecting marine  
521 productivity export production and terrigenous matter supply are ~~ant~~ negatively correlated is  
522 mainly attributed to sedimentary dilution by the biogenic components. However, changes in  
523  $\text{AR}_{\text{Bulk}}$  (and LSR) are obviously largely determined by changes in the accumulation of  
524 siliciclastic material ( $\text{AR}_{\text{Siliciclastics}}$ ), and therefore by changes in terrigenous matter supply

525 ~~(Fig. 4).~~ Accordingly, cold intervals (~~stages-MIS~~ 6, 5.4, 5.2, 4, ~~and to~~ 2) are characterized by  
526 high terrigenous matter supply, whereas warm intervals (~~stages-MIS~~ 5.5, 5.3, 5.1, and 1) show  
527 reduced proxy concentrations or ratios. Notably, a meridional gradient in  $AR_{\text{Siliciclastics}}$  is  
528 observed along the core transect with lower values and therefore potentially decreasing  
529 terrigenous matter supply toward the southernmost site (Fig. 4). The ~~M~~most pronounced  
530 minima in the proxy records are found during interglacials. In core 77KL higher amounts of  
531  $>63 \mu\text{m}$  and of  $\text{CaCO}_3$  concentrations (XRF Ca/Ti log-ratios) occur synchronously, indicating  
532 that changes in  $\text{CaCO}_3$  result from higher foraminiferal abundances. Although independently  
533 derived, covariation is also found between %Terrigen and %Siliciclastics, which are  
534 characterized by almost identical ranges (Fig. 8, Tab. 3).

535 ~~Sediments contain on average  $>85\%$  siliciclastics and only  $<10\%$  coarse material (Table 3),~~  
536 ~~thereby tying terrigenous matter mainly to the fine fractions.~~ K/Ti ratios show a range of 5-7  
537  $\text{mol mol}^{-1}$  in all cores (Fig. ~~ure~~ 8, Tab. ~~le~~ 3). We consider this ratio to be indicative of changes  
538 in the geochemical composition of the terrigenous matter itself. During ~~stage-MIS~~ 5.5 and the  
539 Holocene, %Siliciclastics are reduced to  $\sim 50\%$  at Site 77KL,  $\sim 60\%$  at Site 85KL, and  $\sim 70\%$   
540 at Site 101KL. At the same time, K/Ti ratios decrease to  $\sim 5 \text{ mol mol}^{-1}$ . Minor drops were  
541 recorded during ~~stages-MIS~~ 5.3 and 5.1 ( $\sim 15\%$  in ~~s~~Siliciclastics;  $\sim 0.5 \text{ mol mol}^{-1}$  in K/Ti),  
542 whereas K/Ti ratios increased by  $\sim 1 \text{ mol mol}^{-1}$  during ~~stage-MIS~~ 4 and subsequently  
543 decreased during ~~stage-MIS~~ 3. In core 85KL ~~stage-MIS~~ 6 is characterized by ~~pronounced~~  
544 short-lived maxima in XRF K/Ti log-ratios at  $\sim 173 \text{ ka BP}$  and  $\sim 163 \text{ ka BP}$ . This core and core  
545 101KL also reveal a minor peak in  $>63 \mu\text{m}$  found at  $\sim 133 \text{ ka BP}$ , which occurs  
546 simultaneously with minima in %Siliciclastics but with maxima in  $\text{CaCO}_3$  and TOC. Notably,  
547 highest amounts of  $>63 \mu\text{m}$  were recorded at sites 85KL and 101KL at the end of Termination  
548 II ( $\sim 127\text{-}125 \text{ ka BP}$ ) with maxima of  $\sim 30\%$  and  $\sim 60\%$ , respectively. These maxima are  
549 concurrent with high [C/N]a ratios and lead maxima in TOC and opal concentrations by  $\sim 3$   
550 kyr. During Termination I, the B/A ~~warm-phase~~ is characterized by reductions in  
551 %Siliciclastics and %Terrigen of up to  $\sim 25\%$  and of up to  $\sim 0.5 \text{ mol mol}^{-1}$  in K/Ti. Maxima in  
552  $>63 \mu\text{m}$  were recorded during both, the B/A and the PB. During HS1 ~~Pronounced~~-maxima in  
553 K/Ti are observed, and ~~during the H1 cold phase.~~ ~~D~~during the YD all proxies briefly return to  
554 glacial values, ~~which is~~ followed by a gradual decrease into the Holocene. The described  
555 proxy ranges and their temporal variability almost compare to those reported for the central

556 Okhotsk Sea (Nürnberg and Tiedemann, 2004), ~~which showed except that respective sediment~~  
557 ~~records showed even~~ lower interglacial minima in %Siliciclastics of ~35%.

558 In all cores ~~from Shirshov Ridge significant~~ linear ~~correlations~~ relationships between  
559 concentrations of lithogenous elements Al, Fe, and Ti were found (Fig. 7). This indicates that  
560 these elements originate from the same geochemical source and/or share the same transport  
561 mechanism. [Al] correlated with %Siliciclastics in cores 77KL ( $R^2 = 0.42$ ) and 85KL ( $R^2 =$   
562  $0.74$ ), but not in core 101KL ( $R^2 = 0.08$ ). We consider an influence of scavenging by organic  
563 material and/or bottom sediment resuspension on [Al] (Orians and Bruland, 1986; Nameroff  
564 et al., 2004) insignificant, which is supported by low interglacial concentrations and Al/Ti  
565 ratios that are close to crustal values. Records for [Al], [Fe], and [Ti] follow the same  
566 temporal evolution described for the terrigenous proxies with general high values during most  
567 of the last 180 kyr (~2600-2800  $\mu\text{mol g}^{-1}$  for [Al], ~700-900  $\mu\text{mol g}^{-1}$  for [Fe], ~90-100  $\mu\text{mol}$   
568  $\text{g}^{-1}$  for [Ti]) (Tab. 3). During stage-MIS 5.5 and the Holocene [Al], [Fe], and [Ti] decreased by  
569 up to ~800  $\mu\text{mol g}^{-1}$ , ~300  $\mu\text{mol g}^{-1}$ , and ~30  $\mu\text{mol g}^{-1}$ , respectively. Notably, from MIS 3 to 1  
570 ~~From stage 3 to stage 1,~~ [Fe] became slightly higher in core 77KL than in the other cores  
571 (Figure 7). ~~These results compare to he described those from the temporal evolution overall~~  
572 compares to that recorded in sediment cores from the central Okhotsk Sea (Sato et al., 2002)  
573 and the Antarctic Zone of the Southern Ocean (Latimer and Filippelli, 2001), except that-  
574 ~~However,~~ the respective studies reported on glacial [Al] and [Ti] that were by ~30% lower  
575 than those recorded at Shirshov Ridge. Moreover, these studies described very low interglacial  
576 values (~100  $\mu\text{mol g}^{-1}$  for [Al], ~100  $\mu\text{mol g}^{-1}$  for [Fe], ~10-20  $\mu\text{mol g}^{-1}$  for [Ti]) not found at  
577 our sites. This argues ~~for that thean~~ interglacial reduction in terrigenous fluxes at Shirshov  
578 Ridge was on the order of only ~30-40%.

#### 579 **4.2.2 Geochemical signature**

580 ~~Atomic-Molar~~ Al/Ti and Fe/Al ratios were used to characterize the geochemical signature of  
581 the sediments from Shirshov Ridge. In general, Al/Ti and Fe/Al ratios remained fairly  
582 constant during the last 180 kyr ~~and show with~~ similar ranges at all sites. Only at the end of  
583 both glacial terminations minor increases in Al/Ti and minor decreases in Fe/Al are found.  
584 Distinct glacial-interglacial differences are not observed, indicating that the source of the  
585 terrigenous matter or its underlying transport mechanism did not change. This is an  
586 interesting result, since records of %Siliciclastics, %Terrigen, and lithogenous element

587 concentrations are characterized by ~~significant-strong~~ variations on the glacial-interglacial  
588 level. Al/Ti ratios varied between 24-33 (mol mol<sup>-1</sup>), with short-lived increases (~3) at the end  
589 of ~~stage-MIS~~ 4, and ~~during~~ Terminations I and II. Average ~~down~~core Al/Ti values (~29.5±3;  
590 Tab. 4), as well as surface sediment values from Shirshov Ridge (29.4±4) and from the  
591 eastern Kamchatka continental margin (32.1±3) (unpublished data) ~~are—almost~~  
592 ~~identical~~compare well, which indicates ~~ing~~ that past and modern sources of terrigenous matter  
593 are identical. These values ~~compare-are close~~ to Al/Ti ratios reported for Paleozoic (~29) and  
594 Mesozoic/Cenozoic shales (~32) from the Russian Platform (Ronov and Migdisov, 1971), but  
595 also ~~compare~~ with average values for sediment and continental crust (~28; McLennan, 1995;  
596 Taylor and McLennan, 1995), river particulate and mud (~30; McLennan, 1995), pelagic clay  
597 (~32; McLennan, 1995), as well as the range reported for loess deposits (~26-31; Taylor et al.,  
598 1983; Pye, 1987; McLennan, 1995). Values are clearly lower than that of the North American  
599 shale composite (~38; Gromet et al., 1984), but higher than Al/Ti ratios of oceanic tholeiitic  
600 basalt (~17; Engel et al., 1965) and surface samples from St. George Basin, SE Bering Sea  
601 (~24; Gardner et al., 1980). Nürnberg and Tiedemann (2004) reported a different range for  
602 sediments from the central Okhotsk Sea (~24-45).

603 The ~~overall-variability-ofdowncore~~ Fe/Al ratios ~~was-varied~~ between 0.20-0.34 (mol mol<sup>-1</sup>)  
604 (Tab. 4). ~~This range is also found in surface sediment samples from Shirshov Ridge (0.22-~~  
605 ~~0.39; unpublished data), and it is~~This range is in agreement with ~~downcore~~ results from the  
606 central Okhotsk Sea (~~0.28±0.03; Nürnberg and Tiedemann, 2004).~~ ~~In contrast to Al/Ti, Fe/Al~~  
607 ~~ratios along the core transect become increasingly higher towards the southernmost site since~~  
608 ~~stage 3, with differences of up to ~0.06. A similar range (0.22-0.39) and meridional trend are~~  
609 ~~observed in surface sediment samples from Shirshov Ridge (unpublished data). At the end of~~  
610 ~~both glacial terminations short lived decreases (~0.04) are found.~~ Our Fe/Al ratios compare to  
611 those reported for the North American shale composite and average mud (~0.24; Gromet et  
612 al., 1984; McLennan, 1995), Mesozoic/Cenozoic (~0.26) and Paleozoic (~0.28) Russian  
613 Platform shales (Ronov and Migdisov, 1971), average values for river particulate (~0.25) and  
614 sediment (~0.27) (McLennan, 1995). Oceanic tholeiitic basalt (~0.28; Engel et al., 1965) and  
615 surface samples from St. George Basin (~0.28; Gardner et al., 1980) also apply to the overall  
616 range. The value for bulk continental crust is higher (~0.41; Taylor and McLennan, 1995),  
617 while loess deposits show a lower range between ~0.17-0.25 (Taylor et al., 1983; Pye, 1987;  
618 McLennan, 1995). From these results we conclude that sediments from Shirshov Ridge

619 represent a mixture of geochemical signatures from aeolian sediments (loess) and continental  
620 sources that are supposedly not influenced by North American shales. ~~The continental~~  
621 ~~influence might successively decrease with increasing distance from the coast along the core~~  
622 ~~transect.~~

### 623 4.2.3 Transport mechanism and source area

624 Possible mechanisms of terrigenous matter transport encompass aeolian and fluvial ~~and~~  
625 ~~aeolian~~ supply, as well as sea-ice rafting. ~~Major rivers entering the Bering Sea are the Yukon~~  
626 ~~and Anadyr rivers, which are situated at rather long distances from Shirshov Ridge (cf. Fig.~~  
627 ~~1). Given that further minor rivers in the surrounding of the Bering Sea are rare, we consider~~  
628 ~~particulate material transport by rivers insignificant.~~ Wind transported aerosols present in N  
629 Pacific sediments are restricted to the vicinity of their respective source area, which in our  
630 case are most likely situated in NE Siberia. Model results of global desert dust deposition  
631 show fluxes of 0.5-1.0 g m<sup>-2</sup> yr<sup>-1</sup> for the Bering Sea (Mahowald et al., 2005), which implies  
632 that today aeolian input is negligible. This ~~might, of course, seems to~~ have been different  
633 during past cold intervals as indicated by our higher lithogenous element concentrations and  
634 generally enhanced glacial dust fluxes (e.g., Ruth et al., 2003). Major rivers entering the  
635 Bering Sea are the Yukon and Anadyr rivers, which are situated at rather long distances from  
636 Shirshov Ridge (cf. Fig. 1). Today the Yukon River provides ~63% of the total sediment load  
637 to the Bering Sea and it is suggested that glacial sediments from the Meiji Drift, NW Pacific,  
638 contain a larger fraction of terrigenous material delivered from Yukon-Bering Sea sources  
639 (VanLaningham et al., 2009). Surface sediments from the eastern Bering Sea shelf consist of  
640 Yukon River-derived detrital material (Asahara et al., 2012; Nagashima et al., 2012). Yet it  
641 remains unclear how the terrigenous material is transported from the eastern Bering Sea shelf  
642 to the Meiji Drift in the NW Pacific. ~~Accordingly, w~~We suggest that sea-ice ~~rafting is and has~~  
643 ~~been the prevailing~~plays a considerable role in transporting ~~agent of~~ terrigenous matter ~~at our~~  
644 ~~sites~~toward Shirshov Ridge, ~~although we can not exclude a significant contribution from~~  
645 ~~suspension load carried by the BSC.~~ For the Arctic, Nürnberg et al. (1994) reported on  
646 sediments entrained in sea-ice to be generally fine grained (clayey silts, silty clays) and  
647 mainly composed of quartz, clay minerals and diatom flora. Sediments from the central  
648 Okhotsk Sea, which are also assumed to originate from sea-ice rafting are described as mainly  
649 clay and silt-sized siliciclastics (>65% siliciclastics) featuring dropstones (3-5 cm), and  
650 various lithogenic components (mainly quartz, rock fragments, mica, and dark minerals), with

651 regionally different ice-rafted debris (IRD) composition (Nürnberg and Tiedemann, 2004;  
652 Nürnberg et al., 2011). This sedimentary composition is similar to that found in sediments  
653 recovered from Shirshov Ridge, although IRD records are needed for verification, ~~which is~~  
654 ~~comparable to that of our sediment cores~~. Since dropstones are rather uncommon in our cores,  
655 which, if present, appear as ~~well-well~~-rounded pebbles, and due to the dominance of silt- and  
656 clay-sized terrigenous material we ~~favor-suggest~~ a beach deposit origin and tidal pumping,  
657 suspension freezing and beach-ice formation to be responsible for the entrainment of  
658 terrigenous matter into newly formed sea-ice.

659 The influence of ice in the Bering Sea realm during glacials, either in the form of icebergs or  
660 sea-ice is still debated. Kaufman et al. (1996) suggested that the most recent major ice  
661 advance in SW Alaska occurred between ~90-75 ka BP. For MIS 3 Bigg et al. (2008)  
662 proposed a Kamchatka-Koryak Ice Sheet with marine-terminating ice margins. Our cores lack  
663 clear evidence for iceberg discharge at ~40 ka BP (Bigg et al., 2008), therefore not supporting  
664 their suggested iceberg migration paths. For the LGM, the presence of the Beringian Ice Sheet  
665 (e.g., Grosswald and Hughes, 2002) has been disproved (e.g., Brigham-Grette et al., 2001,  
666 2003; Karhu et al., 2001), and Kamchatkan climate seems to have been too arid for the  
667 development of large continental ice sheets during that time (Barr and Clark, 2011). We  
668 therefore favor sea-ice over iceberg transport ~~due to the dominance of silt- and clay sized~~  
669 ~~terrigenous material, the absence of large dropstones, low variability in >63 µm, and the fact,~~  
670 ~~that today no marine-terminating glaciers exist in the Bering Sea realm. Kaufman et al. (1996)~~  
671 ~~suggested that the most recent major ice advance in SW Alaska occurred between ~90-75 ka~~  
672 ~~BP. For stage 3 the proposed Kamchatka-Koryak Ice Sheet with marine terminating ice~~  
673 ~~margins (Bigg et al., 2008) was disproved (Nürnberg et al., 2011). Our cores lack evidence for~~  
674 ~~iceberg discharge at ~40 ka BP (Bigg et al., 2008), therefore not supporting the suggested~~  
675 ~~iceberg migration paths. For the LGM, the presence of the Beringian Ice Sheet (e.g.~~  
676 ~~Grosswald and Hughes, 2002) has also been disproved (e.g. Brigham-Grette et al., 2001,~~  
677 ~~2003; Karhu et al., 2001), and Kamchatkan climate seems to have been too arid for the~~  
678 ~~development of large continental ice sheets during that time (Barr and Clark, 2011).~~

679 Lisitzin (2002) identified mineralogical provinces for western Bering Sea surface sediments  
680 together with their possible migration paths and proposed that coarse silts and the larger  
681 grain-size fractions (pebbles, gravel, boulder) are controlled by sea-ice, sharing the same  
682 provinces and transport pathways. Accordingly, the Koryak Coast, Olyutorskii Bay, and

683 northern Kamchatka provinces (cf. Fig. 1) ~~likely~~ are potential source areas for the ice-rafted  
684 material ~~in our sediments~~. Anadyr Bay, where modern seasonal sea-ice formation begins  
685 during fall, is as well taken into consideration. The K/Ti ratio is assumed to reflect temporal  
686 changes in sediment sources weathered from acidic (more K) and basaltic (more Ti) source  
687 rocks (Richter et al., 2006). Relatively increased K/Ti ratios are observed at times of  
688 enhanced terrigenous matter supply. If sea-ice rafting is the main driver of these changes, the  
689 geochemical source of the terrigenous matter (and consequently the ice-rafted material) would  
690 be characterized as being relatively increased in K. Of the considered provinces only Anadyr  
691 Bay is reported to contain acidic index rocks (Lisitzin, 2002), although geochemical data ~~do~~  
692 ~~not exist~~ to clearly identify it as the proposed source area of Shirshov Ridge sediments do not  
693 exist. However, ~~that this assumption~~ the source area supposedly lies in the vicinity of Anadyr  
694 Bay is supported by the finding that interannual variability in Bering Sea ice cover is  
695 controlled by wind-driven ice mass advection, which is clearly ~~is~~ southwestward from ~~Anadyr~~  
696 ~~Bay there~~ (Zhang et al., 2010). However, although stronger ocean/bottom currents can not be  
697 excluded as potential transport mechanism for the detrital fractions the available data seem to  
698 congruently argue for a source area that is located on the eastern Bering Sea shelf  
699 (VanLaningham et al., 2009; Asahara et al., 2012; Nagashima et al., 2012).

## 700 **4.3 Environmental changes during the last 180 kyr**

### 701 **4.3.1 Glacial situation**

702 Cold intervals of the last 180 kyr seem to have been subject to strongly reduced, but  
703 maintained ~~primary export production~~ ~~productivity~~ at our sites. At the same time, our records  
704 indicate high input of terrigenous matter, which is in agreement with records from the  
705 Okhotsk Sea (Nürnberg and Tiedemann, 2004; Nürnberg et al., 2011). Although regionally  
706 different, low glacial export production characterizes ~~ds~~ the whole N Pacific during the last 800  
707 kyr (for a review see Kienast et al., 2004). Nürnberg et al. (2011) argued for extreme glacial  
708 ice conditions in the Okhotsk Sea during late stage-MIS 6 with a potentially perennial ice  
709 coverage. From our results, we can not unambiguously argue for similar ~~infer that~~ conditions  
710 during late stage-MIS 6 ~~were significantly different from those during later cold intervals,~~  
711 although the coarse fraction maxima found during Termination II might indicate the sudden  
712 melt of an expanded sea-ice cover that was perennial during the final phase of MIS 6. Glacial  
713 conditions in the Okhotsk Sea are supposed to be similar to the modern winter situation of a

714 strong Siberian High and a weak Aleutian Low, thereby resulting in strong offshore, northerly  
715 winds (Nürnberg and Tiedemann, 2004; Nürnberg et al., 2011). This situation might as well  
716 apply to the Bering Sea and would have resulted in enhanced sea-ice formation during a  
717 generally colder climate, thereby explaining the higher LSR and terrigenous inputs. At  
718 Bowers Ridge, at least for ~~stages-MIS~~ 3 and 2, colder subsurface temperatures are supported  
719 by low total numbers of planktonic foraminifera, dominated by polar species  
720 *Neogloboquadrina pachyderma* (sin.) and reduced/absent numbers of subpolar species  
721 *Globigerina bulloides* (Gorbarenko et al., 2005). A spatially extended sea-ice coverage  
722 fostered by a shortened summer season might have resulted in enhanced upper-ocean  
723 stratification and reduced nutrient supply to the ~~surface-ocean~~euphotic zone. Since primary  
724 productivity is limited by temperature and nutrient availability, the prolonged sea-ice season  
725 during colder intervals in hand with stronger stratification would have consequently led to the  
726 reduction in ~~marine-export~~ productivity observed at our sites. This should be reflected by  
727 ~~stronger-more efficient nutrient-nitrate~~ utilization, and indeed, bulk sediment and diatom-  
728 bound nitrogen isotope ratios ( $\delta^{15}\text{N}$ ) recorded at Bowers Ridge (Brunelle et al., 2007) show  
729 higher glacial than interglacial values (Fig. 9), thereby confirming earlier assumptions of  
730 ~~suppressed-enhanced vertical-mixing~~stratification in the glacial Bering Sea (Nakatsuka et al.,  
731 1995; Brunelle et al., 2007; Kim et al., 2011).

732 ~~In HNLC regions primary production is limited by the availability of Fe (Fe fertilization).  
733 During glacials increasing primary production was observed in the HNLC region of the  
734 equatorial Pacific, implying a link to Fe delivery (Murray et al., 2012). Although the western  
735 Bering Sea basin is considered as HNLC (Tyrrell et al., 2005), we found high glacial [Fe]  
736 values despite low marine productivity. Accordingly, we neglect Fe fertilization as the  
737 limiting factor of primary production on glacial-interglacial timescales in the western Bering  
738 Sea. Support for an extended sea-ice coverage in the Bering Sea during glacial periods comes  
739 from diatom and radiolarian assemblages (Katsuki and Takahashi, 2005; Tanaka and  
740 Takahashi, 2005).~~

741 It has been speculated, that the net-inflow of Alaskan Stream waters into the Bering Sea was  
742 reduced at times when the Bering Strait and/or other Aleutian passes, like Unimak Pass, were  
743 closed due to lower glacial sea-level, thereby affecting Beringian climate (Pushkar et al.,  
744 1999; Tanaka and Takahashi, 2005). During ~~stage-MIS~~ 2, a strengthened Subarctic Front  
745 could have additionally led to a reduced inflow of warmer and nutrient-enriched Pacific



746 surface waters (Gorbarenko et al., 2005). In consequence, nutrient supply to the Bering Sea  
747 should have been further reduced and have resulted in stronger ~~nitrate~~~~nutrient~~ utilization. The  
748 relative sea-level (RSL) reconstruction of Waelbroeck et al. (2002) implies that the Bering  
749 Strait was closed during ~~stage~~-MIS 6, as well as in between ~~stages~~-MIS 4 and 2 (Fig. 9), while  
750 its last major re-opening occurred at 12-11 ka BP (Keigwin et al., 2006). RSL changes in the  
751 Bering Strait are predominantly controlled by eustatic changes and suggested to considerably  
752 influence deep convection in the N Atlantic (Hu et al., 2010). At Bowers Ridge-  $\delta^{15}\text{N}$  values  
753 are highest during ~~stages~~-MIS 3 and 2 (Fig. 9), supporting an influence of RSL on upper-  
754 ocean stratification and, hence, nitrate utilization in the Bering Sea. A closed Bering Strait has  
755 previously been suggested to have resulted in a low-salinity surface layer that reinforced  
756 vertical stratification in the Bering Sea (Sancetta, 1983).

757 The low glacial  $\text{CaCO}_3$  concentrations and abundances of oxic benthic foraminifera species  
758 point towards the presence of corrosive bottom waters as a result of organic matter  
759 degradation under oxic bottom water conditions (Kim et al., 2011). This implies that either  
760  $\text{O}_2$ -rich intermediate water masses were formed in the Bering Sea, or flew in from the Pacific  
761 side. Sea-ice formation in the Bering Sea due to brine rejection results in denser,  $\text{O}_2$ -rich  
762 surface waters (e.g., Niebauer et al., 1999), and thus might have maintained the production  
763 and ventilation of intermediate water. Rella et al. (2012) reported on benthic  $\delta^{18}\text{O}$  excursions  
764 in sediments from the northern slope, which implies that the Bering Sea was a source of  
765 intermediate water during past stadial episodes, which is supported by microfossil  
766 assemblages (Ohkushi et al., 2003). However, as the modern origin of NPIW lies in the  
767 Okhotsk Sea (Yasuda, 1997) and during glacial stages a closed Bering Strait prevented inflow  
768 of surface waters from the Arctic Ocean (Takahashi, 1998, 1999), inflow from the N Pacific  
769 can not be ruled out.

#### 770 **4.3.2 Deglacial situation**

771 During Termination I high ~~marine productivity~~~~export production~~ but low terrigenous input is  
772 observed during the B/A and PB warm phases, whereas the opposite situation occurred during  
773 the HS1 and YD cold phases. Remarkably, SST records from our sites mirror the deglacial  
774 SST evolution recorded in the N Atlantic, supporting quasi-synchrony of Northern  
775 Hemisphere climate changes (Max et al., 2012). Our records suggest that ~~the~~ early deglacial  
776 phase was characterized by~~starts with increasing [C/N]a ratios, LSR, and TOC just after the~~

777 ~~LGM at ~17 ka BP. This is explained by~~ higher input of terrestrial-derived organic matter  
778 ~~derived from flooded shelf areas in the course of sea-level rises and was~~ previously  
779 suggested for the Okhotsk and Bering seas (Ternois et al., 2001; Seki et al., 2003; Khim et al.,  
780 2010). ~~Alternatively, organic matter preservation became better due to poorly-oxygenated~~  
781 ~~conditions at the sediment-water interface.~~ Notably, at the northern slope similar changes  
782 were reported to have occurred ~2 kyr earlier (Khim et al., 2010). This timelag for increased  
783 ~~terrestrial organic~~ carbon input ~~might indicatesuggests~~ that ~~both locationsthe northern~~  
784 ~~slope and Shirshov Ridge~~ were supplied from different sources ~~or by different mechanisms;~~  
785 ~~which for the northern slope might be related to terrestrial runoff from Yukon River~~  
786 ~~denitrifying the eastern continental shelf.~~

787 Our records indicate enhanced sea-ice ~~rafting-influence~~ during HS1 and the YD, which for  
788 our sites is supported by ~~the preseneequalitative reconstructions~~ of the sea-ice-related IP<sub>25</sub>  
789 biomarker (Max et al., 2012) and by increasing abundances of the sea-ice-related diatom  
790 genus *Nitzschia* at Umnak Plateau (Cook et al., 2005). Like during previous cold intervals,  
791 ~~primary productionmarine productivity~~ was restricted by lowered temperature. A sudden  
792 decrease in bulk sedimentary and diatom-bound  $\delta^{15}\text{N}$  (Fig. 9) point to decreased nitrate  
793 utilization (Brunelle et al., 2007, 2010). ~~However, this drop in  $\delta^{15}\text{N}$  is not fully understood~~  
794 ~~since higher nutrient supply due to stronger vertical mixing should have resulted in enhanced~~  
795 ~~export production, which is not observed. as a result of fresh nutrient supply due to stonger~~  
796 ~~vertical mixing. Support for intensified mixing and/or~~ ~~Deglacial changes in~~  
797 ~~ventilation/overturning-overturning in the N Pacific realm during H1 comes have been inferred~~  
798 from ~~reduced~~-ventilation ages ~~in the N Pacific realm~~ (Adkins and Boyle, 1997; Ahagon et al.,  
799 2003; Ohkushi et al., 2004; Galbraith et al., 2007; Sarnthein et al., 2007; Sagawa and Ikehara,  
800 2008; Okazaki et al., 2010; Lund et al., 2011; Jaccard and Galbraith, 2013), ~~benthic~~  
801  ~~$\delta^{18}\text{O}$  foraminiferal isotope data (e.g., Matsumoto et al., 2002; Rella et al., 2012), as well as~~  
802 modeling studies (e.g., Okazaki et al., 2010; Chikamoto et al., 2012; Menviel et al., 2012),  
803 ~~and was related to the potential disappearance of the halocline.~~ ~~Notably, enhanced ventilation~~  
804 ~~in the N Pacific during HS1 seems to have been restricted to ~1400-2400 m depth (Jaccard~~  
805 ~~and Galbraith, 2013), whereas the deep abyssal Pacific was better ventilated during the~~  
806 ~~subsequent B/A (Galbraith et al., 2007). Hence, it was suggested that NPIW formation was~~  
807 ~~more enhanced, that it reached deeper, and that its source might have shifted to the Bering Sea~~

808 during HS1 and during other cold periods (e.g., Matsumoto et al., 2002; Ohkushi et al., 2003;  
809 Rella et al., 2012; Jaccard and Galbraith, 2013).

810 ~~Subsequent to H1, increasing insolation and sea-level rise amplified the surface ocean~~  
811 ~~warming, which might have led to more dynamic ice conditions, northward propagating ice~~  
812 ~~margins, and a prolonged sea-ice-free summer season. Indeed, rising SST and beginning~~  
813 ~~coccolithophorid production are inferred from first detectable concentrations of alkenones~~  
814 ~~(Caissie et al., 2010; Max et al., 2012).~~

815 For tThe onset of the B/A, and to a lesser degree also the PB phase, ~~is characterized by~~  
816 ~~increasing values in all productivity proxies, while LSR and most proxies for terrigenous~~  
817 ~~supply decline. Records of >63  $\mu\text{m}$  instead show a peak, which we attribute to~~our records  
818 imply enhanced marine productivity and the sudden release of IRD from melting sea-ice.  
819 Similar observations regarding changes in marine productivity have previously been reported  
820 for the whole Bering Sea realm (Gorbarenko, 1996; Cook et al., 2005; Gorbarenko et al.,  
821 2005; Okazaki et al., 2005; Khim et al., 2010) and other parts of the N Pacific (Keigwin and  
822 Jones, 1990; Keigwin et al., 1992; Gorbarenko, 1996; Keigwin, 1998; Crusius et al., 2004;  
823 McKay et al., 2004; Okazaki et al., 2005; Gebhardt et al., 2008). Increasing insolation should  
824 have amplified the surface ocean warming and led to more dynamic ice conditions, northward  
825 propagating ice margins, and a prolonged sea-ice-free summer season. Indeed, recent  
826 alkenone- and Mg/Ca-based studies indicate rising SST, strengthened thermal mixed layer  
827 stratification (stronger seasonal contrasts), and the onset of coccolithophorid production  
828 during the B/A (Caissie et al., 2010; Max et al., 2012; Riethdorf et al., 2013). ~~Rising summer~~  
829 ~~SSTs (stronger seasonal contrasts) amplified sea-ice melting and resulted in strengthened~~  
830 ~~mixed layer stratification (Riethdorf et al., in review).~~ Enhanced surface freshening due to  
831 melting sea-ice is supported by higher abundances of radiolarian species *Rhizoplegma boreale*  
832 (Kim et al., 2011), as well as brackish diatom species *Paralia sulcata* (Gorbarenko et al.,  
833 2005). ~~Evidence for reduced ventilation with respect to H1 comes from higher ventilation~~  
834 ~~ages found in the N Pacific (Adkins and Boyle, 1997; Ahagon et al., 2003; Ohkushi et al.,~~  
835 ~~2004; Sagawa and Ikehara, 2008; Okazaki et al., 2010).~~ A maximum in  $\delta^{15}\text{N}$  values (Fig. 9)  
836 implies increased nitrate utilization or even denitrification ~~of seawater nitrate in response to~~  
837 ~~stronger stratification~~ (Brunelle et al., 2007, 2010; Khim et al., 2010). It might further be  
838 speculated, that the increase in marine productivity associated with reduced sea-ice formation  
839 resulted in organic matter supply exceeding its degradation at the seafloor (Kim et al., 2011).

840 In consequence, bottom water conditions might have become dysoxic or anoxic, impeding  
841 benthonic life and favouring laminae formation. This notion ~~is-would be~~ in agreement with  
842 the formation of dysoxic or laminated sediments observed at oxygen minimum zone (OMZ)  
843 depths in the N Pacific and Bering Sea during the B/A and PB (van Geen et al., 2003; Cook,  
844 2006, and references therein) and most probably was related to an intensification of the OMZ  
845 (Zheng et al., 2000). At the same time the respired carbon pool was obviously removed from  
846 the deep basin, which resulted in enhanced carbonate preservation due to a deepened  
847 lysocline, and to an increase in atmospheric CO<sub>2</sub> (e.g. Galbraith et al., 2007).

848 Our records show that at sites 85KL and 101KL the deglacial development during  
849 Termination II does not resemble that of Termination I. Most notably, extremely high  
850 amounts of coarse material are ~~recorded-found~~ at the end of Termination II showing values  
851 that are not reached, which is not observed previously or later at any site. At the same time  
852 minor excursions towards lower Fe/Al but higher Al/Ti ratios were recorded, indicating a  
853 slightly different geochemical composition of the sediments. We attribute these results to the  
854 sudden release of IRD in response to strong melting of a potentially perennial ice coverage  
855 present during the final phase of MIS 6 in agreement with conditions proposed as suggested  
856 for the Okhotsk Sea (Nürnberg et al., 2011). Also, records of benthic δ<sup>18</sup>O do not follow the  
857 LR04 stack, which is indicative of a strong regional effect on the δ<sup>18</sup>O signal, e.g. for example  
858 by melting of continental ice sheets in the Bering Sea realm. This might, of course, also be the  
859 result of constraints in our age models during that timeframe.

### 860 **4.3.3 Interglacial situation**

861 In contrast to the situation during cold intervals, interglacials, as well as warm ~~stages-MIS~~ 5.3  
862 and 5.1 ~~are-were~~ characterized by increased marine productivity and decreased terrigenous  
863 matter supply. ~~Meridional gradients are observed along the core transect with reduced sea-ice~~  
864 ~~influence favouring marine productivity towards the southernmost site. Especially during~~  
865 ~~interglacials~~ Our results-records for Site 77KL better compare to those reported for Bowers  
866 Ridge, whereas records from sites 85KL and 101KL resemble ~~records-those~~ from the northern  
867 slope and the central Okhotsk Sea. Marine productivity as reflected by opal concentrations  
868 ~~was-seems to have been~~ higher during ~~stage-MIS~~ 5.5 than during the Holocene. Interglacial  
869 CaCO<sub>3</sub> concentrations remained at or close to glacial values implying a similar bottom water  
870 calcite saturation state with limited carbonate preservation. The interglacial i~~ncrease~~n area

871 | ~~in~~ marine productivity most probably resulted from warmer temperatures and reduced sea-  
872 | ice formation during a prolonged summer season (stronger seasonal contrasts). However, our  
873 | records imply a reduction of only ~30-40% in terrigenous matter supply. Overall, records of  
874 | XRF Si/Al log-ratios are in phase with mean summer insolation at 65°N (July-September;  
875 | calculated after Laskar ~~et al.~~, 2004; Fig. 9), showing maxima during the warm intervals (  
876 | stages-MIS 5.5, 5.3, 5.1, and 1). This implies a dominant insolation forcing for environmental  
877 | changes in the Bering Sea. At Bowers Ridge,  $\delta^{15}\text{N}$  values are lowest during interglacials  
878 | (Brunelle et al., 2007, 2010) and they also remain low during most of ~~stage-MIS 5~~ (Fig. 9).  
879 | ~~This,~~ indicative of reduced nitrate utilization as a consequence of enhanced vertical mixing,  
880 | which supplies sufficient amounts of and allochthonous-nitrate nutrient supply from the  
881 | subsurface nitrate pool into the euphotic zone. This situation might have been additionally  
882 | fostered-influenced by an open Bering Strait and Unimak Pass, allowing for enhanced inflow  
883 | of ~~relatively warmer and nutrient-enriched~~ water masses from the Alaskan Stream and  
884 | enhanced outflow of relatively fresh surface waters into the Arctic. Reduced sea-ice  
885 | formation, but enhanced nutrient supply and-by stronger vertical mixing as a result of a  
886 | strengthened Alaskan Stream and ~~Bering-Slope-Current~~BSC during higher sea-level has been  
887 | proposed before (Gorbarenko et al., 2005; Okazaki et al., 2005; Kim et al., 2011).  
888 | Accordingly, ~~we consider additional~~ sea-level changes must be considered as additional  
889 | forcing mechanism to foreing to explain the recorded environmental changes.

#### 890 | **4.3.4 Interstadial situation**

891 | High-resolution core logging resulted in the detection of short-lived maxima in our color b\*  
892 | and XRF Ca/Ti log-ratio records during ~~stages-MIS 6 to 3~~. Notably, ~~they-these maxima occur~~  
893 | ~~together with~~ maxima in  $>63 \mu\text{m}$  occur simultaneously. Most peaks were detected in cores  
894 | 85KL and 101KL within which they are characterized by only 1-3 cm sediment thickness  
895 | corresponding to a duration of ~100-300 years. These changes in sediment composition seem  
896 | to be related to D-O events (interstadials) registered in the NGRIP ice core. The most  
897 | prominent events correspond to D-O events 7, 8, 12, 17-21, and 24 (Fig. 5), but events off the  
898 | NGRIP record are found. We consider them as brief intervals of enhanced marine  
899 | productivity, sudden sea-ice melt and-associated with the subsequent release of IRD, and a  
900 | higher bottom water calcite saturation state. However, due to our stratigraphic approach,  
901 | which relies on the NGRIP record, we can neither argue for nor against an in-phase evolution  
902 | between abrupt climate changes recorded in Greenland ice and western Bering Sea sediments.

903 Sediment records from Bowers Ridge (Gorbarenko et al., 2005, 2010), the northern slope  
904 (Kim et al., 2011; Rella et al., 2012), as well as the NE Pacific (Behl and Kennett, 1996;  
905 Hendy and Kennett, 2000; Ortiz et al., 2004) also implied millennial-scale climate changes  
906 | connected to N Atlantic D-O events, especially during ~~stage-MIS~~ 3. Similar features were  
907 detected in stalagmites from China (Wang et al., 2001, 2008), which indicates a Northern  
908 Hemisphere-wide acting atmospheric coupling that is related to the intensity of the East Asian  
909 Monsoon. Kennett and Ingram (1995) proposed that such an atmospheric coupling  
910 mechanism directly affected the ventilation of NPIW. Accordingly, interstadials seem to have  
911 been characterized by weak ventilation of NPIW in combination with increased marine  
912 productivity (Behl and Kennett, 1996; Hendy and Kennett, 2000; Kim et al., 2011) and  
913 warmer SSTs (Gorbarenko et al., 2005). Recently, Kim et al. (2011) reported on D-O event-  
914 related brief episodes of high bulk  $\delta^{15}\text{N}$  values at the northern slope, implying increased  
915 nitrate utilization/denitrification. These results to a lesser degree reflect conditions inferred for  
916 the B/A warm phase and thus might point to the release of deep-sequestered  $\text{CO}_2$  during  
917 interstadials.

918

## 919 **5. Summary and conclusions**

920 | From our results we proposed scenarios for environmental change in the Bering Sea during  
921 glacial, deglacial, and interglacial times which compare to those previously suggested for the  
922 Okhotsk Sea. During the last 180 kyr, the Bering Sea paleoenvironment was characterized by  
923 closely interacting processes controlling marine productivity and terrigenous matter supply.  
924 External forcing is attributed to Northern Hemisphere summer insolation and sea-level  
925 changes controlling atmospheric circulation patterns, sea-ice dynamics and upper-ocean  
926 stratification. Marine productivity, dominated by diatoms, remained low during cold intervals  
927 | (~~stages-MIS~~ 6, 5.4, 5.2, 4, ~~and to~~ 2) when the Bering Strait was closed and summer insolation  
928 was weak. ~~Significant i~~Increases occurred during warm intervals (~~stages-MIS~~ 5.5, 5.3, 5.1, and  
929 1), when insolation was high and the Bering Strait was open. ~~S~~Sediments composition is from  
930 Shirshov Ridge are dominated by terrigenous, siliciclastic material mainly bound to the fine  
931 fractions. Terrigenous matter supply was generally high with reductions of up to ~30-40%  
932 during interglacials. Changes in terrigenous matter supply and marine productivity occurred  
933 | synchronously with ~~antio~~related—negatively correlated proxy behaviour due to the

934 ~~sedimentary dilution by the biogenic components. Meridional gradients were found along our~~  
935 ~~core transect, suggesting stronger s~~Terrigenous input~~ea-ice influence was supposedly stronger~~  
936 ~~toward and, hence, restricted marine productivity towards~~ the northernmost site, ~~and: s~~Sea-ice  
937 ~~rafting~~ is considered as the ~~predominant~~ transport agent for terrigenous matter, limiting  
938 marine productivity during cold intervals. Sedimentary geochemical signatures are a mixture  
939 of aeolian and continental sources, indicating that Shirshov Ridge sediments most likely  
940 originate from ~~sea-ice formation~~material entrained in Anadyr Bay on the eastern Bering Sea  
941 shelf. Especially for the last glacial termination our records support the notion of an  
942 atmospheric, Northern Hemisphere-wide acting climate coupling. The situation during the  
943 HS1 and YD cold phases compared to that of cold intervals with enhanced sea-ice rafting  
944 limiting marine productivity during a shortened summer season (weak seasonal contrasts). In  
945 contrast, the B/A and PB warm phases were characterized by enhanced marine productivity as  
946 a result of a prolonged summer season and reduced sea-ice influence (strong seasonal  
947 contrasts). At the same time, reduced ventilation of intermediate waters is in accordance with  
948 ~~higher~~ stronger nitrate utilization and better CaCO<sub>3</sub> preservation indicative of a release of  
949 deep-sequestered CO<sub>2</sub> to the atmosphere. Moreover, we found supporting evidence for the  
950 occurrence of abrupt environmental changes that are related to interstadials recorded in the  
951 NGRIP ice core ~~and reflect the situation proposed for the B/A.~~

952

953

954

955

956

957

958

959

960

961

962

963 **Appendix A: Age models**

964 Age-depth points for cores SO201-2-77KL, -85KL, and -101KL are given in Tab. A1, A2,  
 965 and A3, respectively.

966

Table A1: Age-Depth Points for Core SO201-2-77KL. Ages <20 ka BP and AMS-<sup>14</sup>C Ages Have Been Derived from Max et al. (2012) and Calendar Ages Are Given With 1σ-ranges (in ka BP).

Core	Depth (cm)	Cal. Age (ka BP)	Approach
SO201-2-77KL	6	2.0 <sup>(1)</sup>	color b* vs. color b* (SO201-2-12KL)
SO201-2-77KL	49	7.6 <sup>(1)</sup>	color b* vs. color b* ( <a href="#">SO201-2-12KL</a> )
SO201-2-77KL	103	10.3	Carbonate Spike 1
SO201-2-77KL	105.5	/	AMS- <sup>14</sup> C dating (10.05-10.15) <sup>(2)</sup>
SO201-2-77KL	115.5	/	AMS- <sup>14</sup> C dating (11.17-11.22) <sup>(3)</sup>
SO201-2-77KL	116	11.2	Carbonate Spike 2
SO201-2-77KL	126	11.6	color b* vs. NGRIP
SO201-2-77KL	155.5	12.62	AMS- <sup>14</sup> C dating (12.61-12.73)
SO201-2-77KL	168.5	13.83	AMS- <sup>14</sup> C dating (13.82-13.97)
SO201-2-77KL	180.5	14.75	AMS- <sup>14</sup> C dating (14.50-14.95)
SO201-2-77KL	187	15.1	color b* vs. color b* (85KL)
SO201-2-77KL	221	17.0	color b* vs. color b* (85KL)
SO201-2-77KL	258	21.5	Ca/Ti vs. Ca/Ti (85KL)
SO201-2-77KL	381	35.5	color b* vs. color b* (85KL)
SO201-2-77KL	393	37.2	color b* vs. color b* (85KL)
SO201-2-77KL	443	42.0	color b* vs. color b* (85KL)
SO201-2-77KL	478	46.9	color b* vs. color b* (85KL)
SO201-2-77KL	596	59.5	color b* vs. color b* (85KL)
SO201-2-77KL	656	64.7	Ca/Ti vs. Ca/Ti (85KL)
SO201-2-77KL	722	70.8	color b* vs. color b* (85KL)
SO201-2-77KL	736	72.3	color b* vs. color b* (85KL)
SO201-2-77KL	777	76.4	color b* vs. color b* (85KL)
SO201-2-77KL	796	77.7	color b* vs. color b* (85KL)
SO201-2-77KL	849	84.7	color b* vs. color b* (85KL)
SO201-2-77KL	898	89.1	Ca/Ti vs. Ca/Ti (85KL)
SO201-2-77KL	986	101.5	Ca/Ti vs. Ca/Ti (85KL)
SO201-2-77KL	1043	108.0	color b* vs. color b* (85KL)
SO201-2-77KL	1100	116.9	color b* vs. color b* (85KL)
SO201-2-77KL	1120	120.2	color b* vs. color b* (85KL)
SO201-2-77KL	1166	124.2	color b* vs. color b* (85KL)

<sup>(1)</sup>Uncertain Age; <sup>(2)</sup>Used to Define Carbonate Spike 1 ([see Max et al., 2012](#)); <sup>(3)</sup>Used to Define Carbonate Spike 2 ([see Max et al., 2012](#)).

967

968

969

970

971



Table A2: Age-Depth Points for Core SO201-2-85KL. Ages <20 ka BP and AMS-<sup>14</sup>C Ages Have Been Derived from Max et al. (2012) and Calendar Ages Are Given With 1 $\sigma$ -Ranges (in ka BP).

Core	Depth (cm)	Cal. Age (ka BP)	Approach
SO201-2-85KL	1	7.6 <sup>(1)</sup>	color b* vs. color b* (SO201-2-12KL)
SO201-2-85KL	26.5	/	AMS- <sup>14</sup> C dating (10.38-10.51) <sup>(2)</sup>
SO201-2-85KL	28	10.3	Carbonate Spike 1
SO201-2-85KL	44	11.2	Carbonate Spike 2
SO201-2-85KL	45.5	/	AMS- <sup>14</sup> C dating (10.79-10.97) <sup>(3)</sup>
SO201-2-85KL	52	11.6	color b* vs. NGRIP
SO201-2-85KL	60.5	13.10	AMS- <sup>14</sup> C dating (13.10-13.22)
SO201-2-85KL	70.5	13.87	AMS- <sup>14</sup> C dating (13.67-13.89)
SO201-2-85KL	77	14.6	color b* vs. NGRIP
SO201-2-85KL	82	14.9	color b* vs. NGRIP
SO201-2-85KL	95.5	15.84	AMS- <sup>14</sup> C dating (15.80-15.82)
SO201-2-85KL	135.5	19.90	AMS- <sup>14</sup> C dating (19.58-19.90)
SO201-2-85KL	155.5	23.78	AMS- <sup>14</sup> C dating (23.71-24.19)
SO201-2-85KL	209	26.2	Transfer of AMS- <sup>14</sup> C Age from Core 101KL, But Not Well Constrained
SO201-2-85KL	266	35.5	color b* vs. NGRIP
SO201-2-85KL	292	36.6	color b* vs. NGRIP
SO201-2-85KL	305	38.2	color b* vs. NGRIP
SO201-2-85KL	350	41.9	RPI vs. PISO-1500 (Laschamp)
SO201-2-85KL	363	43.4	color b* vs. NGRIP
SO201-2-85KL	398	46.9	color b* vs. NGRIP
SO201-2-85KL	433	48.4	color b* vs. NGRIP
SO201-2-85KL	463	51.7	color b* vs. NGRIP
SO201-2-85KL	490	54.2	color b* vs. NGRIP
SO201-2-85KL	567	59.5	color b* vs. NGRIP
SO201-2-85KL	657	64.0	color b* vs. NGRIP
SO201-2-85KL	675	65.0	RPI vs. PISO-1500 (Norwegian-Greenland Sea)
SO201-2-85KL	796	72.3	color b* vs. NGRIP
SO201-2-85KL	853	76.4	color b* vs. NGRIP
SO201-2-85KL	876	77.8	color b* vs. NGRIP
SO201-2-85KL	937	84.7	color b* vs. NGRIP
SO201-2-85KL	976	87.7	color b* vs. NGRIP
SO201-2-85KL	1006	91.7	color b* vs. NGRIP
SO201-2-85KL	1100	104.1	color b* vs. NGRIP
SO201-2-85KL	1149	108.0	color b* vs. NGRIP
SO201-2-85KL	1180	110.2	color b* vs. NGRIP
SO201-2-85KL	1210	113.3	color b* vs. NGRIP
SO201-2-85KL	1224	114.8	color b* vs. NGRIP
SO201-2-85KL	1240	117.0	RPI vs. PISO-1500 (Blake)
SO201-2-85KL	1280	125.0	color b* vs. Sanbao $\delta^{18}\text{O}$ (MIS_5.5 climate optimum)
SO201-2-85KL	1300	130.0 <sup>(4)</sup>	SMP vs. LR04 (MIS 5/6 Boundary)
SO201-2-85KL	1320	132.0	color b* vs. Sanbao $\delta^{18}\text{O}$ (HE11)
SO201-2-85KL	1365	135.0	color b*, Ca/Ti vs. Sanbao $\delta^{18}\text{O}$
SO201-2-85KL	1530	151.0	color b*, Ca/Ti vs. Sanbao $\delta^{18}\text{O}$
SO201-2-85KL	1600	159.0	RPI vs. PISO-1500
SO201-2-85KL	1735	174.0 <sup>(4)</sup>	SMP vs. LR04 (MIS_6 Minimum)
SO201-2-85KL	1813	181.8 <sup>(5)</sup>	Extrapolation

<sup>(1)</sup>Uncertain Age; <sup>(2)</sup>Used to Define Carbonate Spike 1 (see Max et al., 2012); <sup>(3)</sup>Used to Define Carbonate Spike 2 (see Max et al., 2012);

<sup>(4)</sup>Scalar Magnetic Properties (SMP) Correlated with MIS Boundaries of LR04;

<sup>(5)</sup>By Extrapolation Using Linear Sedimentation Rate (LSR).

Table A3: Age-Depth Points for Core SO201-2-101KL. Ages <20 ka BP and AMS-<sup>14</sup>C Ages Have Been Derived from Max et al. (2012) and Calendar Ages Are Given With 1 $\sigma$ -Ranges (in ka BP).

Core	Depth (cm)	Cal. Age (ka BP)	Approach
SO201-2-101KL	4	12.9	Ca/Ti vs. Ca/Ti (85KL)
SO201-2-101KL	10.5	13.56	AMS- <sup>14</sup> C dating (13.69-13.84)
SO201-2-101KL	41	14.6	color b* vs. NGRIP
SO201-2-101KL	67	15.4	color b* vs. NGRIP
SO201-2-101KL	90.5	17.25	AMS- <sup>14</sup> C dating (17.17-17.51)
SO201-2-101KL	110.5	18.95	AMS- <sup>14</sup> C dating (19.54-19.92)
SO201-2-101KL	140	23.78	Transfer of AMS- <sup>14</sup> C Age from Core 85KL
SO201-2-101KL	190.5	25.74	AMS- <sup>14</sup> C dating (25.88-26.35)
SO201-2-101KL	234	28.6	color b* vs. NGRIP
SO201-2-101KL	249	30.3	color b* vs. NGRIP
SO201-2-101KL	260.5	32.0	AMS- <sup>14</sup> C dating (32.12-33.54)
SO201-2-101KL	274	33.5	Ca/Ti vs. Ca/Ti (85KL)
SO201-2-101KL	280	35.1	Ca/Ti vs. Ca/Ti (85KL)
SO201-2-101KL	284	35.7	Ca/Ti vs. Ca/Ti (85KL)
SO201-2-101KL	302	36.9	Ca/Ti vs. Ca/Ti (85KL)
SO201-2-101KL	349	39.7	Ca/Ti vs. Ca/Ti (85KL)
SO201-2-101KL	387	43.1	Ca/Ti vs. Ca/Ti (85KL)
SO201-2-101KL	454	46.9	Ca/Ti vs. Ca/Ti (85KL)
SO201-2-101KL	514	51.6	Ca/Ti vs. Ca/Ti (85KL)
SO201-2-101KL	650	56.6	Ca/Ti vs. Ca/Ti (85KL)
SO201-2-101KL	685	57.8	Ca/Ti vs. Ca/Ti (85KL)
SO201-2-101KL	723	59.7	Ca/Ti vs. Ca/Ti (85KL)
SO201-2-101KL	799	64.1	Ca/Ti vs. Ca/Ti (85KL)
SO201-2-101KL	923	71.7	Ca/Ti vs. Ca/Ti (85KL)
SO201-2-101KL	1005	76.4	color b* vs. color b* (85KL)
SO201-2-101KL	1023	77.8	color b* vs. color b* (85KL)
SO201-2-101KL	1092	84.4	Ca/Ti vs. Ca/Ti (85KL)
SO201-2-101KL	1142	89.1	Ca/Ti vs. Ca/Ti (85KL)
SO201-2-101KL	1236	94.5	color b* vs. color b* (85KL)
SO201-2-101KL	1301	103.5	color b* vs. color b* (85KL)
SO201-2-101KL	1526	116.0	Benthic $\delta^{18}\text{O}$ vs. LR04
SO201-2-101KL	1585	125.0	color b* vs. Sanbao $\delta^{18}\text{O}$ (MIS_5.5 climate optimum)
SO201-2-101KL	1625	130.0	Ca/Ti vs. Ca/Ti (85KL)
SO201-2-101KL	1635	132.0	color b* vs. Sanbao $\delta^{18}\text{O}$ (HE11)
SO201-2-101KL	1657	133.1	Ca/Ti vs. Ca/Ti (85KL)
SO201-2-101KL	1684	134.6	color b* vs. color b* (85KL)
SO201-2-101KL	1738	141.8	Ca/Ti vs. Ca/Ti (85KL)
SO201-2-101KL	1765	145.1	color b* vs. color b* (85KL)
SO201-2-101KL	1804	147.8	Ca/Ti vs. Ca/Ti (85KL)
SO201-2-101KL	1832	149.7 <sup>(1)</sup>	Extrapolation

<sup>(1)</sup>By Extrapolation Using Linear Sedimentation Rate (LSR).

977 **Appendix B: Surface sediment samples**

978 Results of discrete XRF measurements conducted on surface sediment samples recovered in  
 979 direct vicinity of the studied sediment cores using a MultiCorer (MUC) are given in Tab. B1.

Table B1: Site Information, Concentrations of Ba<sub>bio</sub>, and Calculated values for P<sub>new</sub> and PP in Surface Sediment Samples.

<u>Station</u>	<u>Latitude</u>	<u>Longitude</u>	<u>Depth (mbsl)</u>	<u>Tube Depth (cm)</u>	<u>Ba<sub>bio</sub><sup>(1)</sup> (ppm)</u>	<u>P<sub>new</sub><sup>(2)</sup> (gC m<sup>-2</sup> yr<sup>-1</sup>)</u>	<u>PP<sup>(3)</sup> (gC m<sup>-2</sup> yr<sup>-1</sup>)</u>
<u>SO201-2-76MUC</u>	<u>56°19.80'N</u>	<u>170°41.96'E</u>	<u>2137</u>	<u>1-2</u>	<u>932</u>	<u>31.8</u>	<u>113</u>
<u>SO201-2-76MUC</u>	<u>56°19.80'N</u>	<u>170°41.96'E</u>	<u>2137</u>	<u>2-3</u>	<u>1327</u>	<u>54.0</u>	<u>147</u>
<u>SO201-2-76MUC</u>	<u>56°19.80'N</u>	<u>170°41.96'E</u>	<u>2137</u>	<u>3-4</u>	<u>1319</u>	<u>53.5</u>	<u>146</u>
<u>SO201-2-83MUC</u>	<u>57°30.28'N</u>	<u>170°24.82'E</u>	<u>970</u>	<u>0-1</u>	<u>636</u>	<u>19.2</u>	<u>88</u>
<u>SO201-2-83MUC</u>	<u>57°30.28'N</u>	<u>170°24.82'E</u>	<u>970</u>	<u>1-2</u>	<u>681</u>	<u>21.3</u>	<u>92</u>
<u>SO201-2-99MUC</u>	<u>58°52.53'N</u>	<u>170°41.48'E</u>	<u>643</u>	<u>2-3</u>	<u>177</u>	<u>2.9</u>	<u>34</u>

<sup>(1)</sup>via Al using the global average Ba/Al of pelitic rocks of 6.5 mg g<sup>-1</sup> (Wedepohl, 1971)

<sup>(2)</sup>after Nürnberg (1995) using an average AR<sub>Bulk</sub> of 4 g cm<sup>-2</sup> kyr<sup>-1</sup>

<sup>(3)</sup>after Eppley and Peterson (1979)

980  
981  
982  
983  
984  
985  
986  
987  
988  
989  
990  
991  
992  
993  
994  
995

996 **Acknowledgements**

997 This study resulted from the German-Russian joint research project KALMAR, funded by the  
998 German Ministry of Education and Research (BMBF), grant nos. 03G0672A and B. We thank  
999 the captain and crew of R/V Sonne cruise SO201-KALMAR Leg 2 for their professional  
1000 support in recovering high-quality cores. Technical support and laboratory assistance came  
1001 from B. Domeyer, N. Gehre, L. Haxhijaj, P. Appel, and J. Heinze and is gratefully  
1002 acknowledged. E. Maier (AWI-Bremerhaven) conducted additional opal measurements for  
1003 core 77KL. A. Matul (Shirshov Institute of Oceanology, Moscow) provided additional  
1004 benthic foraminiferal tests to improve oxygen isotope stratigraphy for cores 85KL and  
1005 101KL. The data are available via the PANGAEA Data Publisher for Earth & Environmental  
1006 Science (<http://doi.pangaea.de/10.1594/PANGAEA.786307>).

1007

1008

1009

1010

1011

1012

1013

1014

1015

1016

1017

1018

1019

1020

1021

1022

1023 **References**

- 1024 Adkins, J. F. and Boyle, E. A.: Changing atmospheric  $\Delta^{14}\text{C}$  and the record of deep water  
1025 paleoventilation ages, *Paleoceanography*, 12, 337-344. 1997.
- 1026 Ahagon, N., Ohkushi, K., Uchida, M., and Mishima, T.: Mid-depth circulation in the  
1027 northwest Pacific during the last deglaciation: Evidence from foraminiferal radiocarbon ages.  
1028 *Geophys. Res. Lett.*, 30, 2097, doi:10.1029/2003GL018287, 2003.
- 1029 Arzhanova, N. V., Zubarevich, V. L., and Sapozhnikov, V. V.: Seasonal variability of nutrient  
1030 stocks in the euphotic zone and assessment of primary production in the Bering Sea. ~~Min:~~  
1031 Complex studies of the Bering Sea ecosystem, edited by: Kotenev, B. N. and Sapozhnikov, V.  
1032 V., pp. ~~162-179~~, VNIRO, Moscow, ~~162-179~~, 1995.
- 1033 [Asahara, Y., Takeuchi, F., Nagashima, K., Harada, N., Yamamoto, K., Oguri, K., and Tadaï,](#)  
1034 [O.: Provenance of terrigenous detritus of the surface sediments in the Bering and Chukchi](#)  
1035 [Seas as derived from Sr and Nd isotopes: Implications for recent climate change in the Arctic](#)  
1036 [regions, \*Deep-Sea Res. Pt. II\*, 61-64, 155-171, doi:10.1016/j.dsr2.2011.12.004, 2012.](#)
- 1037 Bareille, G., Grousset, F. E., Labracherie, M., Labeyrie, L. D., and Petit, J.-R.: Origin of  
1038 detrital fluxes in the southeast Indian Ocean during the last climatic cycles,  
1039 *Paleoceanography*, 9, 799-819, 1994.
- 1040 Barr, I. D. and Clark, C. D.: Glaciers and climate in Pacific Far NE Russia during the Last  
1041 Glacial Maximum, *J. Quaternary Sci.*, 26, 227-237, doi:10.1002/jqs.1450, 2011.
- 1042 Behl, R. J. and Kennett, J. P.: Brief interstadial events in the Santa Barbara basin, NE Pacific,  
1043 during the past 60 kyr, *Nature*, 379, 243-246, 1996.
- 1044 Bigg, G. R., Clark, C. D., and Hughes, A. L. C.: A last glacial ice sheet on the Pacific Russian  
1045 coast and catastrophic change arising from coupled ice-volcanic interaction, *Earth Planet. Sc.*  
1046 *Lett.*, 265, 559-570, doi:10.1016/j.epsl.2007.10.052, 2008.
- 1047 Blockley, S. P. E., Lane, C. S., Hardiman, M., Rasmussen, S. O., Seierstad, I. K., Steffensen,  
1048 J. P., Svensson, A., Lotter, A. F., Turney, C. S. M., Ramsey, C. B., and INTIMATE members:  
1049 Synchronisation of palaeoenvironmental records over the last 60,000 years, and an extended  
1050 INTIMATE event stratigraphy to 48,000 b2k, *Quaternary Sci. Rev.*, 36, 2-10,  
1051 [doi:10.1016/j.quascirev.2011.09.017](#), 2012.

1052 Boyle, E. A.: Chemical accumulation variations under the Peru current during the past  
1053 130,000 years, *J. Geophys. Res.*, 88, 7667-7680, 1983.

1054 Brigham-Grette, J., Hopkins, D. M., Ivanov, V. F., Basilyan, E. B., Benson, S. L., Heiser, P.  
1055 A., and Pushkar, V. S.: Last Interglacial (isotope stage 5) glacial and sea-level history of  
1056 coastal Chukotka Peninsula and St. Lawrence Island, Western Beringia, *Quaternary Sci. Rev.*,  
1057 20, 419-436, 2001.

1058 Brigham-Grette, J., Gualtieri, L. M., Glushkova, O. Y., Hamilton, T. D., Mostoller, D., and  
1059 Kotov, A.: Chlorine-35 and <sup>14</sup>C chronology support a limited last glacial maximum across  
1060 central Chukotka, northeastern Siberia, and no Beringian ice sheet, *Quaternary Res.*, 59, 386-  
1061 398, [doi:10.1016/S0033-5894\(02\)00000-0](https://doi.org/10.1016/S0033-5894(02)00000-0), 2003.

1062 Broecker, W. S. and Peng, T.-H.: The role of CaCO<sub>3</sub> compensation in the glacial to  
1063 interglacial atmospheric CO<sub>2</sub> change, *Global Biogeochem. Cy.*, 1, 15-29, 1987.

1064 Brunelle, B. G., Sigman, D. M., Cook, M. S., Keigwin, L. D., Haug, G. H., Plessen, B.,  
1065 Schettler, G., and Jaccard, S. L.: Evidence from diatom-bound nitrogen isotopes for subarctic  
1066 Pacific stratification during the last ice age and a link to North Pacific denitrification changes,  
1067 *Paleoceanography*, 22, PA1215, [doi:10.1029/2005PA001205](https://doi.org/10.1029/2005PA001205). 2007.

1068 Brunelle, B. G., Sigman, D. M., Jaccard, S. L., Keigwin, L. D., Plessen, B., Schettler, G.,  
1069 Cook, M. S., and Haug, G. H.: Glacial/interglacial changes in nutrient supply and  
1070 stratification in the western subarctic North Pacific since the penultimate glacial maximum,  
1071 *Quaternary Sci. Rev.*, 29, 2579-2590, [doi:10.1016/j.quascirev.2010.03.010](https://doi.org/10.1016/j.quascirev.2010.03.010), 2010.

1072 ~~Burov, B. V. and Yasonov, P. G.: Introduction into different thermomagnetic analysis of~~  
1073 ~~rocks, Kazanian University Press [in Russian], 1979.~~~~Burov, B. V., Nourgaliev, D. K., and~~  
1074 ~~Iassonov, P. G.: Paleomagnetic analysis, Kazan University Press, Kazan, 167 pp., 1986 (in~~  
1075 ~~Russian).~~

1076 Caissie, B. E., Brigham-Grette, J., Lawrence, K. T., Herbert, T. D., and Cook, M. S.: Last  
1077 Glacial Maximum to Holocene sea surface conditions at Umnak Plateau, Bering Sea, as  
1078 inferred from diatom, alkenone, and stable isotope records, *Paleoceanography*, 25, PA1206,  
1079 [doi:10.1029/2008PA001671](https://doi.org/10.1029/2008PA001671), 2010.

1080 Calvert, S. E. and Fontugne, M. R.: On the late Pleistocene-Holocene sapropel record of  
 1081 climatic and oceanographic variability in the eastern Mediterranean. *Paleoceanography*, 16,  
 1082 78-94, 2001.

1083 Channell, J. E. T., Xuan, C., and Hodell, D. A.: Stacking paleointensity and oxygen isotope  
 1084 data for the last 1.5 Myr (PISO-1500), *Earth Planet. Sc. Lett.*, 283, 14-23,  
 1085 [doi:10.1016/j.epsl.2009.03.012](https://doi.org/10.1016/j.epsl.2009.03.012), 2009.

1086 Chen, C.-T. A.: Shelf-vs. dissolution-generated alkalinity above the chemical lysocline, *Deep-*  
 1087 *Sea Res. Pt. II*, 49, 5365-5375, [doi:10.1016/S0967-0645\(02\)00196-0](https://doi.org/10.1016/S0967-0645(02)00196-0), 2002.

1088 Chikamoto, M. O., Menviel, L., Abe-Ouchi, A., Ohgaito, R., Timmermann, A., Okazaki, Y.,  
 1089 Harada, N., Oka, A., and Mouchet, A.: Variability in North Pacific intermediate and deep  
 1090 water ventilation during Heinrich events in two coupled climate models, *Deep-Sea Res. Pt. II*,  
 1091 61-64, 114-126, [doi:10.1016/j.dsr2.2011.12.002](https://doi.org/10.1016/j.dsr2.2011.12.002), 2012.

1092 Cook, M. S.: The paleoceanography of the Bering Sea during the last glacial cycle, Ph.D.  
 1093 thesis, Massachusetts Institute of Technology, Woods Hole Oceanographic Institution,  
 1094 [Massachusetts Institute of Technology](https://www.mst.mit.edu/), 126 pp., 2006.

1095 Cook, M. S., Keigwin, L. D., and Sancetta, C. A.: The deglacial history of surface and  
 1096 intermediate water of the Bering Sea, *Deep-Sea Res. Pt. II*, 52, 2163-2173,  
 1097 [doi:10.1016/j.dsr2.2005.07.004](https://doi.org/10.1016/j.dsr2.2005.07.004), 2005.

1098 Crusius, J., Pedersen, T. F., Kienast, S., Keigwin, L., and Labeyrie, L.: Influence of northwest  
 1099 Pacific productivity on North Pacific Intermediate Water oxygen concentrations during the  
 1100 Bölling-Alleröd interval (14.7-12.9 ka), *Geology*, 32, 633-636, [doi:10.1130/G20508.1](https://doi.org/10.1130/G20508.1), 2004.

1101 [Dansgaard, W., Johnsen, S. J., Clausen, H. B., Dahl-Jensen, D., Gundestrup, N. S., Hammer,](https://doi.org/10.1038/364218a)  
 1102 [C. U., Hvidberg, C. S., Steffensen, J. P., Svelnbjörnsdottir, A. E., Jouzel, J., and Bond, G.:](https://doi.org/10.1038/364218a)  
 1103 [Evidence for general instability of past climate from a 250-kyr ice-core record, \*Nature\*, 364,  
 1104 \[218-220, 1993.\]\(https://doi.org/10.1038/364218a\)](https://doi.org/10.1038/364218a)

1105 [Debret, M., Desmet, M., Balsam, W., Copard, Y., Francus, P., and Laj, C.: Spectrophotometer](https://doi.org/10.1016/j.margeo.2006.01.005)  
 1106 [analysis of Holocene sediments from an anoxic fjord: Saanich Inlet, British Columbia,](https://doi.org/10.1016/j.margeo.2006.01.005)  
 1107 [Canada, \*Mar. Geol.\*, 229, 15-28, doi:10.1016/j.margeo.2006.01.005, 2006.](https://doi.org/10.1016/j.margeo.2006.01.005)

1108 Dehairs, F., Stroobants, N., and Goeyens, L.: Suspended barite as a tracer of biological  
 1109 activity in the Southern Ocean, *Mar. Chem.*, 35, 399-410, 1991.

- 1110 De La Rocha, C. L.: The biological pump, in: *Treatise on Geochemistry*, Vol. 6, edited by:  
1111 Elderfield, H., pp. ~~83-111~~, Elsevier, Amsterdam, 83-111, 2007.
- 1112 DeMaster, D.: The supply and accumulation of silica in the marine environment, *Geochim.*  
1113 *Cosmochim. Ac.*, 45, 1715-1732, 1981.
- 1114 Duce, R. A. and Tindale, N. W.: Atmospheric transport of iron and its deposition in the ocean,  
1115 *Limnol. Oceanogr.*, 36, 1715-1726, 1991.
- 1116 Dullo, W.-C., Baranov, B., and van den Bogaard, C. (Eds.): FS Sonne Fahrtbericht / Cruise  
1117 Report SO201-2 KALMAR, Busan/Korea-Tomakomai/Japan, 30.08.-08.10.2009, IFM-  
1118 GEOMAR Report 35, Leibniz Institute of Marine Sciences, Kiel, 233 pp., 2009.
- 1119 Dymond, J. and R. Collier, R.: Particulate barium fluxes and their relationships to biological  
1120 productivity, *Deep-Sea Res. Pt. II*, 43, 1283-1308, 1996.
- 1121 Dymond, J., Suess, E., and Lyle, M.: Barium in deep-sea sediment: a geochemical proxy for  
1122 paleoproductivity, *Paleoceanography*, 7, 163-181, 1992.
- 1123 Emile-Geay, J., Cane, M. A., Naik, N., Seager, R., Clement, A. C., and van Geen, A.: Warren  
1124 revisited: Atmospheric freshwater fluxes and “Why is no deep water formed in the North  
1125 Pacific“, *J. Geophys. Res.*, 108, 3178, doi:10.1029/2001JC001058, 2003.
- 1126 Engel, A. E. J., Engel, C. G., and Havens, R. G.: Chemical characteristics of oceanic basalts  
1127 and the upper Miocene, *Geol. Soc. Am. Bull.*, 76, 719-734, 1965.
- 1128 Enkin, R. J., Baker, J., Nourgaliev, D., Iassonov, P., and Hamilton, T. S.: Magnetic hysteresis  
1129 parameters and Day plot analysis to characterize diagenetic alteration in gas hydrate-bearing  
1130 sediments, *J. Geophys. Res.*, 112, B06S90, doi:10.1029/2006JB004638, 2007.
- 1131 Eppley, R. W. and Peterson, B. J.: Particulate organic matter flux and planktonic new  
1132 production in the deep ocean, *Nature*, 282, 677-680, 1979.
- 1133 Feely, R. A., Sabine, C. L., Lee, K., Millero, F. J., Lamb, M. F., Greeley, D., Bullister, J. L.,  
1134 Key, R. M., Peng, T.-H., Kozyr, A., Ono, T., and Wong, C. S.: In situ calcium carbonate  
1135 dissolution in the Pacific Ocean, *Global Biogeochem. Cy.*, 16, 1144,  
1136 doi:10.1029/2002GB001866, 2002.



1137 Francois, R., Honjo, S., Manganini, S. J., Ravizza, G. E.: Biogenic barium fluxes to the deep  
1138 sea: Implications for paleoproductivity reconstruction, *Global Biogeochem. Cy.*, 9, 289-303,  
1139 1995.

1140 Galbraith, E. D., Jaccard, S. L., Pedersen, T. F., Sigman, D. M., Haug, G. H., Cook, M.,  
1141 Southon, J. R., and Francois, R.: Carbon dioxide release from the North Pacific abyss during  
1142 the last deglaciation, *Nature*, 449, 890-893, [doi:10.1038/nature06227](https://doi.org/10.1038/nature06227), 2007.

1143 Galbraith, E. D., Kienast, M., Jaccard, S. L., Pedersen, T. F., Brunelle, B. G., Sigman, D. M.,  
1144 and Kiefer, T.: Consistent relationship between global climate and surface nitrate utilization  
1145 in the western subarctic Pacific throughout the last 500 ka, *Paleoceanography*, 23, PA2212,  
1146 [doi:10.1029/2007PA001518](https://doi.org/10.1029/2007PA001518), 2008.

1147 Ganeshram, R. S., Calvert, S. E., Pedersen, T. F., and Cowie, G. L.: Factors controlling the  
1148 burial of organic carbon in laminated and bioturbated sediments off NW Mexico:  
1149 Implications for hydrocarbon preservation, *Geochim. Cosmochim. Ac.*, 63, 1723-1734, 1999.

1150 [Ganeshram, R. S., Francois, R., Commeau, J., and Brown-Leger, S. L.: An experimental](#)  
1151 [investigation of barite formation in seawater, \*Geochim. Cosmochim. Ac.\*, 67, 14, 2599-2605,](#)  
1152 [doi:10.1016/S0016-7037\(03\)00164-9, 2003.](#)

1153 Gardner, J. V., Dean, W. E., and Vallier, T. L.: Sedimentology and geochemistry of surface  
1154 sediments, outer continental shelf, southern Bering Sea, *Mar. Geol.*, 35, 299-329, 1980.

1155 Gebhardt, H., Sarnthein, M., Grootes, P. M., Kiefer, T., Kühn, H., Schmieder, F., and Röhl,  
1156 U.: Paleonutrient and productivity records from the subarctic North Pacific for Pleistocene  
1157 glacial terminations I to V. *Paleoceanography*, 23, PA4212, [doi:10.1029/2007PA001513](https://doi.org/10.1029/2007PA001513),  
1158 2008.

1159 Gingele, F., Zabel, M., Kasten, S., Bonn, W. J., and Nürnberg, C. C.: Biogenic barium as a  
1160 proxy for paleoproductivity: Methods and limitations of application—, [Hain](#): Use of proxies in  
1161 paleoceanography—, [Examples from the South Atlantic](#), edited by: Fischer, G. and Wefer, G.,  
1162 [pp. 345-364](#), Springer, Berlin, [345-364](#), 1999.

1163 Goñi, M. A., Ruttenberg, K. C., and Eglinton, T. I.: A reassessment of the sources and  
1164 importance of land-derived organic matter in surface sediments from the Gulf of Mexico.  
1165 *Geochim. Cosmochim. Ac.*, 62, 3055-3075, 1998.

1166 Gorbarenko, S. A.: Stable isotope and lithologic evidence of late-glacial and Holocene  
1167 oceanography of the northwestern Pacific and its marginal seas, *Quaternary Res.*, 46, 230-  
1168 250, 1996.

1169 Gorbarenko, S. A., Khusid, T. A., Basov, I. A., Oba, T., Southon, J. R., and Koizumi, I.:  
1170 Glacial Holocene environment of the southeastern Okhotsk Sea: Evidence from geochemical  
1171 and paleontological data, *Palaeogeogr. Palaeocl.*, 177, 237-263, [doi:10.1016/S0031-  
1172 0182\(01\)00335-2](https://doi.org/10.1016/S0031-0182(01)00335-2), 2002a.

1173 Gorbarenko, S. A., Nürnberg, D., Derkachev, A. N., Astakhov, A. S., Southon, J. R., and  
1174 Kaiser, A.: Magnetostratigraphy and tephrochronology of the Upper Quaternary sediments in  
1175 the Okhotsk Sea: Implication of terrigenous, volcanogenic and biogenic matter supply, *Mar.*  
1176 *Geol.*, 183, 107-129, [doi:10.1016/S0025-3227\(02\)00164-0](https://doi.org/10.1016/S0025-3227(02)00164-0), 2002b.

1177 Gorbarenko, S. A., Basov, I. A., Chekhovskaya, M. P., Southon, J., Khusid, T. A., and  
1178 Artemova, A. V.: Orbital and millenium scale environmental changes in the southern Bering  
1179 Sea during the last glacial-Holocene: Geochemical and paleontological evidence, *Deep-Sea*  
1180 *Res. Pt. II*, 52, 2174-2185, [doi:10.1016/j.dsr2.2005.08.005](https://doi.org/10.1016/j.dsr2.2005.08.005), 2005.

1181 Gorbarenko, S. A., Wang, P., Wang, R., and Cheng, X.: Orbital and suborbital environmental  
1182 changes in the southern Bering Sea during the last 50 kyr, *Palaeogeogr. Palaeocl.*, 286, 97-  
1183 106, [doi:10.1016/j.palaeo.2009.12.014](https://doi.org/10.1016/j.palaeo.2009.12.014), 2010.

1184 Gromet, L. P., Dymek, R. F., Haskin, L. A., and Korotev, R. L.: The "North American shale  
1185 composite": Its compilation, major and trace element characteristics, *Geochim. Cosmochim.*  
1186 *Ac.*, 48, 2469-2482, 1984.

1187 Grosswald, M. G. and Hughes, T. J.: The Russian component of an Arctic Ice Sheet during  
1188 the Last Glacial Maximum, *Quaternary Sci. Rev.*, 21, 121-146, [doi:10.1016/S0277-  
1189 3791\(01\)00078-6](https://doi.org/10.1016/S0277-3791(01)00078-6), 2002.

1190 Hartnett, H. E., Keil, R. G., Hedges, J. I., and Devol, A. H.: Influence of oxygen exposure  
1191 time on organic carbon preservation in continental margin sediments, *Nature*, 391, 572-574,  
1192 1998.

1193 Haug, G. H., Sigman, D. M., Tiedemann, R., Pedersen, T. F., and Sarnthein, M.: Onset of  
1194 permanent stratification in the subarctic Pacific Ocean, *Nature*, 401, 779-782, 1999.

1195 Haug, G. H., Ganopolski, A., Sigman, D. M., Rosell-Mele, A., Swann, G. E. A., Tiedemann,  
1196 R., Jaccard, S. L., Bollmann, J., Maslin, M. A., Leng, M. J., and Eglinton, G.: North Pacific  
1197 seasonality and the glaciation of North America 2.7 million years ago, *Nature*, 433, 821-825,  
1198 | [doi:10.1038/nature03332](https://doi.org/10.1038/nature03332), 2005.

1199 Hedges, J. I., Clark, W. A., Quay, P. D., Richey, J. E., Devol, A. H., and de M. Santos, U.:  
1200 Compositions and fluxes of particulate organic material in the Amazon River, *Limnol.*  
1201 *Oceanogr.*, 31, 717-738, 1986.

1202 Hedges, J. I., Baldock, J. A., Gélinas, Y., Lee, C., Peterson, M., and Wakeham, S. G.:  
1203 Evidence for non-selective preservation of organic matter in sinking marine particles, *Nature*,  
1204 409, 801-804, 2001.

1205 Hendy, I. L. and Kennett, J. P.: Dansgaard-Oeschger cycles and the California Current  
1206 System: Planktonic foraminiferal response to rapid climate change in Santa Barbara Basin,  
1207 | Ocean Drilling Program ~~hole~~-Hole 893A, *Paleoceanography*, 15, 30-42, 2000.

1208 Honda, M. C., Imai, K., Nojiri, Y., Hoshi, F., Sugawara, T., and Kusakabe, M.: The biological  
1209 pump in the northwestern North Pacific based on fluxes and major components of particulate  
1210 matter obtained by sediment-trap experiments (1997-2000), *Deep-Sea Res. Pt. II*, 49, 5595-  
1211 | 5625, [doi:10.1016/S0967-0645\(02\)00201-1](https://doi.org/10.1016/S0967-0645(02)00201-1), 2002.

1212 [Honjo, S.: Particle fluxes and modern sedimentation in the polar oceans, in: Polar](#)  
1213 [Oceanography, Part B. Chemistry, Biology, and Geology, edited by Smith, W.D., Academic](#)  
1214 [Press, New York, pp. 687-739, 1990.](#)

1215 Hu, A., Meehl, G. A., Otto-Bliesner, B. L., Waelbroeck, C., Han, W., Loutre, M.-F.,  
1216 Lambeck, K., Mitrovica, J. X., and Rosenbloom, N.: Influence of Bering Strait flow and  
1217 North Atlantic circulation on glacial sea-level changes, *Nat. Geosci.*, 3, 118-121,  
1218 | [doi:10.1038/ngeo729](https://doi.org/10.1038/ngeo729), 2010.

1219 Itaki, T., Uchida, M., Kim, S., Shin, H.-S., Tada, R., and Khim, B.-K.: Late Pleistocene  
1220 stratigraphy and palaeoceanographic implications in northern Bering Sea slope sediments:  
1221 | Evidence from the radiolarian species *Cycladophora davisiana*, *J. Quaternary Sci.*, 24, 856-  
1222 865, [doi:10.1002/jqs.1356](https://doi.org/10.1002/jqs.1356), 2009.

- 1223 | [Jaccard, S.L. and Galbraith, E. D.: Direct ventilation of the North Pacific did not reach the](#)  
1224 | [deep ocean during the last deglaciation, \*Geophys. Res. Lett.\*, 40, 199-203,](#)  
1225 | [doi:10.1029/2012GL054118, 2013.](#)
- 1226 | Jaccard, S. L., Haug, G. H., Sigman, D. M., Pedersen, T. F., Thierstein, H. R., and Röhl, U.:  
1227 | Glacial/interglacial changes in subarctic North Pacific stratification, *Science*, 308, 1003-1008,  
1228 | [doi:10.1126/science.1108696, 2005.](#)
- 1229 | Jaccard, S. L., Galbraith, E. D., Sigman, D. M., Haug, G. H., Francois, R., Pedersen, T. F.,  
1230 | Dulski, P., and Thierstein, H. R.: Subarctic Pacific evidence for a glacial deepening of the  
1231 | oceanic respired carbon pool, *Earth Planet. Sc. Lett.*, 277, 156-165,  
1232 | [doi:10.1016/j.epsl.2008.10.017, 2009.](#)
- 1233 | Jaccard, S. L., Galbraith, E. D., Sigman, D. M., and Haug, G. H.: A pervasive link between  
1234 | Antarctic ice core and subarctic Pacific sediment records over the past 800 kyrs, *Quaternary*  
1235 | *Sci. Rev.*, 29, 206-212, [doi:10.1016/j.quascirev.2009.10.007, 2010.](#)
- 1236 | Jansen, J. H. F., van der Gaast, S. J., Koster, B., and Vaars, A. J.: CORTEX, a shipboard  
1237 | XRF-scanner for element analyses in split sediment cores, *Mar. Geol.*, 151, 143-153, 1998.
- 1238 | Karhu, J. A., Tschudi, S., Saarnisto, M., Kubik, P., and Schlüchter, C.: Constraints for the  
1239 | latest glacial advance on Wrangel Island, Arctic Ocean, from rock surface exposure dating,  
1240 | *Global Planet. Change*, 31, 447-451, 2001.
- 1241 | Katsuki, K. and Takahashi, K.: Diatoms as paleoenvironmental proxies for seasonal  
1242 | productivity, sea-ice and surface circulation in the Bering Sea during the late Quaternary,  
1243 | *Deep-Sea Res. Pt. II*, 52, 2110-2130, [doi:10.1016/j.dsr2.2005.07.001, 2005.](#)
- 1244 | Kaufman, D. S., Forman, S. L., Lea, P. D., and Wobus, C. W.: Age of pre-late-Wisconsin  
1245 | glacial-eastuarine sedimentation, Bristol Bay, Alaska, *Quaternary Research*, 45, 59-72,  
1246 | [doi:10.1016/j.quascirev.2003.09.007, 2004.](#)
- 1247 | Keigwin, L.D. (1998), *Glacial-age hydrography of the far northwest Pacific Ocean*,  
1248 | *Paleoceanography*, 13, 323-339, 1996.
- 1249 | Keigwin, L. D. and Jones, G. A.: Deglacial climatic oscillations in the Gulf of California,  
1250 | *Paleoceanography*, 5, 1009-1023, 1990.

- 1251 Keigwin, L. D., Jones, G. A., and Froelich, P. N.: A 15,000 year paleoenvironmental record  
1252 from Meiji Seamount, far northwestern Pacific, *Earth Planet. Sc. Lett.*, 111, 425-440, 1992.
- 1253 Keigwin, L. D., Donnelly, J. P., Cook, M. S., Driscoll, N. W., and Brigham-Grette, J.: Rapid  
1254 sea-level rise and Holocene climate in the Chukchi Sea, *Geology*, 34, 861-864,  
1255 doi:10.1130/G22712.1, 2006.
- 1256 Kennett, J. P. and Ingram, B. L.: A 20,000-year record of ocean circulation and climate  
1257 change from the Santa Barbara basin, *Nature*, 377, 510-514, 1995.
- 1258 Khim, B.-K., Kim, S., Uchida, M., and Itaki, T.: High organic carbon deposition in the  
1259 northern margin of the Aleutian Basin (Bering Sea) before the last deglaciation, *Ocean Sci.*,  
1260 | 45, 203-211, [doi:10.1007/s12601-010-0019-y](https://doi.org/10.1007/s12601-010-0019-y), 2010.
- 1261 Kienast, S. S., Hendy, I. L., Crusius, J., Pedersen, T. F., and Calvert, S.: Export production in  
1262 the subarctic North Pacific over the last 800 kyrs: No evidence for iron fertilization? *J.*  
1263 *Oceanogr.*, 60, 189-203, 2004.
- 1264 Kim, S., Khim, B. K., Uchida, M., Itaki, T., and Tada, R.: Millennial-scale paleoceanographic  
1265 events and implication for the intermediate-water ventilation in the northern slope area of the  
1266 Bering Sea during the last 71 kyrs, *Global Planet. Change*, 79, 89-98,  
1267 | [doi:10.1016/j.gloplacha.2011.08.004](https://doi.org/10.1016/j.gloplacha.2011.08.004), 2011.
- 1268 Klump, J., Hebbeln, D., and Wefer, G.: The impact of sediment provenance on barium-based  
1269 productivity estimates, *Mar. Geol.*, 169, 259-271, 2000.
- 1270 Laskar, J., Robutel, P., Joutel, F., Gastineau, M., Correia, A. C. M., and Levrard, B.: A long-  
1271 term numerical solution for the insolation quantities of the Earth, *Astron. Astrophys.*, 428,  
1272 261-285, doi:10.1051/0004-6361:20041335, 2004.
- 1273 Latimer, J. C. and Filippelli, G. M.: Terrigenous input and paleoproductivity in the Southern  
1274 Ocean, *Paleoceanography*, 16, 627-643, 2001.
- 1275 Lisiecki, L. and Raymo, M.: A Pliocene-Pleistocene stack of 57 globally distributed benthic  
1276  $\delta^{18}\text{O}$  records, *Paleoceanography*, 20, PA1003, doi:10.1029/2004PA001071, 2005.
- 1277 Lisitzin, A. P.: *Sea ice and iceberg sedimentation in the ocean: Recent and past*, Springer-  
1278 | Verlag, Berlin, 563 pp., 2002.

- 1279 [Lund, D. C., Mix, A. C., and Southon, J.: Increased ventilation age of the deep northeast](#)  
1280 [Pacific Ocean during the last deglaciation, \*Nat. Geosci.\*, 4, 771-774, doi:10.1038/ngeo1272,](#)  
1281 [2011.](#)
- 1282 Mahowald, N. M., Baker, A. R., Bergametti, G., Brooks, N., Duce, R. A., Jickells, D.,  
1283 Kubilay, N., Prospero, J. M., and Tegen, I.: Atmospheric global dust cycle and iron inputs to  
1284 the ocean, *Global Biogeochem. Cy.*, 19, GB4025, doi:10.1029/2004GB002402, 2005.
- 1285 Malakhov, M. I., Gorbarenko, S. A., Malakhova, G. Y., Harada, N., Vasilenko, Y. P., Bosin,  
1286 A. A., Goldberg, E. L., and Derkachev, A. N.: Petromagnetic parameters of bottom sediments  
1287 as indicators of the climatic and environmental changes in the central zone of the Sea of  
1288 Okhotsk during the last 350 kyr, *Russ. Geol. Geophys.*, 50, 973-982,  
1289 doi:10.1016/j.rgg.2009.10.006, 2009.
- 1290 Mantua, N. J., Hare, S. R., Zhang, Y., Wallace, J. M., and Francis, R. C.: A Pacific  
1291 interdecadal climate oscillation with impacts on salmon production, *B. Am. Meteorol. Soc.*,  
1292 78, 1069-1079, 1997.
- 1293 Marchitto, T. M., Lynch-Stieglitz, J., and Hemming, S. R.: Deep Pacific CaCO<sub>3</sub>  
1294 compensation and glacial-interglacial atmospheric CO<sub>2</sub>, *Earth Planet. Sc. Lett.*, 231, 317-336,  
1295 [doi:10.1016/j.epsl.2004.12.024](#), 2005.
- 1296 [Matsumoto, K., Oba, T., Lynch-Stieglitz, J., and Yamamoto, H.: Interior hydrography and](#)  
1297 [circulation of the glacial Pacific Ocean, \*Quaternary Sci. Rev.\*, 21, 1693-1704,](#)  
1298 [doi:10.1016/S0277-3791\(01\)00142-1](#), 2002.
- 1299 ~~[Matul, A., Abelman, A., Tiedemann, R., Kaiser, A., and Nürnberg, D.: Late Quaternary](#)~~  
1300 ~~[polycystine radiolarian datum events in the Sea of Okhotsk, \*Geo-Mar. Lett.\*, 22, 25-32, 2002.](#)~~
- 1301 Max, L., Riethdorf, J.-R., Tiedemann, R., Smirnova, M., Lembke-Jene, L., Fahl, K.,  
1302 Nürnberg, D., Matul, A., and Mollenhauer, G.: Sea surface temperature variability and sea-ice  
1303 extent in the subarctic northwest Pacific during the past 15,000 years, *Paleoceanography*, 27,  
1304 PA3213, doi:10.1029/2012PA002292, 2012.
- 1305 McDonald, D., Pedersen, T. F., and Crusius, J.: Multiple late Quaternary episodes of  
1306 exceptional diatom production in the Gulf of Alaska, *Deep-Sea Res. Pt. II*, 46, 2993-3017,  
1307 1999.

1308 McKay, J. L., Pedersen, T. F., and Kienast, S. S.: Organic carbon accumulation over the last  
1309 16 kyr off Vancouver Island, Canada: Evidence for increased marine productivity during the  
1310 deglacial, *Quaternary Sci. Rev.*, 23, 261-281, [doi:10.1016/j.quascirev.2003.07.004](https://doi.org/10.1016/j.quascirev.2003.07.004), 2004.

1311 McLennan, S. M.: Sediments and soils: Chemistry and abundances, in: *Rock physics and*  
1312 *phase relations: A handbook of physical constants*, edited by: Ahrens, T. J., ~~pp. 8-20~~, AGU  
1313 Reference Shelf 3, AGU, Washington, [8-20](#), 1995.

1314 Menviel, L., Timmermann, A., Elison Timm, O., Mouchet, A., Abe-Ouchi, A., Chikamoto,  
1315 M. O., Harada, N., Ohgaito, R., and Okazaki, Y.: Removing the North Pacific halocline:  
1316 Effects on global climate, ocean circulation and the carbon cycle, *Deep-Sea Res. Pt. II*, 61-64,  
1317 106-113, [doi:10.1016/j.dsr2.2011.03.005](https://doi.org/10.1016/j.dsr2.2011.03.005), 2012.

1318 Middelburg, J. J., Soetaert, K., and Herman, P. M. J.: Empirical relationships for use in global  
1319 diagenetic models, *Deep-Sea Res. Pt. I*, 44, 327-344, 1997.

1320 Müller, P.: C/N ratios in Pacific deep-sea sediments: effect of inorganic ammonium and  
1321 organic nitrogen compounds sorbed by clays, *Geochim. Cosmochim. Ac.*, 41, 765-776, 1977.

1322 Müller, P. and Schneider, R.: An automated leaching method for the determination of opal in  
1323 sediments and particulate matter, *Deep-Sea Res. Pt. I*, 40, 425-444, 1993.

1324 Murray, R. W., Leinen, M., and Knowlton, C. W.: Links between iron input and opal  
1325 deposition in the Pleistocene equatorial Pacific Ocean, *Nat. Geosci.*, 5, 270-274,  
1326 [doi:10.1038/ngeo1422](https://doi.org/10.1038/ngeo1422), 2012.

1327 [Nagashima, K., Asahara, Y., Takeuchi, F., Harada, N., Toyoda, S., and Tada, R.: Contribution](#)  
1328 [of detrital materials from the Yukon River to the continental shelf sediments of the Bering](#)  
1329 [Sea based on the electron spin resonance signal intensity and crystallinity of quartz, \*Deep-Sea\*](#)  
1330 [Res. Pt. II, 61-64, 145-154, doi:10.1016/j.dsr2.2011.12.001, 2012.](#)

1331 Nakatsuka, T., Watanabe, K., Handa, N., Matsumoto, E., and Wada, E.: Glacial to interglacial  
1332 surface nutrient variations of Bering deep basins recorded by  $\delta^{13}\text{C}$  and  $\delta^{15}\text{N}$  of sedimentary  
1333 organic matter, *Paleoceanography*, 10, 1047-1061, 1995.

1334 Nameroff, T. J., Calvert, S. E., and Murray, J. W.: Glacial-interglacial variability in the  
1335 eastern tropical North Pacific oxygen minimum zone recorded by redox-sensitive trace  
1336 metals, *Paleoceanography*, 19, PA1010, [doi:10.1029/2003PA000912](https://doi.org/10.1029/2003PA000912), 2004.

1337 Narita, H., Sato, M., Tsunogai, S., Murayama, M., Ikehara, M., Nakatsuka, T., Wakatsuchi,  
1338 M., Harada, N., and Ujiie, Y.: Biogenic opal indicating less productive northwestern North  
1339 Pacific during the glacial ages, *Geophys. Res. Lett.*, 29, 1732, doi:10.1029/2001GL014320,  
1340 2002.

1341 Nelson, D. M., Tréguer, P., Brzezinski, M. A., Leynaert, A., and Quéguiner, B.: Production  
1342 and dissolution of biogenic silica in the ocean: Revised global estimates, comparison with  
1343 regional data and relationship to biogenic sedimentation, *Global Biogeochem. Cy.*, 9, 359-  
1344 372, 1995.

1345 Niebauer, H. J.: Effects of El Niño—Southern Oscillation and North Pacific weather patterns  
1346 on interannual variability in the subarctic Bering Sea, *J. Geophys. Res.*, 93, 5051-5068, 1988.

1347 Niebauer, H. J.: Variability in Bering Sea ice cover as affected by a regime shift in the North  
1348 Pacific in the period 1947-1996, *J. Geophys. Res.*, 103, 27717-27737, 1998.

1349 Niebauer, H. J., Alexander, V., and Henrichs, S.M.: A time-series study of the spring bloom  
1350 at the Bering Sea ice edge I. Physical processes, chlorophyll and nutrient chemistry. *Cont.*  
1351 *Shelf Res.*, 15, 1859-1877, 1995.

1352 Niebauer, H. J., Bond, N. A., Yakunin, L. P., and Plotnikov, V. V.: An update on the  
1353 climatology and sea ice of the Bering Sea. In: *Dynamics of the Bering Sea*, edited by:  
1354 Loughlin, T. R. and Ohtani, K., pp. 29-59, University of Alaska Sea Grant, [Fairbanks, Alaska,](#)  
1355 [29-59](#), 1999.

1356 North Greenland Ice Core Project members: High-resolution record of northern hemisphere  
1357 climate extending into the last interglacial period, *Nature*, 431, 147-151,  
1358 [doi:10.1038/nature02805](#), 2004.

1359 Nürnberg, C. C.: Bariumfluss und Sedimentation im südlichen Südatlantik-Hinweise auf  
1360 Produktivitätsänderungen im Quartär, *GEOMAR Reports* 38, Research Center for Marine  
1361 Geosciences (GEOMAR), Kiel, 105 pp., 1995.

1362 Nürnberg, C. C., Bohrmann, G., Schlüter, M., and Frank, M.: Barium accumulation in the  
1363 Atlantic sector of the Southern Ocean: Results from 190,000-year records. *Paleoceanography*,  
1364 12, 594-603, 1997.

1365 Nürnberg, D. and Tiedemann, R.: Environmental change in the Sea of Okhotsk during the last  
1366 1.1 million years, *Paleoceanography*, 19, PA4011, doi:10.1029/2004PA001023, 2004.



1367 Nürnberg, D., Wollenburg, I., Dethleff, D., Eicken, H., Kassens, H., Letzig, T., Reimnitz, E.,  
1368 and Thiede, J.: Sediments in Arctic sea ice: Implications for entrainment, transport and  
1369 release, *Mar. Geol.*, 119, 185-214, 1994.

1370 Nürnberg, D., Dethleff, D., Tiedemann, R., Kaiser, A., and Gorbarenko, S. A.: Okhotsk Sea  
1371 ice coverage and Kamchatka glaciation over the last 350 ka – Evidence from ice-rafted debris  
1372 and planktonic  $\delta^{18}\text{O}$ , *Palaeogeogr. Palaeoclimatol.*, 310, 191-205, [doi:10.1016/j.palaeo.2011.07.011](https://doi.org/10.1016/j.palaeo.2011.07.011),  
1373 2011.

1374 Ohkushi, K., Itaki, T., and Nemoto, N.: Last glacial-Holocene change in intermediate-water  
1375 ventilation in the northwestern Pacific, *Quaternary Sci. Rev.*, 22, 1477-1484,  
1376 [doi:10.1016/S0277-3791\(03\)00082-9](https://doi.org/10.1016/S0277-3791(03)00082-9), 2003.

1377 Ohkushi, K., Uchida, M., Ahagon, N., Mishima, T., and Kanematsu, T.: Glacial intermediate  
1378 water ventilation in the northwestern Pacific based on AMS radiocarbon dating, *Nucl.*  
1379 *Instrum. Meth. B*, 223-224, 460-465, [doi:10.1016/j.nimb.2004.04.087](https://doi.org/10.1016/j.nimb.2004.04.087), 2004.

1380 Okada, M., Takagi, M., Narita, H., and Takahashi, K.: Chronostratigraphy of sediment cores  
1381 from the Bering Sea and the subarctic Pacific based on paleomagnetic and oxygen isotopic  
1382 analyses, *Deep-Sea Res. Pt. II*, 52, 2092-2109, [doi:10.1016/j.dsr2.2005.08.004](https://doi.org/10.1016/j.dsr2.2005.08.004), 2005.

1383 Okazaki, Y., Takahashi, K., Asahi, H., Katsuki, K., Hori, J., Yasuda, H., Sagawa, Y., and  
1384 Tokuyama, H.: Productivity changes in the Bering Sea during the late Quaternary, *Deep-Sea*  
1385 *Res. Pt. II*, 52, 2150-2162, [doi:10.1016/j.dsr2.2005.07.003](https://doi.org/10.1016/j.dsr2.2005.07.003), 2005.

1386 Okazaki, Y., Timmermann, A., Menviel, L., Harada, N., Abe-Ouchi, A., Chikamoto, M. O.,  
1387 Mouchet, A., and Asahi, H.: Deepwater formation in the North Pacific during the Last Glacial  
1388 Maximum, *Science*, 329, 200-204, [doi:10.1126/science.1190612](https://doi.org/10.1126/science.1190612), 2010.

1389 [Okazaki, Y., Sagawa, T., Asahi, H., Horikawa, K., and Onodera, J.: Ventilation changes in](https://doi.org/10.5194/cp-8-17-2012)  
1390 [the western North Pacific since the last glacial period, \*Clim. Past\*, 8, 17-24, doi:10.5194/cp-8-](https://doi.org/10.5194/cp-8-17-2012)  
1391 [17-2012, 2012.](https://doi.org/10.5194/cp-8-17-2012)

1392 Oriens, K. J. and Bruland, K. W.: The biogeochemistry of aluminium in the Pacific Ocean,  
1393 *Earth Planet. Sc. Lett.*, 78, 397-410, 1986.

1394 Ortiz, J. D., O'Connell, S. B., DelViscio, J., Dean, W., Carriquiry, J. D., Marchitto, T., Zheng,  
1395 Y., and van Geen, A.: Enhanced marine productivity off western North America during warm  
1396 climate intervals of the past 52 k.y., *Geology*, 32, 521-524, [doi:10.1130/G20234.1](https://doi.org/10.1130/G20234.1), 2004.

- 1397 Overland, J. E., Adams, J. M., and Bond, N. A.: Decadal variability of the Aleutian Low and  
1398 its relation to high-latitude circulation, *J. Climate*, 12, 1542-1548, 1999.
- 1399 Overland, J. E., Bond, N. A., and Adams, J. M.: The relation of surface forcing of the Bering  
1400 Sea to large-scale climate patterns, *Deep-Sea Res. Pt. II*, 49, 5855-5868, [doi:10.1016/S0967-](https://doi.org/10.1016/S0967-0645(02)00322-3)  
1401 [0645\(02\)00322-3](https://doi.org/10.1016/S0967-0645(02)00322-3), 2002.
- 1402 Paillard, D., Labeyrie, L., and Yiou, P.: Macintosh program performs time-series analysis,  
1403 EOS T. [Am. Geophys. Un., 77, p. 379, doi:10.1029/96EO00259,](https://doi.org/10.1029/96EO00259) ~~transactions, 77, 379,~~ 1996.
- 1404 Pondaven, P., Ragueneau, O., Tréguer, P., Hauvespre, A., Dezileau, L., and Reyss, J. L.:  
1405 Resolving the 'opal paradox' in the Southern Ocean, *Nature*, 405, 168-172, 2000.
- 1406 Pushkar, V. S., Roof, S. R., Cherepanova, M. V., Hopkins, D. M., and Brigham-Grette, J.:  
1407 Paleogeographic and paleoclimatic significance of diatoms from middle Pleistocene marine  
1408 and glaciomarine deposits on Baldwin Peninsula, northwestern Alaska, *Palaeogeogr.*  
1409 *Palaeocl.*, 152, 67-85, 1999.
- 1410 Pye, K.: *Aeolian dust and dust deposits*, Academic Press, London, 334 pp., 1987.
- 1411 Ragueneau, O., Tréguer, P., Leynaert, A., Anderson, R. F., Brzezinski, M. A., DeMaster, D.  
1412 J., Dugdale, R. C., Dymond, J., Fischer, G., Francois, R., Heinze, C., Maier-Reimer, E.,  
1413 Martin-Jézéquel, V., Nelson, D. M., and Quéguiner, B.: A review of the Si cycle in the  
1414 modern ocean: recent progress and missing gaps in the application of biogenic opal as a  
1415 paleoproductivity proxy, *Global Planet. Change*, 26, 317-365, 2000.
- 1416 Rasmussen, S. O., Andersen, K. K., Svensson, A. M., Steffensen, J. P., Vinther, B. M.,  
1417 Clausen, H. B., Siggaard-Andersen, M.-L., Johnsen, S. J., Larsen, L. B., Dahl-Jensen, D.,  
1418 Bigler, M., Röthlisberger, R., Fischer, H., Goto-Azuma, K., Hansson, M. E., and Ruth, U.: A  
1419 new Greenland ice core chronology for the last glacial termination, *J. Geophys. Res.*, 111,  
1420 D06102, [doi:10.1029/2005JD006079](https://doi.org/10.1029/2005JD006079), 2006.
- 1421 Redfield, A. C., Ketchum, B. H., and Richards, F. A.: The influence of organisms on the  
1422 composition of seawater. In: *The Sea*, Vol. 2, edited by: Hill, M. N., ~~pp. 26-77,~~ Wiley-  
1423 Interscience, New York, [26-77](https://doi.org/10.1002/9781118164729.ch2), 1963.
- 1424 Reed, R. K., Khen, G. V., Stabeno, P. J., and Verkhunov, A. V.: Water properties and flow  
1425 over the deep Bering Sea basin, summer 1991, *Deep-Sea Res. Pt. I*, 40, 2325-2334, 1993.

1426 Rella, S. F., Tada, R., Nagashima, K., Ikehara, M., Itaki, T., Ohkushi, K., Sakamoto, T.,  
1427 Harada, N., and Uchida, M.: Abrupt changes of intermediate water properties on the  
1428 northeastern slope of the Bering Sea during the last glacial and deglacial period,  
1429 *Paleoceanography*, 27, PA3203, doi:10.1029/2011PA002205, 2012.

1430 Richter, T., van der Gaast, S., Koster, B., Vaars, A., Gieles, R., de Stigter, H., De Haas, H.,  
1431 and van Weering, T.: The Avaatech XRF core scanner: technical description and applications  
1432 to NE Atlantic sediments, in: *New Techniques in Sediment Core Analyses*, edited by:  
1433 *Rothwell, R.G.*, Geol. Soc. Spec. Publ., 267, 39-50, doi:10.1144/GSL.SP.2006.267.01.03,  
1434 2006.

1435 Riethdorf, J.-R., Max, L., Nürnberg, D., Lembke-Jene, L., and Tiedemann, R.: Deglacial  
1436 development of (sub) sea surface temperature and salinity in the subarctic northwest Pacific:  
1437 Implications for upper-ocean stratification, ~~in review at~~ *Paleoceanography*, accepted  
1438 manuscript online, doi:10.1002/palo.20014, 2013.-

1439 Ronov, A. B. and Migdisov, A. A.: Geochemical history of the crystalline basement and the  
1440 sedimentary cover of the Russian and North American platforms, *Sedimentology*, 16, 137-  
1441 185, 1971.

1442 Rösler, H. J. and Lange, H.: *Geochemical tables*, Elsevier, New York, 468 pp., 1972.

1443 Sagawa, T. and Ikehara, K.: Intermediate water ventilation change in the subarctic northwest  
1444 Pacific during the last deglaciation, *Geophys. Res. Lett.*, 35, L24702,  
1445 doi:10.1029/2008GL035133, 2008.

1446 Ruth, U., Wagenbach, D., Steffensen, J. P., and Bigler, M.: Continuous record of  
1447 microparticle concentration and size distribution in the central Greenland NGRIP ice core  
1448 during the last glacial period, *J. Geophys. Res.*, 108 (D3), 4098, doi:10.1029/2002JD002376,  
1449 2003.

1450 Sancetta, C.: Effect of Pleistocene glaciation upon oceanographic characteristics of the North  
1451 Pacific Ocean and Bering Sea, *Deep-Sea Res.*, 30, 8A, 851-869, 1983.

1452 Sarnthein, M., Statterger, K., Dreger, D., Erlenkeuser, H., Grootes, P., Haupt, B. J., Jung, S.,  
1453 Kiefer, T., Kuhnt, W., Pflaumann, U., Schäfer-Neth, C., Schulz, H., Schulz, M., Seidov, D.,  
1454 Simstich, J., van Kreveld, S., Vogelsang, E., Völker, A., and Weinelt, M.: Fundamental  
1455 modes and abrupt changes in North Atlantic circulation and climate over the last 60 ky –

1456 Concepts, reconstruction and numerical modeling. *In*: The northern North Atlantic: A  
1457 changing environment, edited by: Schäfer, P., Ritzrau, W., Schlüter, M., and Thiede, J., pp.  
1458 ~~365-410~~, Springer, Berlin, 365-410, 2001.

1459 Sarnthein, M., Grootes, P. M., Kennett, J. P., and Nadeau, M.-J.: <sup>14</sup>C reservoir ages show  
1460 deglacial changes in ocean currents and carbon cycle. *In*: Past and Future Changes of the  
1461 Oceanic Meridional Overturning Circulation: Mechanisms and Impacts, edited by:  
1462 Schmittner, A., Chiang, J. C. H., and Hemming, S. R., pp. ~~175-196~~, AGU Monograph Series  
1463 173, AGU, Washington, D.C., 175-196, 2007.

1464 Sato, M. M., Narita, H., and Tsunogai, S.: Barium increasing prior to opal during the last  
1465 termination of glacial ages in the Okhotsk Sea sediments, *J. Oceanogr.*, 58, 461-467, 2002.

1466 Schlitzer, R.: Ocean Data View, <http://odv.awi.de/>, (last access: 6 August 2012), 2011.

1467 Schmitz, B.: The TiO<sub>2</sub>/Al<sub>2</sub>O<sub>3</sub> ratio in the Cenozoic Bengal abyssal fan sediments and its use  
1468 as a paleostream energy indicator, *Mar. Geol.*, 76, 195-206, 1987.

1469 Schneider, R. R., Price, B., Müller, P. J., Kroon, D., and Alexander, I.: Monsoon related  
1470 variations in Zaire (Congo) sediment load and influence of fluvial silicate supply on marine  
1471 productivity in the east equatorial Atlantic during the last 200,000 years, *Paleoceanography*,  
1472 12, 463-481, 1997.

1473 Seki, O., Kawamura, K., Nakatsuka, T., Ohnishi, K., Ikehara, M., and Wakatsuchi, M.:  
1474 Sediment core profiles of long-chain n-alkanes in the Sea of Okhotsk: Enhanced transport of  
1475 terrestrial organic matter from the last deglaciation to the early Holocene, *Geophys. Res.*  
1476 *Lett.*, 30, 1001, doi:10.1029/2001GL014464, 2003.

1477 Shackleton, N. J. and Hall, M. A.: Oxygen and carbon isotope stratigraphy of Deep Sea  
1478 Drilling Project Hole 552A: Plio-Pleistocene glacial history. *In*: Initial Reports DSDP, 81,  
1479 edited by: Roberts, D. G., Schnitker, D., ~~et al~~ Backman, J., Baldauf, J. G., Desprairies, A.,  
1480 Homrighausen, R., Huddleston, P., Kaltenback, A. J., Krumsiek, K. A. O., Morton, A. C.,  
1481 Murray, J. W., Westberg-Smith, J., and Zimmermann, H. B., pp. ~~599-609~~, ~~Washington (U.S.~~  
1482 ~~Govt. Printing Office)~~, Washington, 599-609, doi:10.2973/dsdp.proc.81.116.1984, 1984.

1483 Shigemitsu, M., Narita, H., Watanabe, Y. W., Harada, N., and Tsunogai, S.: Ba, Si, U, Al, Sc,  
1484 La, Th, C and <sup>13</sup>C/<sup>12</sup>C in a sediment core in the western subarctic Pacific as proxies of past  
1485 biological production, *Mar. Chem.*, 106, 442-455, doi:10.1016/j.marchem.2007.04.004, 2007.

1486 Sigman, D. M. and Boyle, E. A.: Glacial/interglacial variations in atmospheric carbon  
1487 dioxide, *Nature*, 407, 859-869, 2000.

1488 Sigman, D. M., Jaccard, S. L., and Haug, G. H.: Polar ocean stratification in a cold climate,  
1489 *Nature*, 428, 59-63, [doi:10.1038/nature02357](https://doi.org/10.1038/nature02357), 2004.

1490 Sigman, D. M., Hain, M. P., and Haug, G. H.: The polar ocean and glacial cycles in  
1491 atmospheric CO<sub>2</sub> concentration, *Nature*, 466, 47-55, [doi:10.1038/nature09149](https://doi.org/10.1038/nature09149), 2010.

1492 Springer, A. M., McRoy, C. P., and Flint, M. V.: The Bering Sea green belt: shelf-edge  
1493 processes and ecosystem production, *Fish. Oceanogr.*, 5, 205-223, 1996.

1494 Stabeno, P. J., Schumacher, J. D., and Ohtani, K.: The physical oceanography of the Bering  
1495 Sea, *In: Dynamics of the Bering Sea*, edited by: Loughlin, T. R. and Ohtani, K., [pp. 1-28](#),  
1496 University of Alaska Sea Grant, [Fairbanks, Alaska, 1-28](#), 1999.

1497 Stein, R.: Arctic Ocean sediments: Processes, proxies, and paleoenvironment, *in: Vol. 2 of*  
1498 *Developments in Marine Geology*, [vol. 2](#), edited by: Chamley, H., Elsevier, Amsterdam, 592  
1499 pp., 2008.

1500 Széreméta, N., Bassinot, F., Balut, Y., Labeyrie, L., and Pagel, M.: Oversampling of  
1501 sedimentary series collected by giant piston corer: Evidence and corrections based on 3.5-kHz  
1502 chirp profiles, *Paleoceanography*, 19, PA1005, [doi:10.1029/2002PA000795](https://doi.org/10.1029/2002PA000795), 2004.

1503 Takahashi, K.: The Bering and Okhotsk Sea: Modern and past paleoceanographic changes  
1504 and gateway impact, *J. Asian Earth Sci.*, 16, 49-58, 1998.

1505 Takahashi, K.: Paleoceanographic changes and present environment of the Bering Sea, *In:*  
1506 *Dynamics of the Bering Sea*, edited by: Loughlin, T. R. and Ohtani, K., [pp. 365-385](#),  
1507 University of Alaska Sea Grant, [Fairbanks, Alaska, 365-385](#), 1999.

1508 Takahashi, K.: The Bering Sea and paleoceanography, *Deep-Sea Res. Pt. II*, 52, 2080-2091,  
1509 [doi:10.1016/j.dsr2.2005.08.003](https://doi.org/10.1016/j.dsr2.2005.08.003), 2005.

1510 Takahashi, T., Sutherland, S. C., Sweeney, C., Poisson, A., Metzl, N., Tilbrook, B., Bates, N.,  
1511 Wanninkhof, R., Feely, R. A., Sabine, C., Olafsson, J., and Nojiri, Y.: Global sea—air CO<sub>2</sub>  
1512 flux based on climatological surface ocean pCO<sub>2</sub> and seasonal biological and temperature  
1513 effects, *Deep-Sea Res. Pt. II*, 49, 1601-1622, [doi:10.1016/S0967-0645\(02\)00003-6](https://doi.org/10.1016/S0967-0645(02)00003-6), 2002a.

- 1514 Takahashi, K., Fujitani, N., and Yanada, M.: Long term monitoring of particle fluxes in the  
1515 Bering Sea and the central subarctic Pacific Ocean, 1990-2000, *Progr. Oceanogr.*, 55, 95-112,  
1516 [doi:10.1016/S0079-6611\(02\)00072-1](https://doi.org/10.1016/S0079-6611(02)00072-1), 2002b.
- 1517 [Takahashi, K., Ravelo, A. C., Alvarez Zarikian, C. A., and the Expedition 323 Scientists:  
1518 Bering Sea Paleoceanography, Proceedings of the Integrated Ocean Drilling Program, 323,  
1519 Tokyo \(Integrated Ocean Drilling Program Management International, Inc.\),  
1520 doi:10.2204/iodp.proc.323.2011.](https://doi.org/10.2204/iodp.proc.323.2011)
- 1521 Tanaka, S. and Takahashi, K.: Late Quaternary paleoceanographic changes in the Bering Sea  
1522 and the western subarctic Pacific based on radiolarian assemblages, *Deep-Sea Res. Pt. II*, 52,  
1523 2131-2149, [doi:10.1016/j.dsr2.2005.07.002](https://doi.org/10.1016/j.dsr2.2005.07.002), 2005.
- 1524 Taylor, S. R.: Abundance of chemical elements in the continental crust: a new table,  
1525 *Geochim. Cosmochim. Ac.*, 28, 1273-1285, 1964.
- 1526 Taylor, S. R. and McLennan, S. M.: The geochemical evolution of the continental crust, *Rev.*  
1527 *Geophys.*, 33, 241-265, 1995.
- 1528 Taylor, S. R., McLennan, S. M., and McCulloch, M. T.: Geochemistry of loess, continental  
1529 crust composition and crustal model ages, *Geochim. Cosmochim. Ac.*, 47, 1897-1905, 1983.
- 1530 Ternois, Y., Kawamura, L., Keigwin, L., Ohkouchi, N., and Nakatsuka, T.: A biomarker  
1531 approach for assessing marine and terrigenous inputs to the sediments of Sea of Okhotsk for  
1532 the last 27,000 years, *Geochim. Cosmochim. Ac.*, 65, 791-802, 2001.
- 1533 Thunell, R. C., Varela, R., Llano, M., Collister, J., Muller-Karger, F., and Bohrer, R.: Organic  
1534 carbon fluxes, degradation, and accumulation in an anoxic basin: Sediment trap results from  
1535 the Cariaco Basin, *Limnol. Oceanogr.*, 45, 300-308, 2000.
- 1536 Tjallingii, R., Röhl, U., Kölling, M., and Bickert, T.: Influence of the water content on X-ray  
1537 fluorescence core-scanning measurements in soft marine sediments, *Geochem. Geophys.*  
1538 *Geosy.*, 8, Q02004, [doi:10.1029/2006GC001393](https://doi.org/10.1029/2006GC001393), 2007.
- 1539 Tomczak, M. and Godfrey, J. S.: *Regional oceanography: An introduction*, Elsevier Science  
1540 Ltd., Oxford, 391 pp., 1994.

1541 Tyrrell, T., Merico, A., Waniek, J. J., Wong, C. S., Metzl, N., and Whitney, F.: Effect of  
1542 seafloor depth on phytoplankton blooms in high-nitrate, low-chlorophyll (HNLC) regions, *J.*  
1543 *Geophys. Res.*, 110, G02007, doi:10.1029/2005JG000041, 2005.

1544 van Geen, A., Zheng, Y., Bernhard, J. M., Cannariato, K. G., Carriquiry, J., Dean, W. E.,  
1545 Eakins, B. W., Ortiz, J. D., and Pike, J.: On the preservation of laminated sediments along the  
1546 western margin of North America, *Paleoceanography*, 18, 1098, doi:10.1029/2003PA000911,  
1547 2003.

1548 [VanLaningham, S., Piasias, N. G., Duncan, R. A., and Clift, P. D.: Glacial-interglacial](#)  
1549 [sediment transport to the Meiji Drift, northwest Pacific Ocean: Evidence for timing of](#)  
1550 [Beringian outwashing, \*Earth Planet. Sci. Lett.\*, 277, 64-72, doi:10.1016/j.epsl.2008.09.033,](#)  
1551 [2009.](#)

1552 Waelbroeck, C., Labeyrie, L., Michel, E., Duplessy, J. C., McManus, J. F., Lambeck, K.,  
1553 Balbon, E., and Labracherie, M.: Sea-level and deep water temperature changes derived from  
1554 benthic foraminifera isotopic records, *Quaternary Sci. Rev.*, 21, 295-305, doi:10.1016/S0277-  
1555 [3791\(01\)00101-9](#), 2002.

1556 Wang, Y. J., Cheng, H., Edwards, R. L., An, Z. S., Wu, J. Y., Shen, C.-C., and Dorale, J. A.:  
1557 A high-resolution absolute-dated Late Pleistocene monsoon record from Hulu cave, China,  
1558 *Science*, 294, 2345-2348, 2001.

1559 Wang, Y., Cheng, H., Edwards, R. L., Kong, X., Shao, X., Chen, S., Wu, J., Jiang, X., Wang,  
1560 X., and An, Z.: Millennial- and orbital-scale changes in the East Asian monsoon over the past  
1561 224,000 years, *Nature*, 451, 1090-1093, doi:10.1038/nature06692, 2008.

1562 Warren, B.: Why is no deepwater formed in the North Pacific? *J. Mar. Res.*, 41, 327-347,  
1563 1983.

1564 Wedepohl, K. H.: Environmental influences on the chemical composition of shales and clays,  
1565 in: *Physics and chemistry of the Earth*, edited by: Ahrens, L., Press, K., Runcorn, S., and  
1566 Urey, H., pp. ~~307-333~~, Pergamon Press, Oxford, [307-333](#), 1971.

1567 Yarincik, K. M., Murray, R. W., and Peterson, L. C.: Climatically sensitive eolian and  
1568 hemipelagic deposition in the Cariaco Basin, Venezuela, over the past 578,000 years: Results  
1569 from Al/Ti and K/Al, *Paleoceanography*, 15, 210-228, 2000.

1570 Yasonov, P. G., Nourgaliev, D. C., Bourov, B. V., and Heller, F.: A modernized coercivity  
1571 spectrometer, *Geol. Carpath.*, 49, 224-226, 1998.

1572 Yasuda, I.: The origin of the North Pacific Intermediate Water, *J. Geophys. Res.*, 102, 893-  
1573 909, 1997.

1574 Zhang, J., Woodgate, R., and Moritz, R.: Sea ice response to atmospheric and oceanic forcing  
1575 in the Bering Sea, *J. Phys. Oceanogr.*, 40, 1729-1747, [doi:10.1175/2010JPO4323.1](https://doi.org/10.1175/2010JPO4323.1), 2010.

1576 Zheng, Y., van Geen, A., Anderson, R. F., Gardner, J. V., and Dean, W. E.: Intensification of  
1577 the northeast Pacific oxygen minimum zone during the Bölling-Alleröd warm period,  
1578 *Paleoceanography*, 15, 528-536, 2000.

1579 Ziegler, M., Jilbert, T., de Lange, G. J., Lourens, L. J., and Reichart, G.-J.: Bromine counts  
1580 from XRF scanning as an estimate of the marine organic carbon content of sediment cores,  
1581 *Geochem. Geophys. Geosy.*, 9, Q05009, [doi:10.1029/2007GC001932](https://doi.org/10.1029/2007GC001932), 2008.

1582

1583

1584

1585

1586

1587

1588

1589

1590

1591

1592

1593

1594

1595

1596



1597 **Tables**

Table 1: Site Information.

Core	Latitude	Longitude	Depth (m <u>b.s.l.</u> )	Recovery (m)
SO201-2-77KL	56°19.83'N	170°41.98'E	2135	11.78
SO201-2-85KL	57°30.30'N	170°24.77'E	968	18.13
SO201-2-101KL	58°52.52'N	170°41.45'E	630	18.32

1598

1599

1600

1601

1602

1603

1604

1605

1606

1607

1608

1609

1610

1611

1612

1613

1614

1615

1616

1617

1618

1619

Table 2: Statistics of Parameters Approximating Marine Productivity.

Parameter	SO201-2-77KL		SO201-2-85KL		SO201-2-101KL	
	Avg.	StDev.	Avg.	StDev.	Avg.	StDev.
TOC (wt.%)	0.85	0.30	0.96	0.36	0.88	0.16
[C/N] <sub>a</sub>	13.0	2.9	11.9	1.6	12.4	1.6
Opal (wt.%)	9.5	9.7	3.3	3.2	2.9	1.3
CaCO <sub>3</sub> (wt.%)	1.9	3.2	1.9	2.2	1.2	0.7
Ba <sub>bio</sub> <sup>(1)</sup> (ppm)	733	330	436	141	260	85
P <sub>New</sub> <sup>(2)</sup> (gC m <sup>-2</sup> yr <sup>-1</sup> )	50.6	47.5	34.9	21.5	29.9	21.1
PP <sup>(3)</sup> (gC m <sup>-2</sup> yr <sup>-1</sup> )	131.9	54.2	113.1	34.8	102.9	37.6

<sup>(1)</sup>via Al using the global average Ba/Al of pelitic rocks of 6.5 mg g<sup>-1</sup> (Wedepohl, 1971)

<sup>(2)</sup>after Nürnberg (1995)

<sup>(3)</sup>after Eppley and Peterson (1979)

1620

1621

1622

1623

1624

1625

1626

1627

1628

1629

1630

1631

1632

1633

1634

1635

1636

1637

1638

Table 3: Statistics of Parameters Approximating Terrigenous Matter Supply.

Parameter	SO201-2-77KL		SO201-2-85KL		SO201-2-101KL	
	Avg.	StDev.	Avg.	StDev.	Avg.	StDev.
>63 $\mu\text{m}$ (wt.%)	5.6	3.1	7.5	5.4	7.9	7.4
%Siliciclastics	88.9	8.8	94.1	4.4	94.9	1.5
%Terrigen (Al-norm.) <sup>(1)</sup>	82.7	10.2	88.2	7.3	89.3	5.9
%Terrigen (Ti-norm.) <sup>(2)</sup>	76.6	9.6	84.4	8.4	83.8	6.2
[Ti] ( $\mu\text{mol g}^{-1}$ )	86.4	10.9	95.2	9.5	94.5	7.0
[Fe] ( $\mu\text{mol g}^{-1}$ )	762	112	792	96	740	90
[Al] ( $\mu\text{mol g}^{-1}$ )	2578	316	2751	227	2783	185

<sup>(1)</sup>using [Al] = 3117  $\mu\text{mol g}^{-1}$  of average continental crust (Taylor and McLennan, 1995)

<sup>(2)</sup>using [Ti] = 112.8  $\mu\text{mol g}^{-1}$  of average continental crust (Taylor and McLennan, 1995)

1639

1640

1641

1642

1643

1644

1645

1646

1647

1648

1649

1650

1651

1652

1653

1654

1655

1656

1657

1658

Table 4: Ranges, Averages and Variability of Atomic-Molar Elemental Ratios in Cores SO201-2-77KL, -85KL, and -101KL.

	SO201-2-77KL		SO201-2-85KL		SO201-2-101KL	
	Al/Ti	Fe/Al	Al/Ti	Fe/Al	Al/Ti	Fe/Al
Average	29.9	0.30	29.0	0.29	29.5	0.26
<del>Standard deviation</del> <u>Dev.</u>	1.5	0.03	1.5	0.02	1.2	0.02
Maximum	34.1	0.34	32.3	0.36	32.4	0.30
Minimum	24.9	0.17	22.1	0.23	27.8	0.21

1659

1660

1661

1662

1663

1664

1665

1666

1667

1668

1669

1670

1671

1672

1673

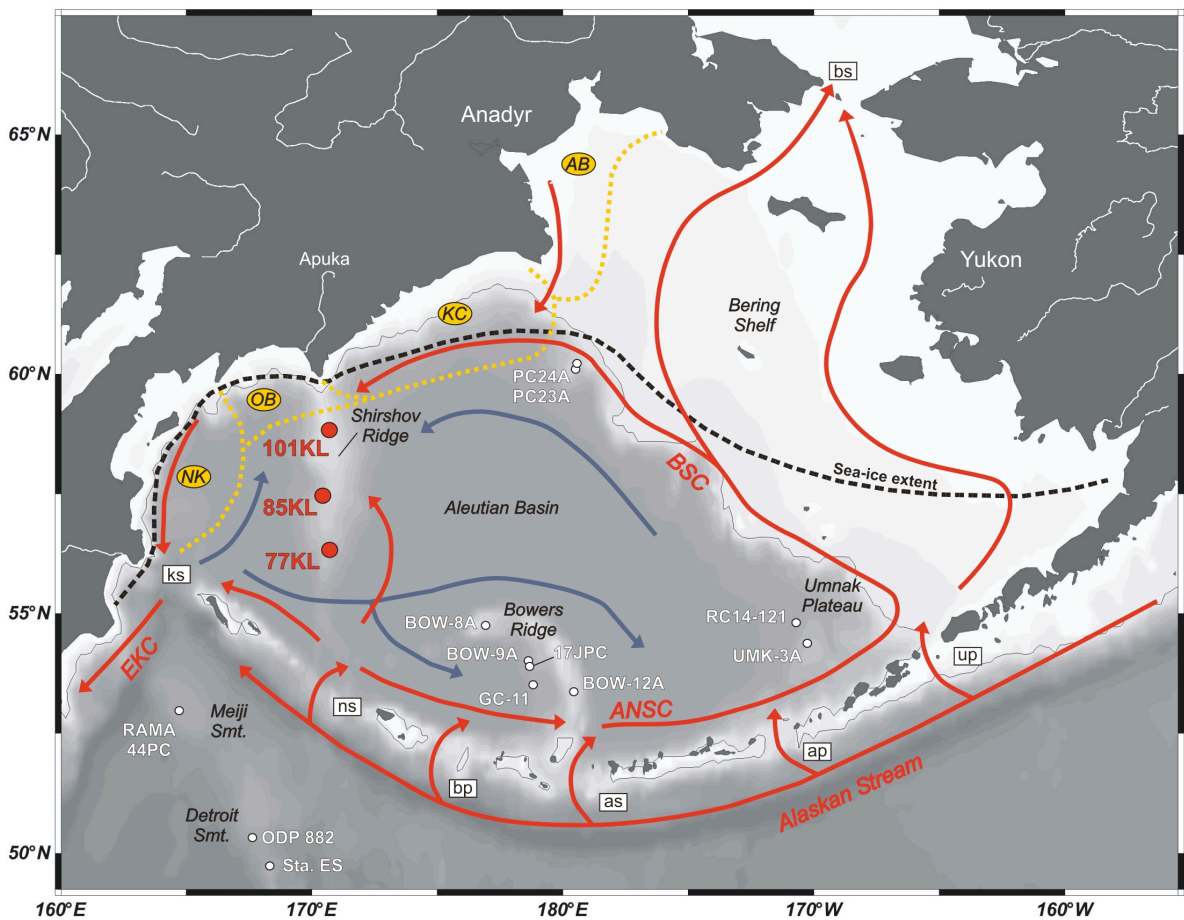
1674

1675

1676

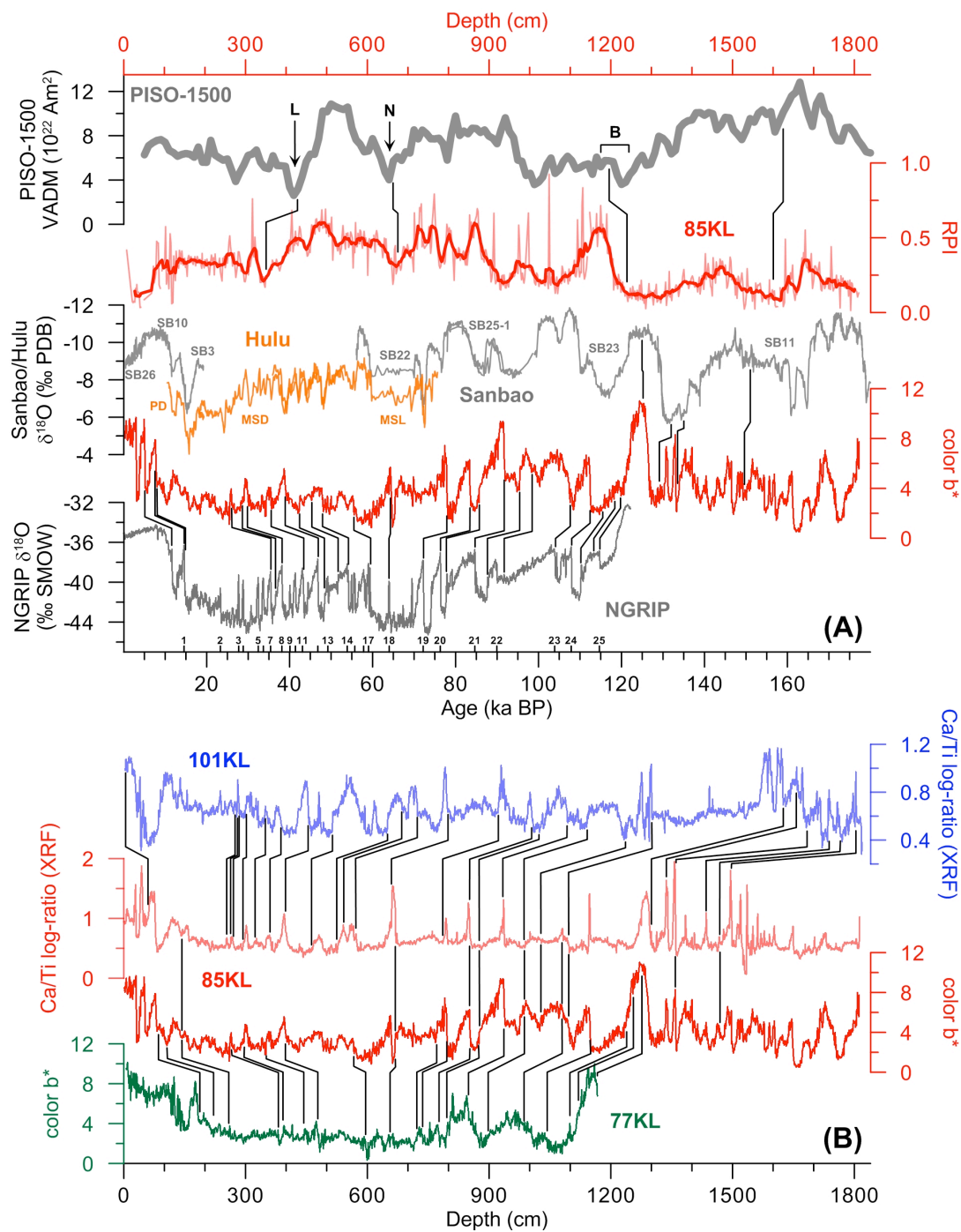
1677

1678



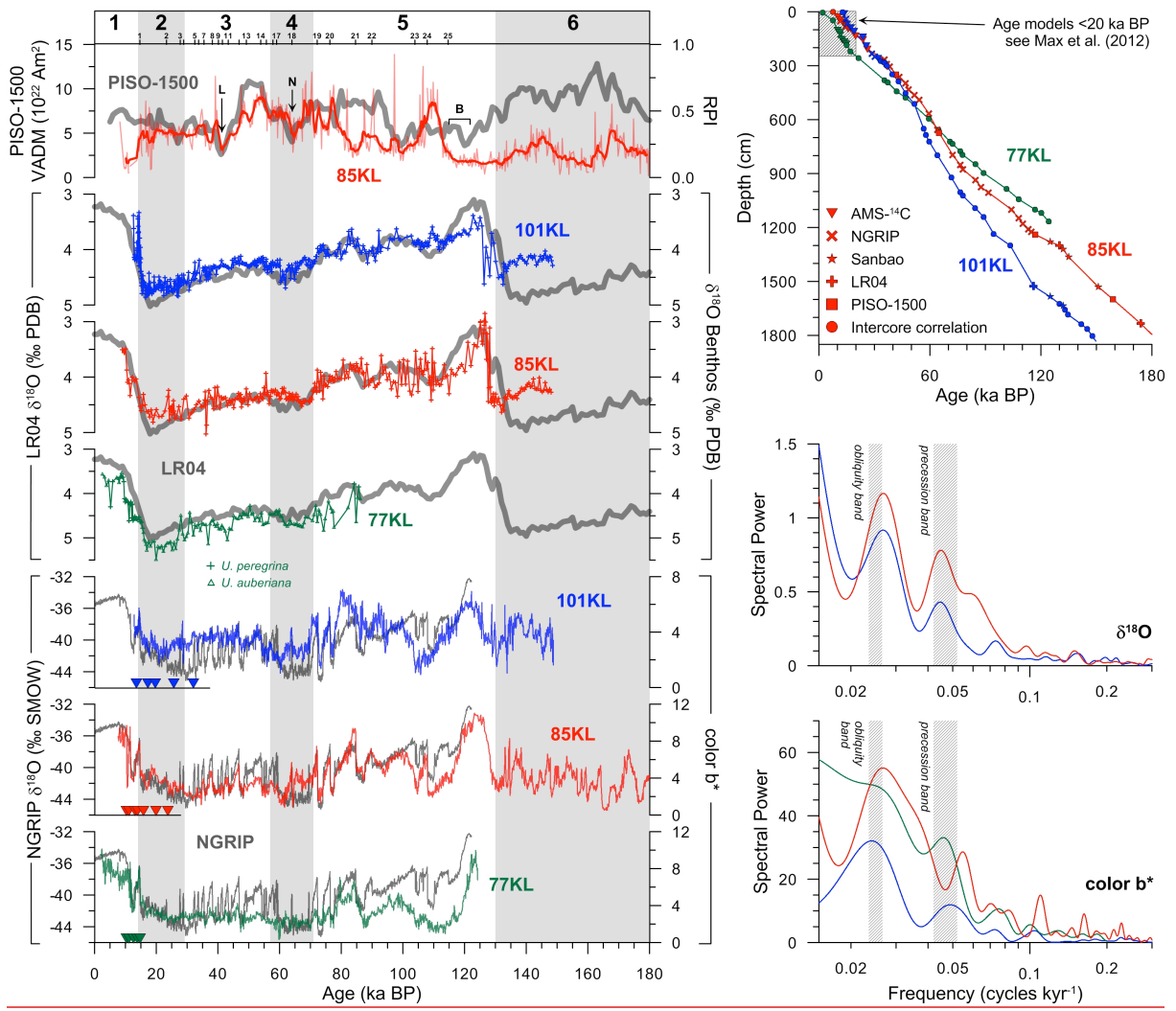
1681

1682 Figure 1: Bathymetric map of the study area with 250 m isobathe. Locations of sediment  
 1683 cores SO201-2-77KL, -85KL, and -101KL are marked by red dots. White dots indicate  
 1684 reference records referred to in this study. Meiji Seamount: RAMA44PC (Keigwin et al.,  
 1685 1992). Detroit Seamount: ODP Site 882 (Jaccard et al., 2005), KH99-3 Sta. ES (Narita et al.,  
 1686 2002). Bowers Ridge: GC-11 (Gorbarenko, 1996; Gorbarenko et al., 2005, 2010), KH99-3-  
 1687 BOW-8A, -9A, and -12A (Katsuki and Takahashi, 2005; Okada et al., 2005; Okazaki et al.,  
 1688 2005; Tanaka and Takahashi, 2005), HLY02-02-17JPC (Brunelle et al., 2007, 2010). Umnak  
 1689 Plateau: KH99-3-UMK-3A (Okada et al., 2005; Okazaki et al., 2005; Tanaka and Takahashi,  
 1690 2005), RC14-121 (Cook et al., 2005). Northern slope: MR06-04-PC23A and -PC24A (Itaki et  
 1691 al., 2009; Khim et al., 2010; Kim et al., 2011; Rella et al., 2012). Dashed black line indicates  
 1692 average maximum sea-ice extent (after Niebauer et al., 1999; Zhang et al., 2010). Dotted  
 1693 yellow line shows mineralogical provinces of coarse silts (after Lisitzin, 2002). The surface  
 1694 and deep circulation patterns (after Stabeno et al., 1999) are indicated by red and blue arrows,  
 1695 respectively. Mineralogical provinces: NK = Northern Kamchatka, OB = Olyutorskii Bay, KC  
 1696 = Koryak Coast, AB = Anadyr Bay. Surface currents: ANSC = Aleutian North Slope Current,  
 1697 BSC = Bering Slope Current, EKC = East Kamchatka Current. Straits: ks = Kamchatka Strait,  
 1698 ns = Near Strait, bp = Buldir Pass, as = Amchitka Strait, ap = Amukta Pass, up = Unimak  
 1699 Pass, bs = Bering Strait. This map was generated with "Ocean Data View" (Schlitzer, 2011).

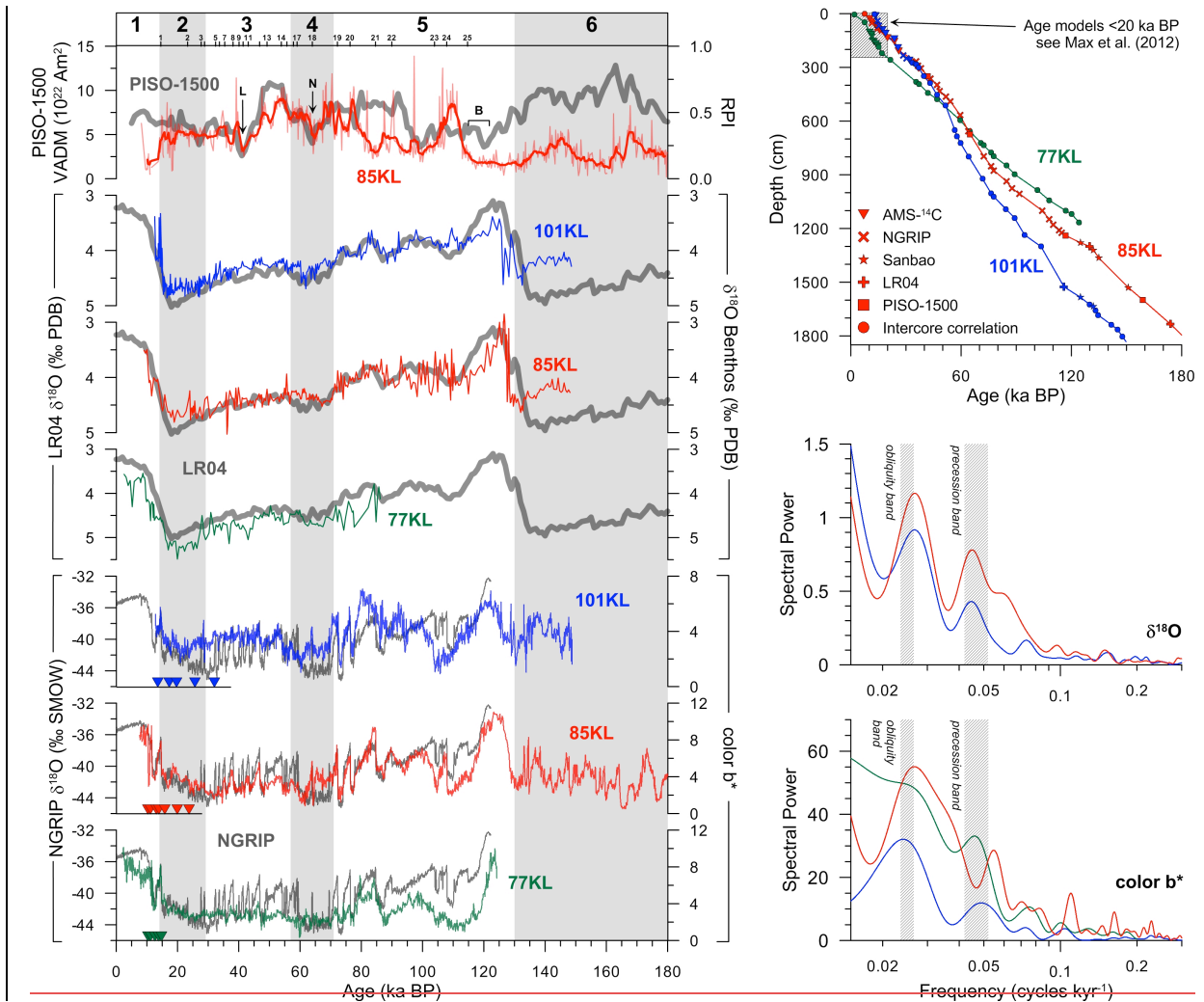


1701

1702 Figure 2: (A) Correlation of sediment core SO201-2-85KL with the PISO-1500 (thick grey  
 1703 line) paleomagnetic reference record (Channell et al., 2009) based on relative paleointensity  
 1704 (RPI, smoothed by a 5-point-running average), as well as with the Sanbao (grey lines) and  
 1705 Hulu (orange lines) stalagmite  $\delta^{18}\text{O}$  records (Wang et al., 2001, 2008) and the NGRIP  $\delta^{18}\text{O}$   
 1706 record (NGRIP members, 2004; GICC05 timescale, Rasmussen et al., 2006) based on color  
 1707  $b^*$ . Black lines mark correlation lines. The Laschamp (L), Norwegian-Greenland Sea (N), and  
 1708 Blake (B) paleomagnetic events are indicated. Bottom numbers mark D-O events. (B)  
 1709 Intercore correlation of sediment cores SO201-2-77KL (green) and -101KL (blue) with core -  
 1710 85KL (red) is based on color  $b^*$  and XRF Ca/Ti log-ratio records.



1711



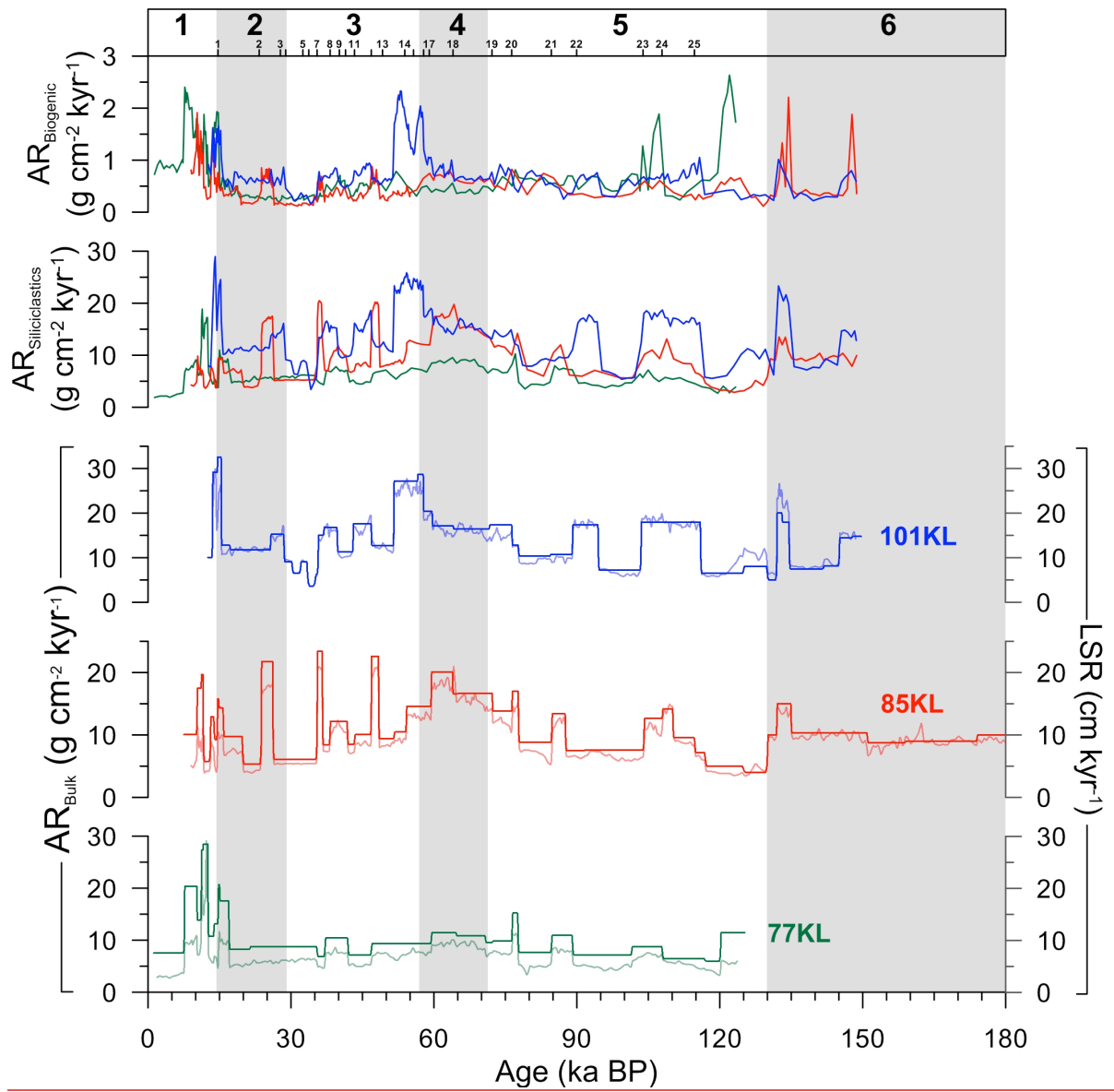
1712

1713 Figure 3: Left: Comparison of proxy records from sediment cores SO201-2-77KL (green  
 1714 lines), -85KL (red lines), and -101KL (blue lines) with published reference records (grey  
 1715 lines). Age models are primarily based on the graphic correlation between color b\* records  
 1716 and the NGRIP  $\delta^{18}\text{O}$  record (NGRIP members, 2004; GICC05 timescale, Rasmussen et al.,  
 1717 2006). Benthic  $\delta^{18}\text{O}$  values from *U. peregrina* (plus symbols) and *U. auberiana* (open  
 1718 triangles) are in agreement with the global reference stack LR04 (Lisiecki and Raymo, 2005).  
 1719 Relative paleointensity (RPI, smoothed by a 5-point-running average) recorded in core 85KL  
 1720 compares with the paleomagnetic reference record PISO-1500 (Channell et al., 2009). L, N,  
 1721 and B mark the Laschamp, Norwegian-Greenland Sea, and Blake paleomagnetic events.  
 1722 Absolute age control is provided by AMS- $^{14}\text{C}$ -dating (coloured triangles; see Max et al.,  
 1723 2012). Top numbers indicate Marine Isotope Stages (boundaries after Lisiecki and Raymo,  
 1724 2005) and D-O events. Upper right: Age versus depth diagram showing the age-depth points  
 1725 and their underlying stratigraphic approach (see also Appendix A). Lower right: Spectral  
 1726 analysis of benthic  $\delta^{18}\text{O}$  and color b\* records performed in the time domain revealed  
 1727 dominant cyclicities that lie within the frequency bands of Earth's obliquity and precession  
 1728 cycles.

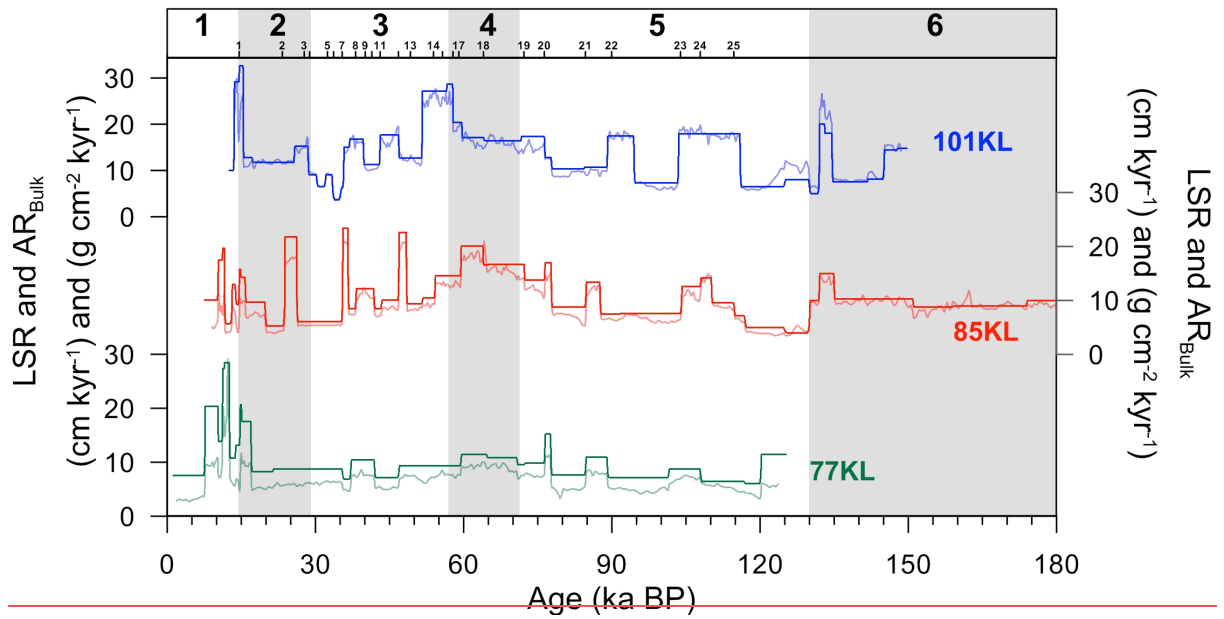
1729

1730



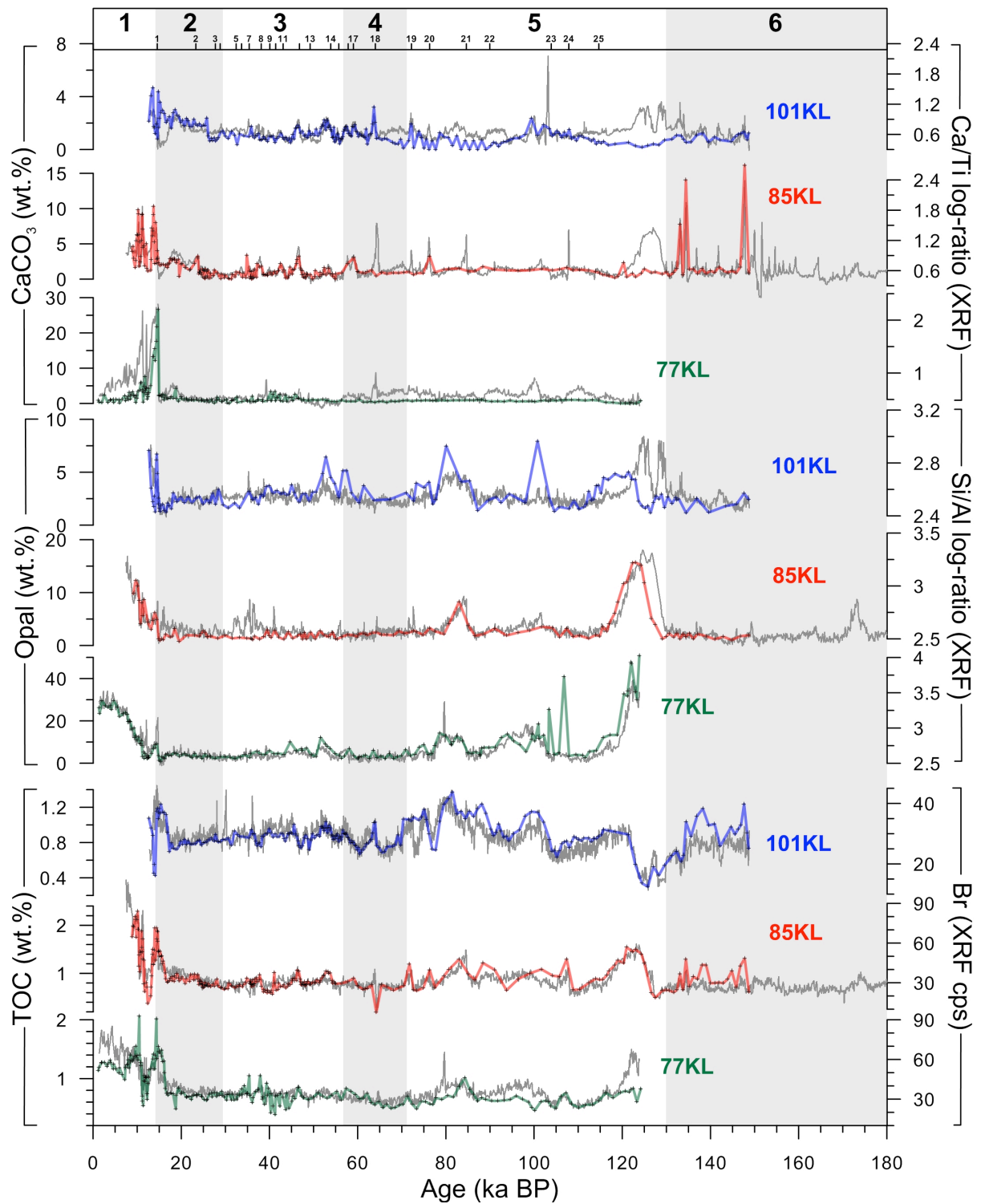


1731



1732  
1733  
1734  
1735  
1736  
1737  
1738  
1739  
1740  
1741  
1742  
1743  
1744  
1745  
1746  
1747  
1748  
1749  
1750  
1751  
1752  
1753  
1754  
1755

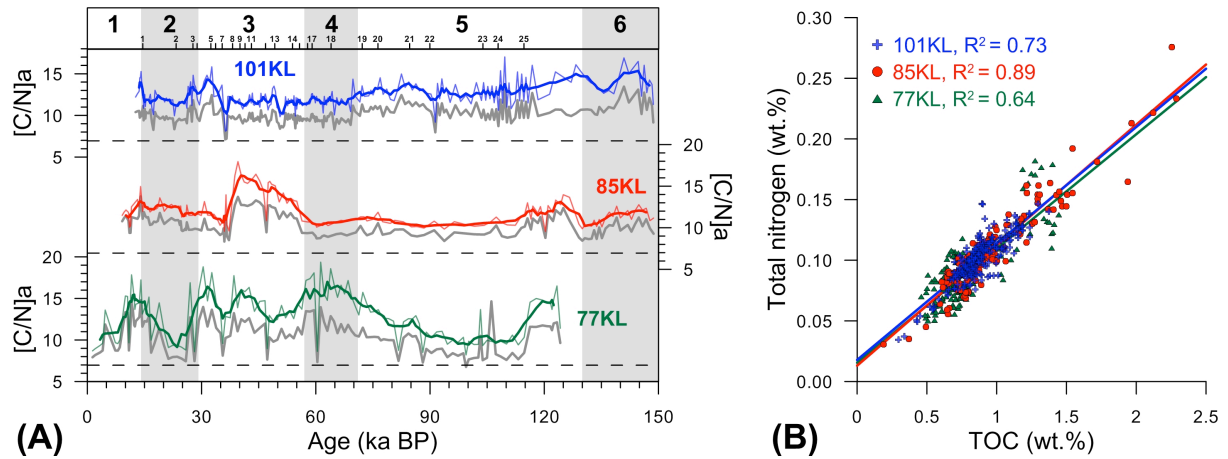
Figure 4: Linear sedimentation rates (LSR) and bulk accumulation rates ( $AR_{Bulk}$ ; transparent lines) of sediment cores SO201-2-77KL (green), -85KL (red), and -101KL (blue). LSR and  $AR_{Bulk}$  are plotted on the same scale per core, as well as accumulation rates of Siliciclastics ( $AR_{Siliciclastics}$ ) and biogenic components (sum of  $CaCO_3$ , TOC, and opal;  $AR_{Biogenic}$ ).



1756

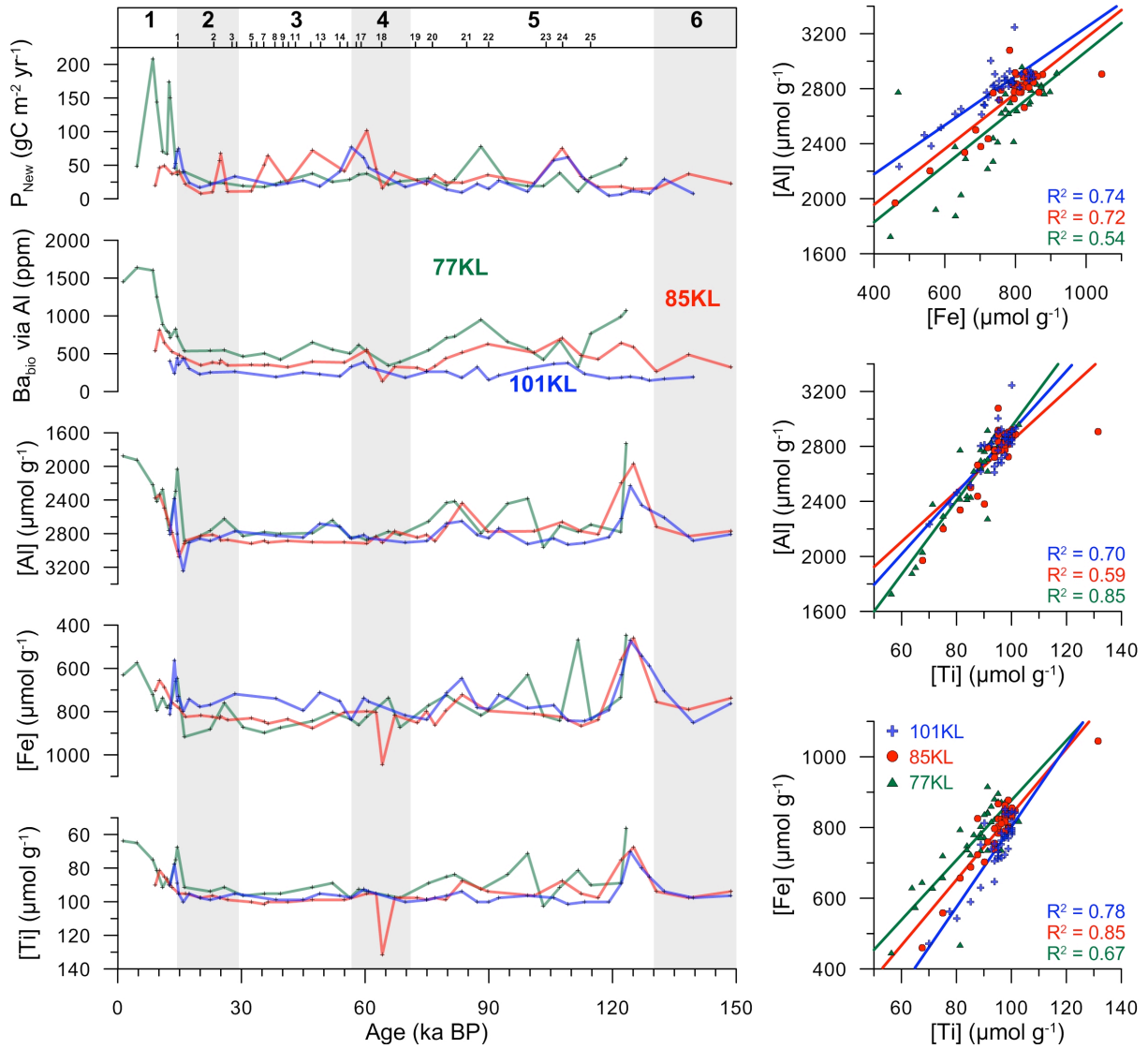
1757 Figure 5: Proxy records from cores SO201-2-77KL (green lines), -85KL (red lines), and -  
 1758 101KL (blue lines) approximating changes in marine productivity over the last 180 kyr.  
 1759 Concentrations of TOC, biogenic opal, and CaCO<sub>3</sub> (coloured lines), are shown in comparison  
 1760 to XRF records of Br (in cps), as well as XRF Si/Al and Ca/Ti log-ratios (underlying grey  
 1761 lines), respectively.

1762



1763 (A) **Atomic** [C/N]<sub>a</sub> ratios (coloured lines, smoothed by a 5-point-running average),  
 1764 corrected for inorganic nitrogen compounds, and uncorrected **molar** C/N ratios (underlying  
 1765 grey lines) for cores SO201-2-77KL (green line), -85KL (red line), and -101KL (blue line)  
 1766 over the past 150 kyr. Dashed horizontal lines mark a C/N ratio of 7. Lower values represent  
 1767 typically marine-derived organic matter. (B) Linear regressions between TOC and TN  
 1768 conducted for each core result in intercept-values that reflect the amount of inorganic nitrogen  
 1769 (TIN). TN contents corrected for TIN were subsequently used to calculate [C/N]<sub>a</sub> ratios.  
 1770

1771  
 1772  
 1773  
 1774  
 1775  
 1776  
 1777  
 1778  
 1779  
 1780  
 1781  
 1782  
 1783  
 1784  
 1785  
 1786  
 1787  
 1788  
 1789  
 1790



1791

1792 Figure 7: Left: Concentrations of lithogenous elements Ti, Fe, and Al (angular brackets), as  
 1793 as well as of biogenic barium ( $Ba_{bio}$ ) and new production ( $P_{New}$ ) for the last 150 kyr.  $P_{New}$  was  
 1794 calculated from  $Ba_{bio}$  using the equation of Nürnberg (1995):  $P_{New} = 3.56 * F Ba_{bio}^{1.504} * z^{-0.0937}$ ,  
 1795 where  $F Ba_{bio} = AR Ba_{bio} / [0.209 * \log_{10}(AR_{Bulk} * 1000) - 0.213]$  (Dymond et al., 1992), and  $z =$   
 1796 water depth (in m).  $F Ba_{bio}$  is the flux of biogenic Ba to the seafloor (in  $\mu\text{g cm}^{-2} \text{yr}^{-1}$ ),  $AR$   
 1797  $Ba_{bio}$  is the accumulation rate of biogenic Ba (in  $\text{mg cm}^{-2} \text{kyr}^{-1}$ ). Note that for records of [Ti],  
 1798 [Fe], and [Al] Y-axes are inverted. Right: Correlation between lithogenous elements and  
 1799 respective linear correlation coefficients ( $R^2$ ) indicate a shared terrigenous source of these  
 1800 elements.

1801

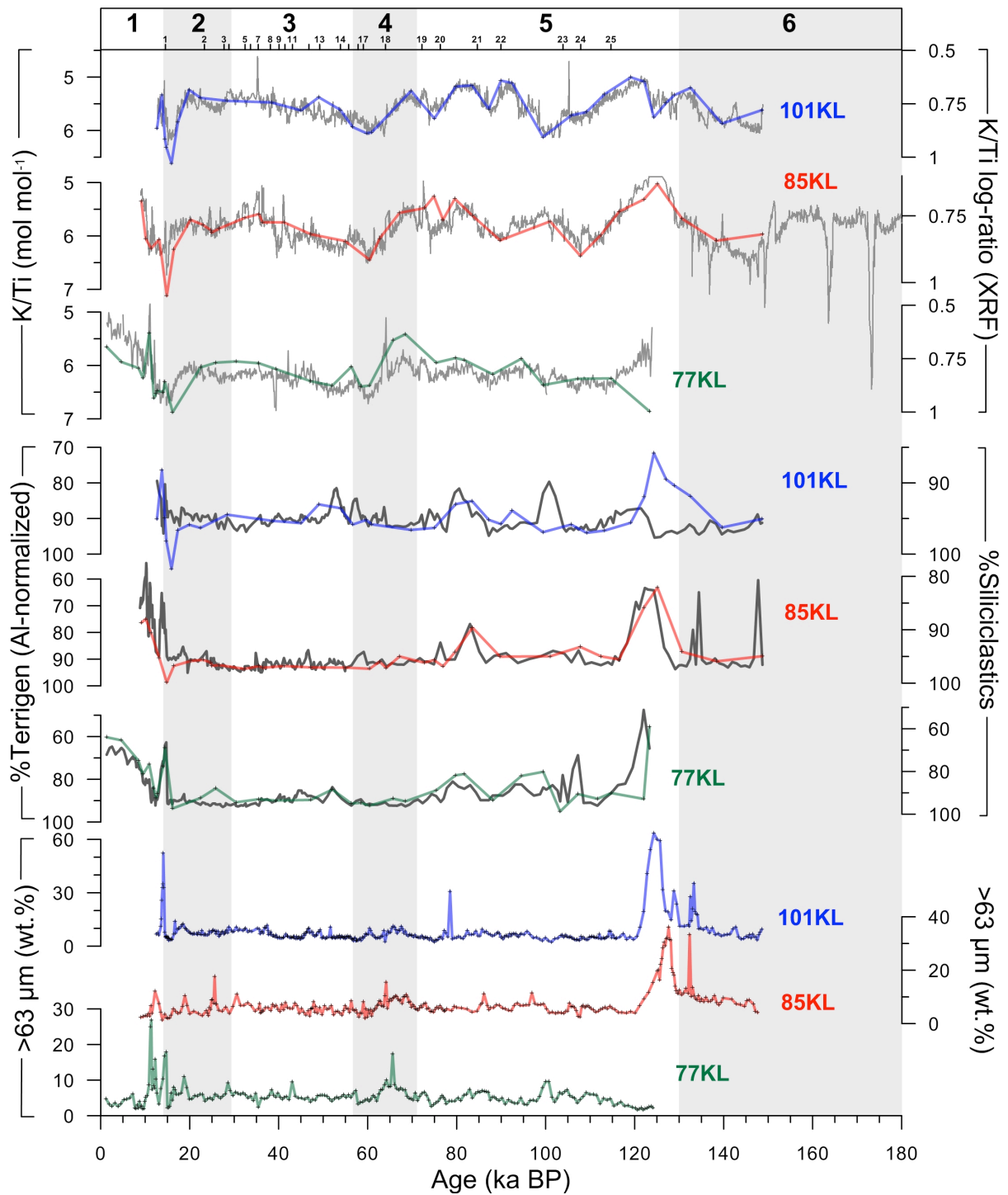
1802

1803

1804

1805

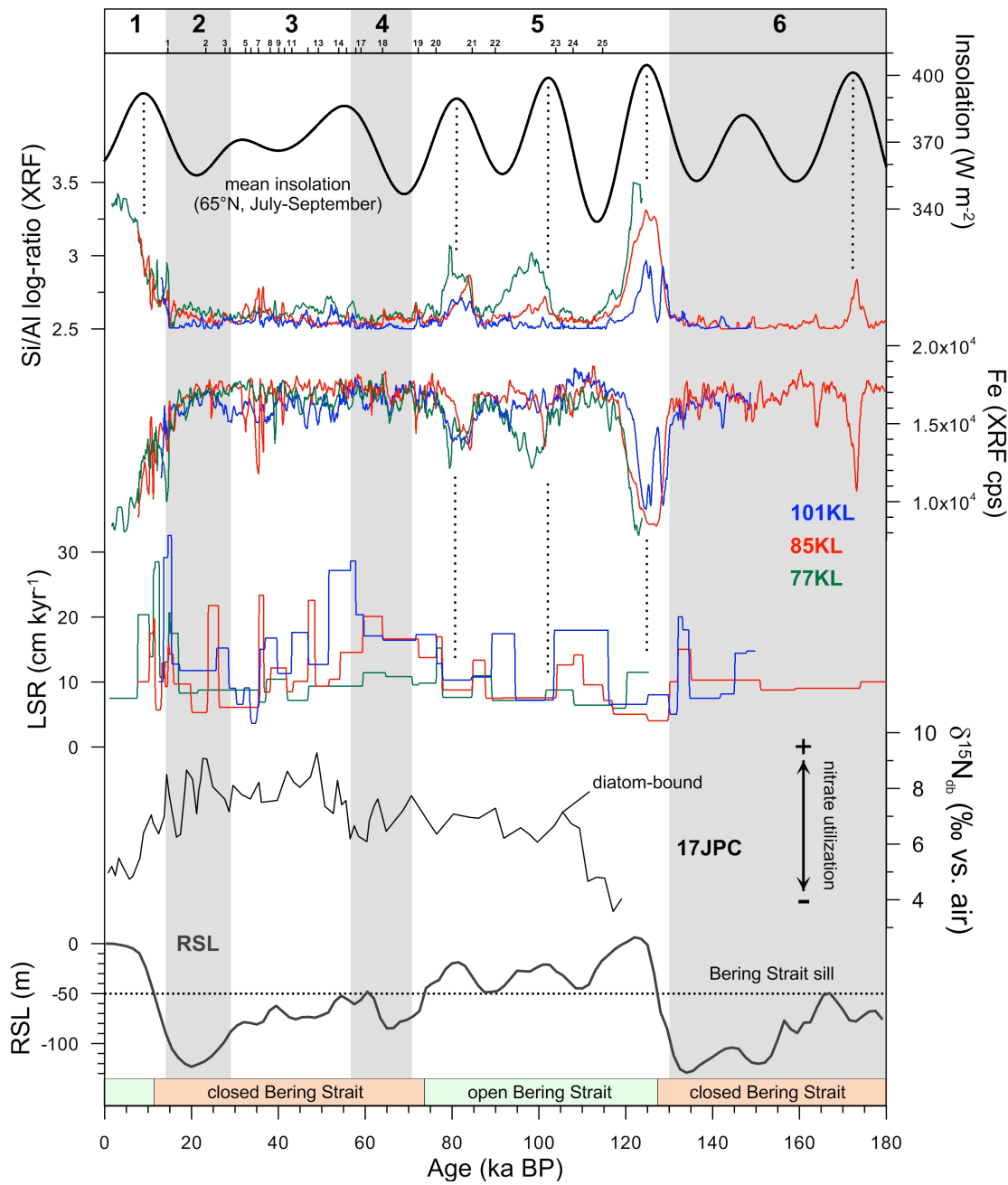
1806



1808

1809 Figure 8: Records approximating changes in terrigenous matter supply over the past 180 kyr.  
 1810 Relative contents of coarse material (>63 μm), terrigenous matter (normalized to Al  
 1811 | concentrations of continental crust; Taylor and McLennan, 1995), and atomic-molar K/Ti  
 1812 | ratios (coloured lines), in comparison to relative amounts of siliciclastics, and XRF K/Ti log-  
 1813 | ratios (underlying grey lines) for cores SO201-2-77KL (green lines), -85KL (red lines), and -  
 1814 | 101KL (blue lines). Note that all Y-axes are inverted, except for >63 μm.

1815



1817

1818 Figure 9: Records of XRF Si/Al log-ratios reflecting changes in biogenic opal concentrations  
 1819 (marine productivity), XRF records of Fe (in cps) reflecting relative changes in terrigenous  
 1820 matter supply, and linear sedimentation rates (LSR) at sites SO201-2-77KL (green lines), -  
 1821 85KL (red lines), and -101KL (blue lines) for the last 180 kyr. Logging data are smoothed by  
 1822 | 5-point-running averages. Relative sea-level (RSL) is after Waelbroeck et al. (2002). The  
 1823 | dashed horizontal line indicates the sill depth of the Bering Strait (~50 m). Summer insolation  
 1824 | at 65°N (July-August) was calculated after Laskar et al. (2004). Records of diatom-bound  
 1825 | nitrogen isotope ratios ( $\delta^{15}N_{db}$ ), assumed to reflect changes in nitrate utilization, are shown  
 1826 | for Bowers Ridge core 17JPC (Brunelle et al., 2007). Comparison of these records suggests  
 1827 | that marine productivity and terrigenous matter supply are subject to external forcing by  
 1828 | summer insolation and sea-level changes.